CHALMERS
UNIVERSITY OF TECHNOLOGY

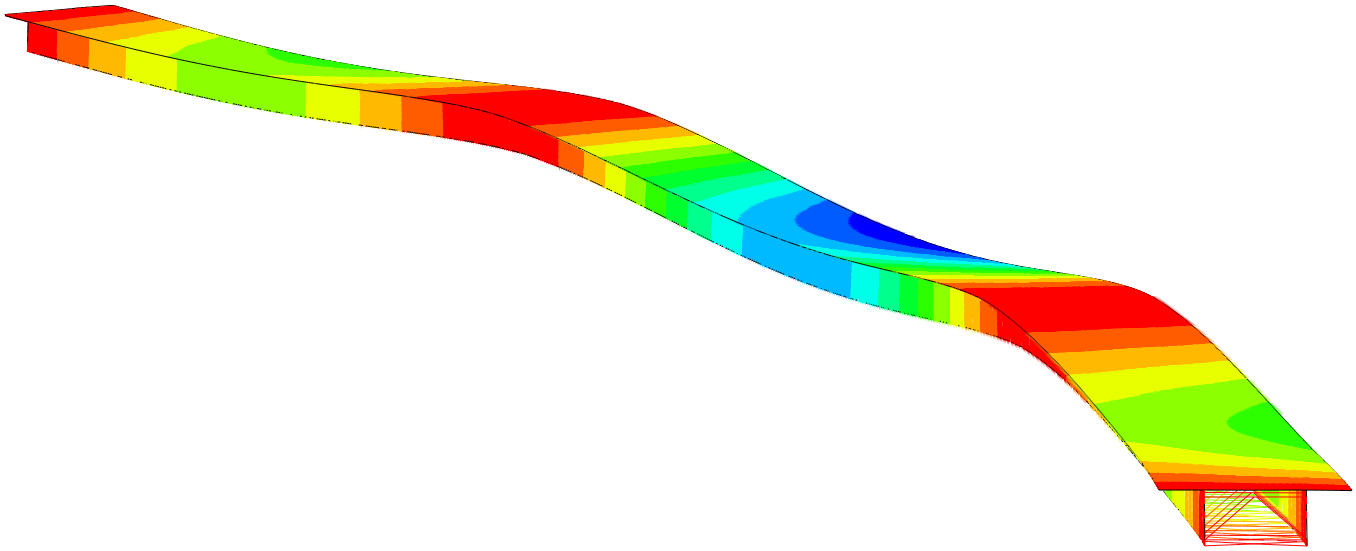

Modelling and Design of Curved Composite I- and Box Girder Bridges

Master's thesis in Master Program Structural Engineering and Building Technology

OFELIA FREDRIKSSON
SIRI SALANDER

DEPARTMENT OF ARCHITECTURE AND CIVIL ENGINEERING

CHALMERS UNIVERSITY OF TECHNOLOGY
Gothenburg, Sweden 2022
www.chalmers.se

Master's thesis ACEX30

Modelling and Design of Curved Composite I- and Box Girder Bridges

OFELIA FREDRIKSSON
SIRI SALANDER

CHALMERS
UNIVERSITY OF TECHNOLOGY

Department of Architecture and Civil Engineering
Division of Structural Engineering
Lightweight Structures Group
Chalmers University of Technology
Gothenburg, Sweden 2022

Modelling and Design of Curved Composite I- and Box Girder Bridges

OFELIA FREDRIKSSON
SIRI SALANDER

Supervisor: Christoffer Svedholm, ELU Konsult AB
Co-supervisor and examiner: Mohammad al-Emrani, Department of Architecture and Civil Engineering
Co-supervisor: Erik Flinck, ELU Konsult AB
Co-supervisor: Erik Olsson, ELU Konsult AB

Department of Architecture and Civil Engineering
Division of Structural Engineering
Lightweight Structures Group
Chalmers University of Technology
SE-412 96 Gothenburg
Telephone +46 31 772 1000

Cover: Displacement field for the shell model of a curved I-girder bridge. Own material.

Department of Architecture and Civil Engineering
Gothenburg, Sweden 2022

Modelling and Design of Curved Composite I- and Box Girder Bridges

OFELIA FREDRIKSSON
SIRI SALANDER
Department of Architecture and Civil Engineering
Chalmers University of Technology

Abstract

Design and modelling of curved composite bridges is a complex art, with few existing guidelines in European standards. By introducing a curvature to the bridge, behaviours such as torsion will highly influence its performance and the design demands will therefore include the torsional stiffness. Naturally, a box girder section would be an appropriate design choice, however, a twin I-girder section could be economically motivated if equipped with a lower plan bracing. This thesis aims to investigate the design and modelling of curved composite bridges. This is done by firstly, discussing appropriate numerical modelling strategies, as there is a need for simplified beam models during the conceptual design phase. Here, the concluding result shows that a spatial beam model is a more suitable beam model, both for the I- and the box girder bridge. Based on these findings, the most advantageous cross-section design at varying radii is investigated by presenting the optimised volume of the I- or box girder bridge. In summary, this part of the study indicates that an I-girder cross-section is the most material-efficient down to a 300 meters radius of curvature. For bridges more curved than that, the box girder bridge results in the least amount of steel. The thesis concludes by presenting a design procedure for curved composite bridges that could be utilised in practice within this field.

Keywords: Steel bridges, Composite Bridges, Curved bridges, I- and box girder bridges, Torsion, Warping, Material-efficient

Acknowledgements

First of all, we would like to give our special thanks to our main supervisors: Christoffer Svedholm at *ELU Konsult AB* and Mohammad al-Emrani at *Chalmers University of Technology*. Their committment to our project has not gone unnoticed and we are ever so grateful for their perspectives and knowledge within the field. We also wish to acknowledge the support and dedication that our supervisors Erik Flinck and Erik Olsson at *ELU Konsult AB* generously have shown. During the whole project, the company of *ELU Konsult AB* has provided us with a welcoming and valuable working environment, and for that we wish to extend our special thanks. Last but not least, our appreciation also goes out to our opponents Leo Adolfsson and Oskar Vestin who devoted themselves to their mission.

Ofelia Fredriksson and Siri Salander, Gothenburg, June 2022

Contents

List of Figures **x**

List of Tables **xii**

1 Introduction **1**
1.1 Background . . . 1
1.2 Aim and objectives . . . 1
1.3 Scope and limitations . . . 2
1.4 Method . . . 2
1.5 Outline of thesis . . . 3

2 Theory **4**
2.1 Design of curved bridges . . . 4
2.1.1 Structural components and details . . . 4
2.1.2 Construction . . . 6
2.2 Effect of curvature . . . 7
2.2.1 Torsion . . . 7
2.2.2 Fatigue . . . 9
2.3 Revision of published models . . . 10
2.3.1 Equivalent straight beam model . . . 10
2.3.2 Grillage model . . . 12
2.3.3 Spatial beam model . . . 13

3 Idealised bridge **14**
3.1 Bridge description . . . 14
3.2 Finite element model . . . 16
3.2.1 Equivalent straight beam model . . . 16
3.2.2 Grillage model . . . 17
3.2.3 Spatial beam model . . . 18
3.2.4 3D shell model . . . 18
3.3 Results and discussion . . . 19
3.3.1 Global design . . . 20
3.3.2 Details . . . 27

4 Case study **31**
4.1 Bridge description . . . 31
4.1.1 Loads . . . 32

4.1.2 Load combinations 34
4.1.3 Requirements 35
4.2 Optimisation 36
4.3 Results and discussion 39
4.3.1 Global design 39
4.3.2 Details 42

5 Conclusion **43**
5.1 Design guide 43
5.2 Further research 44

Bibliography **44**

A Cross-section of idealised bridge design **II**

B Supplementary results: radius of 300 meters **III**

C Supplementary results: bending and shear stresses **X**

D Calculation of internal forces of cross-bracing **XIX**

E Geometrical values for Solvalla bridge **XXV**

F Calculations for one cross-section in the case study **XXVI**

G Supplementary result: Case study **XXXIX**

List of Figures

2.1 Two common cross-sections for curved composite bridges. 4
2.2 Common structural components of a composite bridge. 5
2.3 Examples of horizontal bracing. 6
2.4 Torsion induced by curvature. 7
2.5 Torsion stiffness of a composite bridge. 8
2.6 Welds on the cross-bracing and the corresponding detail category [14]. 9
2.7 View of equivalent straight beam model. 11
2.8 View of grillage model. 12
2.9 View of spatial beam model. 13

3.1 Geometry of the idealised bridge. 14
3.2 Geometry of the I-girder bridge's cross-section. 15
3.3 Geometry of the box girder bridge's cross-section. 15
3.4 Boundary conditions of the idealised bridge. 16
3.5 Equivalent torque. 17
3.6 Grillage model with applied load. 18
3.7 Spatial beam model with applied load. 18
3.8 Shell model for I-girder bridge. 19
3.9 Shell model for box girder bridge. 19
3.10 Paths for retrieving xy-data from shell model. 20
3.11 Displacement for I-girder bridge during construction. 21
3.12 Displacement for I-girder bridge during service life. 22
3.13 Displacement for box girder bridge during construction. 23
3.14 Displacement for box girder bridge during service life. 24
3.15 Bending stresses for the box girder bridge during service life and with a radius of 900 meters. 26
3.16 Shear stresses for the box girder bridge during service life and with a radius of 900 meters. 27
3.17 Axial force in cross-bracing from the shell model of the I-girder bridge. 27
3.18 Axial force in cross-bracing from the shell model of the box girder bridge. 28
3.19 Truss model of cross-bracing [6]. 28
3.20 Axial force in lower plan bracing from the shell model. 29
3.21 Position of the highest stressed lower plan bracing. 29

4.1 Geometry of Solvalla Bridge. 31
4.2 Cross-section of Solvalla bridge. 32

4.3 Illustration of how the forces act on Solvalla Bridge. 33
4.4 Traffic load model LM71 for the dimensioning cases. 34
4.5 Shear force due to torsion. 36
4.6 Flowchart over the analysis of Solvalla Bridge. 37
4.7 Final results of case study: Steel masses for optimised cross-sections at different radii. 41

5.1 Developed flowchart over modelling approach and design procedure . 44

B.1 Bending stress for I-girder bridge with radius of 300 meters. IV
B.2 Bending stress for box girder bridge with radius radius of 300 meters. V
B.3 Shear stress for I-girder bridge with radius of 300 meters. VI
B.4 Shear stress for box girder bridge with radius of 300 meters. VII
B.5 Displacement for I-girder bridge with radius of 300 meters. VIII
B.6 Displacement for box girder bridge with radius of 300 meters. IX

C.1 Bending stress for I-girder bridge during construction. XI
C.2 Bending stress for I-girder bridge during service life. XII
C.3 Bending stress for box girder bridge during construction. XIII
C.4 Bending stress for box girder bridge during service life. XIV
C.5 Shear stress for I-girder bridge during construction. XV
C.6 Shear stress for I-girder bridge during service life. XVI
C.7 Shear stress for box girder bridge during construction. XVII
C.8 Shear stress for box girder bridge during service life. XVIII

E.1 Positions of the parts that constitutes the cross-bracing and the plan bracing. XXV

List of Tables

2.1 Typical geometrical values for I- and box girder steel bridges [3]. . . . 5
2.2 Element properties for equivalent straight beam model for box girder bridge. . . . 11
2.3 Element properties for equivalent straight beam model for I-girder bridge. . . . 12
2.4 Element properties for grillage model. . . . 12
2.5 Element properties for spatial beam model. . . . 13

3.1 Applied load for the idealised bridge. . . . 15
3.2 Material properties for the idealised bridge. . . . 16
3.3 Total vertical reaction force. . . . 20
3.4 Convergence study for shell model. . . . 20
3.5 Deviations from shell model[1)]: maximum field displacement for I-girder. 25
3.6 Deviations from shell model: maximum field displacement for box girder. . . . 25
3.7 Deviations from shell model: maximum axial forces in the diagonals, upper and lower chords of the cross-bracing. . . . 29
3.8 Forces in lower plan bracing. . . . 30

4.1 Material properties for the Solvalla Bridge. . . . 32
4.2 Loads that act on Solvalla Bridge. . . . 33
4.3 ψ-factor for load combination [23]. . . . 35
4.4 Settings for the genetic algorithm. . . . 37
4.5 Varying geometrical parameters in [mm] for the I-girder bridge. . . . 38
4.6 Varying geometrical parameters in [mm] for the box girder bridge. . . . 38
4.7 Verification of the rail traffic load position. . . . 39
4.8 Utilisation ratios for all studied radii from the first optimisation. . . . 40
4.9 Final utilisation ratios for all studied radii. . . . 41

A.1 Geometries of the I- and box girder cross-sections II

E.1 Measurements of the parts that constitutes the cross-bracing and the plan bracing. . . . XXV

1
Introduction

1.1 Background

Steel-concrete composite bridges are a prominent choice when designing robust structures such as railway or highway bridges. Especially, the composite action combines the advantages of steel structures' low self-weight and simple prefabrication with the economical benefit of the reinforced concrete. Eurocode includes design of steel-concrete composite bridges, but for curved bridges it only states that: "Where the steel section of a composite member is curved in plan, the effects of curvature should be taken into account" [1]. It is therefore up to the engineer to specify how these effect should be considered during modelling.

In practice, curved composite bridges are commonly made with either twin I-girders or a box girder, which both entails advantages and disadvantages. A box girder section possesses high torsional stiffness, something that is particularly essential when the bridge is curved. On the contrary, an I-girder section provide an economical benefit and is consequently often preferred by the client. Even though this type of cross-section have a lower torsional stiffness, it can be equipped with a plan bracing system to increase it. However, depending on the magnitude of the curvature, a suspicion of whether or not the I-girder is still economically motivated arises. Currently, several simplified models for designing curved composite bridges have been published and adapted by the industry but they do not make it clear when an I- or a box beam results in the most optimised solution.

1.2 Aim and objectives

The aim is to formulate a design procedure for curved composite I- and box girder bridges. In order to achieve this, the key questions to be answered are:

1. What are the published models used in practice for curved composite bridges and for which design case is a model suitable, both regarding construction and service life?
2. When is it advantageous or disadvantageous to use an I- or a box girder system for a curved composite bridge?
3. How could a design procedure for curved composite bridges be defined in a practical way?

1.3 Scope and limitations

This project will investigate the design and modelling of horizontally curved steel-concrete composite bridges with an I- and a box cross-section. The design will focus on the bridge geometry with regard to the curvature and thus different radii will be investigated. Excluded design features, which is also affected by curvature, includes the bridge width and span length, along with the form and spacing of the cross-beams and plan bracing. The numerical modelling will be limited to one construction phase to keep the design on a general level. A static analysis assuming linear elastic behaviour will be performed, thereby excluding any non-linearity. Dynamic effects of variable loads will only be considered by an amplifying dynamic factor according to Eurocode.

1.4 Method

Firstly, a comprehensive literature review will be conducted. This includes studying of Swedish design codes for bridges, design and construction of composite I- and box girder bridges, as well as, the effect of torsion, warping and fatigue on curved bridges. The literature review will also include already published models for design of curved composite bridges with open and closed cross-section.

Secondly, finite element modelling will be performed in Brigade Plus using Python scripts. The published design models will be compared to a linear elastic 3D shell model that can predict the stress field of a curved I- and box girder bridge. The numerical modelling will first be performed on an idealised bridge with regard to the geometry and the load, in order to see the isolated effects of curvature on a bridge with open and closed cross-section. Thereafter, a case study of Solvalla Bridge will be accomplished to investigate when an I- or a box girder section is most advantageous. This is examined by performing an optimisation of the two cross-section types, using the MatLab application *Global optimisation toolbox*.

Finally, a design procedure will be proposed based on the result of the finite element modelling. This procedure includes recommendations regarding when a published model is most suitable and when it is most appropriate to use an I- or a box section. The procedure should be practical to use for a specific design case, such that it easily can be implemented by the industry.

1.5 Outline of thesis

Chapter 2 treats the theory of design of steel-concrete composite bridges and how effects acting on steel are influenced by curvature. Published current models for analysis of curved composite bridges are revised.

Chapter 3 presents the study of the idealised bridge. It describes the development of the numerical models in Brigade and further, it presents the results together with evaluations and discussions.

Chapter 4 presents the case study of Solvalla Bridge. It describes the development of the numerical models in Brigade and further, it presents the results together with evaluations and discussions.

Chapter 5 draws conclusions in order to answer the thesis aim and to propose a design procedure. It also discusses questions regarding future research.

2
Theory

2.1 Design of curved bridges

When designing a curved composite bridge, there are commonly two beam bridge systems to consider: the I- and the box girder system [2], see Figure 2.1. These can be referred to as an open and a closed section, where, as the names suggest, the steel together with the concrete may enclose the section. Hence, the box girder bridge is a closed section and the I-girder bridge an open section. However, when the I-girder bridge is constructed with a lower plan bracing system, its behaviour reassembles that of a closed section instead.

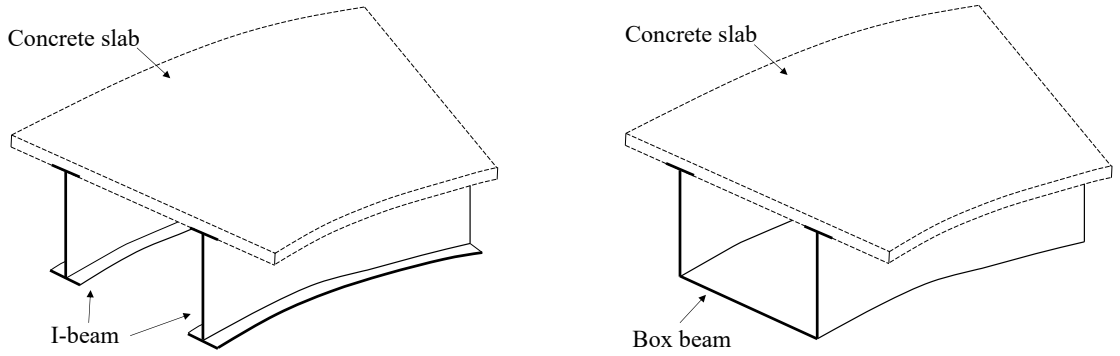

(a) I-girder bridge (open section). **(b)** Box girder bridge (closed section).

Figure 2.1: Two common cross-sections for curved composite bridges.

2.1.1 Structural components and details

Curved I- and box girder bridges are built up of many structural components, which purpose may change from construction phase to service life as well as when compared to a straight bridge. The main design features of its superstructure are the steel girders with an I- or a box section, the concrete slab, the cross-beams and the plan bracing, as illustrated in Figure 2.2.

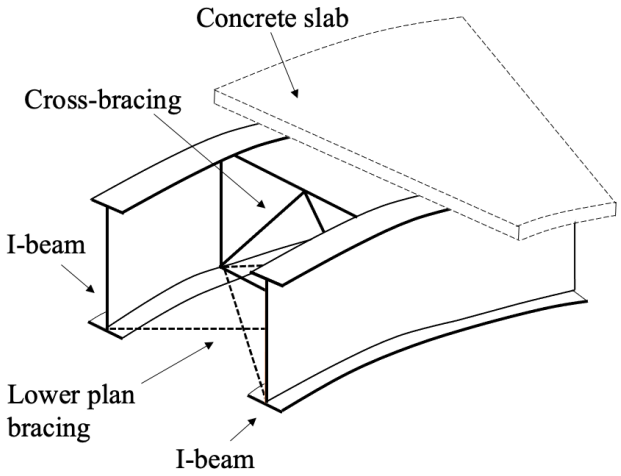

Figure 2.2: Common structural components of a composite bridge.

Firstly, the longitudinal I- or box girders are the primary elements of the structure and their main task is to transfer the loads acting on the bridge deck to the supports [3]. There exist common reference values for conventional bridge design, which can be used during the conceptual design phase of curved bridges. These typical dimensions are introduced in Table 2.1 for both I- and box girders. From the table, it is apparent that a box girder bridge can be made longer and slender than an I-girder bridge, which is due to its higher stiffness. All the same, when it comes to the smaller spans, the I-girder bridge is generally economically justified over the box girder bridge [2].

Table 2.1: Typical geometrical values for I- and box girder steel bridges [3].

Variable	I-girder section	Box section	Unit
Length of spans, L	up to 125	up to 300	m
Slenderness of the cross-section, L/H	20 to 28	25 to 30	-
Width of top flange, b_{tf}	300 to 1200	[1)]	mm
Thickness of top flange, t_{tf}	15 to 70	16 to 40	mm
Thickness of web, t_w	10 to 22	10 to 22	mm
Width of bottom flange, b_{bf}	400 to 1400	[2)]	mm
Thickness of bottom flange, t_{bf}	20 to 90	10 to 50	mm

1) Recommended design values not given.

2) Equals the centre-to-centre distance between webs.

Furthermore, the cross-bracing, designed as diaphragms, trusses, or frames, are located above the piers and abutments of the bridge and then at consistent distances in between. While in a straight bridge, the cross-beams function is to prevent lateral torsional buckling during construction, their role becomes more significant for a curved bridge where they serve as load-carrying components [4]. Without cross-bracing, the structure would be unstable, due to their function as the added restraint to handle torsion of the bridge [5]. The cross-beams should also maintain the shape of the cross-section, since both curved I- and box girder bridges are stressed by

distortion [6]. This implies a design that can handle the stresses due to torsion, seeing that the cross-bracing distributes the torque to the main girders. Moreover, the spacing of the cross-beams becomes an important design feature, since curved bridges naturally demands more cross-beams than straight bridges. For larger curvature, there will therefore be a need of more cross-bracing and thereby also a higher material consumption [4].

2.1.2 Construction

The construction phase entails challenges, as the final stability of the structure is not yet achieved. Before the concrete slab has been cast, both the I- and box girder bridge behave as open cross-sections and therefore, their vulnerability to torsion has to be considered during the design of the bridge. One alternative is to equip the bridge with a temporary top horizontal bracing [3]. These can be designed with different forms as illustrated in Figure 2.3. Since there are no presence of fatigue loads in the construction phase, the choice of horizontal bracing is not governed by secondary load effects and may be more freely chosen based on construction method [3].

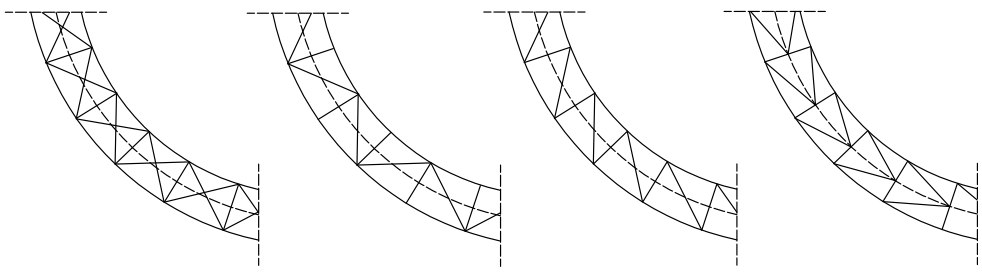

Figure 2.3: Examples of horizontal bracing.

The temporary bracing will act as the slab during construction and increase the torsion stiffness of the structure. It can be placed either at the same level as the cross-beams or at the top of the top flange [3]. If the latter position is chosen, it cannot be taken away after the slab has been cast and cured. Therefore, attention will have to be made to ensure the plan bracing is properly maintained throughout the service life. Equipping the bridge with temporary bracing implies additional costs for the material and construction. The additional welding work also induces stresses in the steel structure, which have to be considered when assessing the fatigue strength.

There are numerous ways to construct a bridge, each depending on the site and the design of the bridge. One cost-efficient approach is to lift the steel structure into place by cranes positioned at ground level [7]. The lifting of a single curved I-girder will induce rotation during the lift [4]. The stability of the I-girder steel structure can be ensured if pairs of girders are lifted simultaneously with cross-bracing already in place.

For sites where lifting is deemed impossible, the more complex construction method of launching can be applicable instead. The components are assembled at one or two ends and the bridge segment is driven forward on roller to the next support. A tapered truss structure, called launching nose, is attached to the main girders in the leading bridge segment in order to reduce the cantilever effect [8]. This launching method suggests that the bridge possesses sufficient horizontal bending and torsion stiffness, and therefore, a closed cross-section is preferable [7]. This can be achieved by launching a box girder bridge with the full composite section or by using temporary top bracing. It is, however, more common to launch only the steelwork to limit the self-weight of the cantilever part [7].

2.2 Effect of curvature

A curved bridge will experience additional stresses compared to a straight bridge merely due to the geometry. Torsion, warping, and fatigue are relevant phenomena of these bridges and therefore, this section explains for their behaviour and how they are affected by the curvature.

2.2.1 Torsion

Figure 2.4a serves as an illustrative example of how torsion is introduced by considering the segment *ds* of a curved I-girder. Regardless if the girder is curved or straight, the flanges are liable to bending stresses due to the self-weight. In a simplified manner, the bending moment, M_y, can be substituted by an axial force couple, N, acting with the opposite direction at the level of the top and bottom flange [9], see Figure 2.4b. Distinctive for curved girders is that this axial force has an horizontal component, H, which will be apparent along the length of the beam. The addition of a horizontal force couple implies that an horizontal or a torsional moment restraint is needed to achieve equilibrium [5]. In practice, this added restraint will be the cross-bracing.

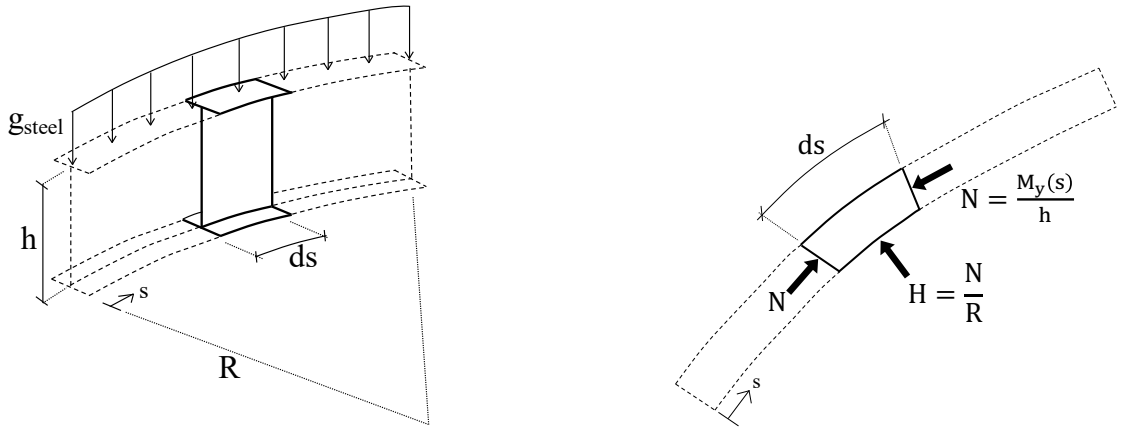

(a) Segment of an I-girder. **(b)** Plan view of segment.

Figure 2.4: Torsion induced by curvature.

Torsion can be resisted in two ways: by St. Venant torsion (uniform torsion) or by warping (non-uniform torsion). The component that contributes to the torsion stiffness of the bridge depends on the type of cross-section. Generally, an open cross-section resists torsion by warping and a closed by St. Venant torsion [5]. One I-girder have negligible torsion stiffness by itself, however, twin I-girders can resist torsion by warping when they are connected by the cross-bracing. This implies that the horizontal force couple will be resisted by a vertical force couple at the position of the cross-bracing [5] as illustrated in Figure 2.5a. The effect of torsion on a global level is an added component to the normal and shear stresses. On the other hand, a box girder bridge resists the horizontal force couple by means of a uniform shear flow, see Figure 2.5b. For the box section to utilise the St. Venant torsion resistance, distortion of the cross-section have to be prevented [5]. This is achieved by adequate cross-bracing.

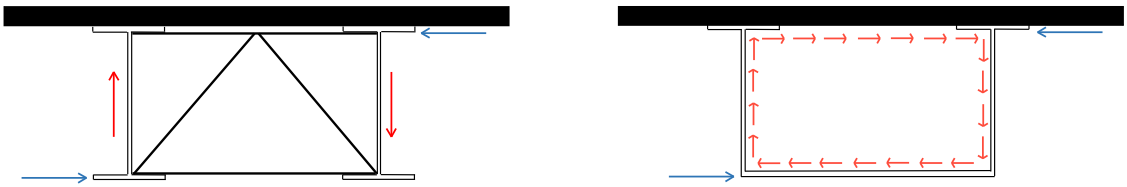

(a) Resistance in warping. **(b)** Resistance in St. Venant torsion.

Figure 2.5: Torsion stiffness of a composite bridge.

The two different behaviours for resisting torsion are integrated in the modelling by a torsional constant. For an open section with thin-walled components, this cross-sectional property is determined as described in Equation 2.1. The corresponding constant for a closed cross-section is determined by Bredt's second formula [10], see Equation 2.2. For a composite bridge, it is the concrete slab that closes the cross-section and will therefore influence the stiffness distribution of the bridge. Even though the slab is moderately thick, its additional stiffness is added according to Equation 2.1. It is worth noting that the closed cross-section has a higher torsional stiffness than an open section, which is captured by the two different equations.

$$I_t = \frac{1}{3} \cdot \sum_{i=1}^{n} s_i \cdot t_i^3 \tag{2.1}$$

$$I_t = \frac{(2CC)^2 \cdot h^2}{\frac{h_w}{t_w} + \frac{CC}{t_{bf}} + \frac{h_w}{t_w} + \frac{CC}{t_{slab}}} \tag{2.2}$$

where s = length, t = thickness, CC = distance between webs,
h = section height, h_w = web height, t_w = web thickness,
t_{bf} = bottom flange thickness, t_{slab} = slab thickness

If a twin I-girder bridge is equipped with a lower plan bracing, the bridge will behave as a closed cross-section and thus the torsion constant should capture this change of behaviour. This is included by substituting the bracing with a fictional steel sheet and using an equivalent thickness in Equation 2.2 [18].

2.2.2 Fatigue

The phenomena of fatigue is relevant when ductile materials are exposed to fluctuating loads, as is expected for a railway bridge. For every cycle of loading, damage caused by secondary load effects is accumulated in the details of the structure and accordingly, failure can occur below the elastic limit at these areas [11]. Curved composite bridges are to a greater extent affected by secondary load effects. When horizontal curvature is introduced to a composite bridge, it results in transversely uneven distribution of the self-weight loading. This in turn leads to greater stresses on the details at the outer curve of the bridge, something that needs to be accounted for [12]. Another consequence of the curvature is that the outer web plate becomes longer than the inner one. This leads to a greater spacing of the vertical cross-bracing and furthermore, to smaller rigidity at the outer web versus the inner web [13].

For I- and box girder bridges there are multiple controls concerning fatigue that have to be performed, most of them regarding joints of the cross-beams. Figure 2.6a shows an example of details that are relevant for the cross-bracing. They are numbered as follows: 1) the weld connecting the cross-beams to the top and bottom flange, 2) the weld connecting the cross-beams to the web. In addition to these, the but welds which connects the main girders to one another should be verified.

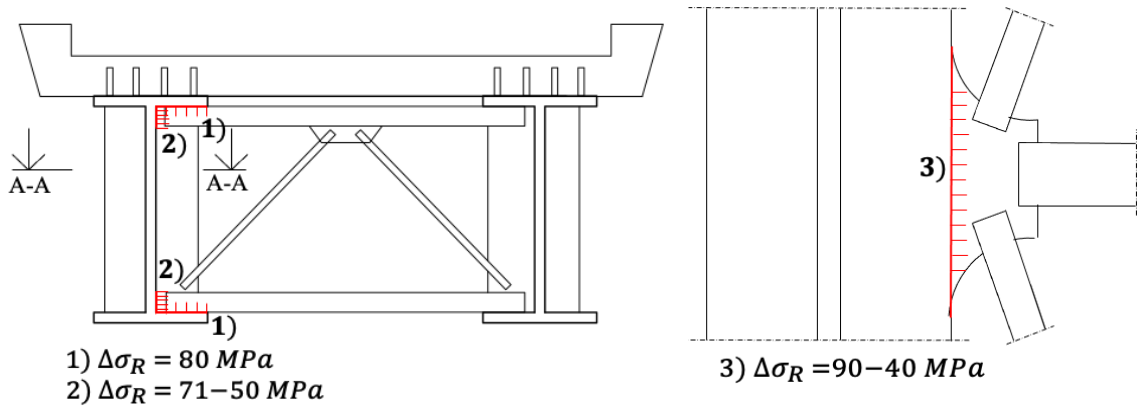

(a) Section view of cross-bracing. **(b)** Section A-A.

Figure 2.6: Welds on the cross-bracing and the corresponding detail category [14].

When comparing the two cross-sections in question, it becomes obvious that the necessary closer spacing of cross-bracing, as well as, the plan bracing system of the I girder bridge results in more connection details, which leads to the illation that I-girder bridges will be more exposed to fatigue. The additional detail is illustrated in Figure 2.6b with the numbering: 3) the weld between the gusset plate, where the cross- and plan bracing is attached, and the bottom flange. The detail category of the gusset plate is very dependent on if its edges are hard or smooth, as this will effect the geometrical stress concentration. Therefore, the detail category may vary between 40 and 90 MPa[14].

2.3 Revision of published models

The most general way to model a curved bridge is to set up a three dimensional shell model. Shell elements are 3D elements that are appropriate to use to represent components where the thickness is significantly smaller than the other dimensions [15]. Since both an I- and a box girder bridge are composed of components that satisfy this condition, a shell model is applicable. However, it can be time consuming since the model is complex. This type of model is also not optimal for design, since a new model have to be created for each iteration. It is therefore desirable to simplify the shell model to a beam model. This thesis will focus on three different beam models with varying degree of simplicity:

1. The equivalent straight beam model, also known as Simplified method [5] or V-load method [16]
2. The grillage model
3. The spatial beam model

Following sections will serve as an introduction to the theory behind the three models in question.

2.3.1 Equivalent straight beam model

One simplified way to model a curved bridge is to substitute the geometry with an equivalent straight bridge [16]. The span length of the straight bridge is assumed to be $L = R \cdot \alpha$, where R is the radius of curvature (to the centre of the bridge) and α is the central angle of the circle sector [5]. The effect of curvature is introduced as an additional load, which is done in two different approaches since I- and box girder bridges resist torsion in different ways.

For a box girder bridge, an equivalent torque is added to represent the effect of curvature, as illustrated in Figure 2.7a. This torque have a magnitude of $m_T = \frac{-M_y(s)}{R}$, with $M_y(s)$ being the varying distribution of bending moment along the length of the beam. On the other hand, the I-girder bridge have a torsion stiffness that includes warping. Hence, the equivalent torque is divided by the centre-to-centre distance between the main girders, CC, and applied as a force couple with magnitude $\frac{\pm M_y(s)/R}{cc}$, see Figure 2.7b.

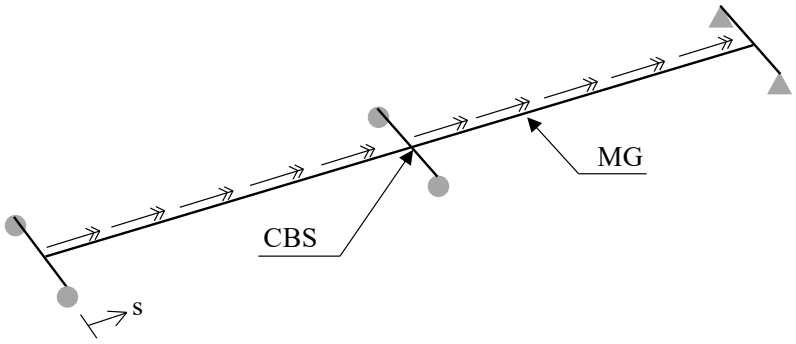

(a) Box girder bridge.

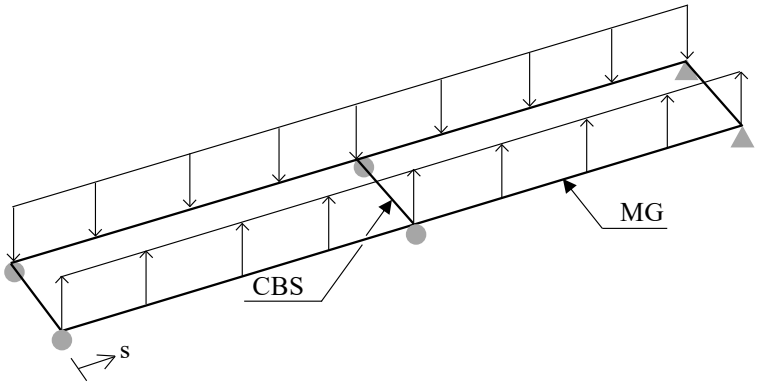

(b) I-girder bridge.

Figure 2.7: View of equivalent straight beam model.

Besides the different approaches of how to introduce the equivalent load, the two bridge types are also distinguished by their geometry as indicated in Figure 2.7. The box girder bridge is modelled with one straight main girder, (MG), whilst the I-girder bridge instead is modelled as two straight main girders. In both cases, cross-beams at the support, (CBS), are added. The beam elements represent different parts of the bridge and are therefore assigned different cross-sectional properties, see Table 2.2 and Table 2.3. The MG-elements represent the I-girders or the box and an effective width with regard to shear lag is given for both the concrete slab and the bottom steel flange. The CBS-elements are assumed rigid to model the support conditions at the position of the bearings.

Table 2.2: Element properties for equivalent straight beam model for box girder bridge. The cross-sectional properties I_y,I_z and I_t relates to the entire cross-section.

Element	**Moment of inertia**			**Torsion constant**	**Young's modulus**
	Vertical	Horizontal	Product		
MG	I_y	I_z	0	I_t	E_s
CBS	$\gg I_y$	$\gg I_z$	0	0	∞

Table 2.3: Element properties for equivalent straight beam model for I-girder bridge. The cross-sectional properties I_y,I_z and I_t relates to the entire cross-section.

Element	**Moment of inertia**			**Torsion constant**	**Young's modulus**
	Vertical	Horizontal	Product		
MG	$I_y/2$	$I_z/2$	0	$I_t/2$	E_s
CBS	$\gg I_y/2$	$\gg I_z/2$	0	0	∞

2.3.2 Grillage model

One of the most commonly adapted models for capturing the behaviour of both straight and curved bridges is the grillage model [17]. This model is composed of either curved beams or straight beams that are placed in the same radius as the curved bridge. Unlike the equivalent straight beam model, the grillage model is consistent for both a box and an I-section, as illustrated in Figure 2.8. It consists of CBS-elements and two MG-elements that corresponds to the twin I-girders or the box. Cross-beams, (CB), are also placed at the position of the cross-bracing along the length of the bridge. These elements represent both the cross-bracing and the slab with a width equal to the centre-to-centre distance between the cross-beams. The CB- and CBS-elements compose the out-of-plane stiffness of the slab and cross-bracing, whereas the in-plane stiffness is added to the MG-elements [18]. The assigned cross-sectional properties are found in Table 2.4.

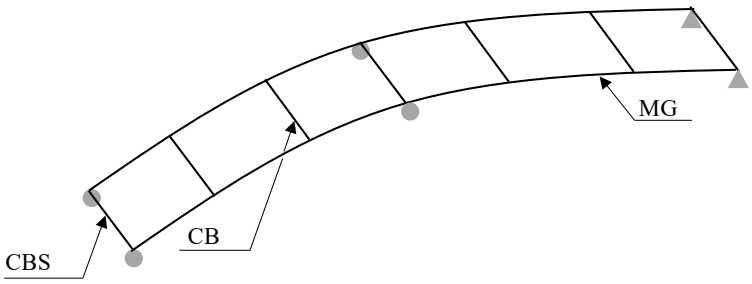

Figure 2.8: View of grillage model.

Table 2.4: Element properties for grillage model. I_y,I_z and I_t relates to the entire cross-section.

Element	**Moment of inertia**			**Torsion constant**	**Young's modulus**
	Vertical	Horizontal	Product		
MG	$I_y/2$	$I_z/2$	0	$I_t/2$	E_s
CB	$I_{y.slab}$	$I_{x.slab}$	0	0	E_s
CBS	$I_{y.slab}$	$I_{x.slab}$	0	0	E_s

The grillage model can be improved to better simulate the three dimensional behaviour by implementing beam elements with seven degrees of freedom (DOFs) instead of the common six [19]. However, this type of beam element is not standardised for most FE-softwares and will not be used in this study.

2.3.3 Spatial beam model

As a further development of the grillage model, the spatial beam model was developed to cover a more advanced behaviour, such as local bending, section distortion, and warping effects [10]. Compared to the grillage model, a third fictitious longitudinal beam is added to the grid, which allows for the possibility to assign the longitudinal elements different cross-sectional properties, see Figure 2.9. The longitudinal elements are divided so that the main girders take the vertical loading and the central girder, (CG), takes the horizontal loading. This suggests that the MG-elements are assigned the bending stiffness whereas the CG-element possesses the torsion stiffness, see Table 2.5. The CB- and CBS-elements are modelled as rigid links.

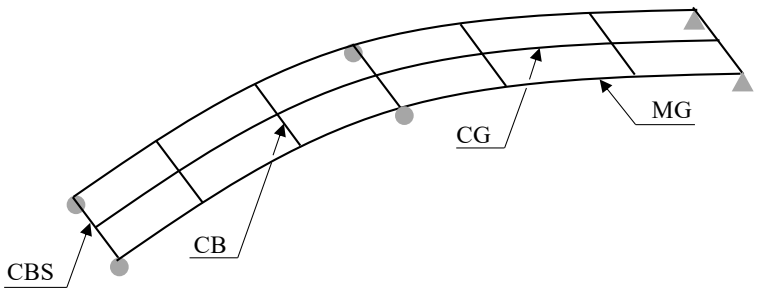

Figure 2.9: View of spatial beam model.

Table 2.5: Element properties for spatial beam model. I_y,I_z and I_t relates to the entire cross-section.

Element	**Moment of inertia**			**Torsion constant**	**Young's modulus**
	Vertical	Horizontal	Product		
MG	$I_y/2$	0	0	0	E_s
CG	0	I_z	0	I_t	E_s
CB	1	1	0	0	∞
CBS	$\gg I_y/2$	$\gg I_z$	0	0	∞

3
Idealised bridge

The study of the idealised bridge is conducted to isolate the effect of curvature by simplifying the geometry and the applied load. The aim of this analysis is to answer the first objective: for which design case is a model suitable, both regarding construction and service life?

3.1 Bridge description

The idealised bridge consists of continuous twin or box girder(s) with a total length of 200 meters divided into three spans, as illustrated in Figure 3.1. The end spans have a length equal to 80 % of the mid-span's length, so as to have approximately the same field moment in all spans. The webs of the girder(s) have a centre-to-centre distance of 4.5 meters.

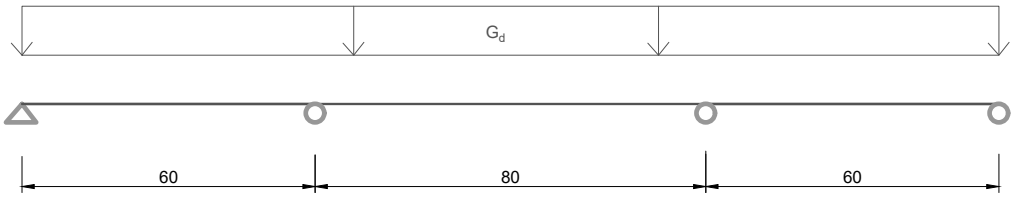

Figure 3.1: Geometry of the idealised bridge.

The analysis is performed in two different phases to capture the bridge behaviour during both construction and service life. This results in four modelling cases for the I- and box girder bridge, all of them illustrated in Figure 3.2 and Figure 3.3. The figures also clarifies the chosen form of cross-beams: a truss bracing, which has a centre-to-centre distance of 2 meters. Most of the bridge´s cross-section is kept constant during the analysis and the exact values chosen for the modelling are presented in Appendix A. It is only the horizontal radius of the bridge that will vary in the analysis, which is a radius that is constant for all three spans of the bridge.

During the construction phase, it is assumed that the whole steel structure has been erected and the concrete slab has been cast but not yet hardened. This assumption is made since the specification of construction method is outside the limits of the thesis. In this stage, the load of the concrete slab is added to the self-weight of the bridge, but no contribution to sectional properties are regarded since the concrete is not fully cured. However, the I- and box girder bridge still act as closed sections

due to the temporary top horizontal bracing. The temporary bracing is placed at the top of the flanges, as illustrated in Figures 3.2a and 3.3a, whereas the lower plan bracing for the I-girder bridge is located at the same level as the cross-beams.

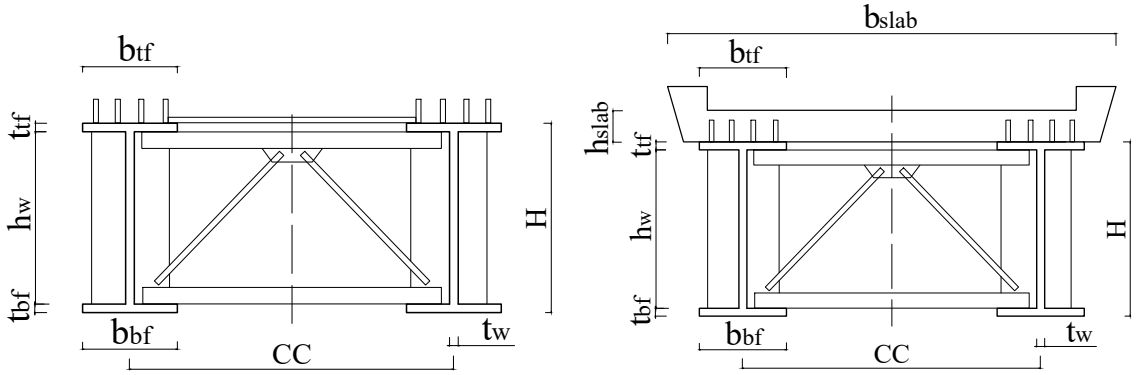

(a) During construction. **(b)** During service life.

Figure 3.2: Geometry of the I-girder bridge's cross-section.

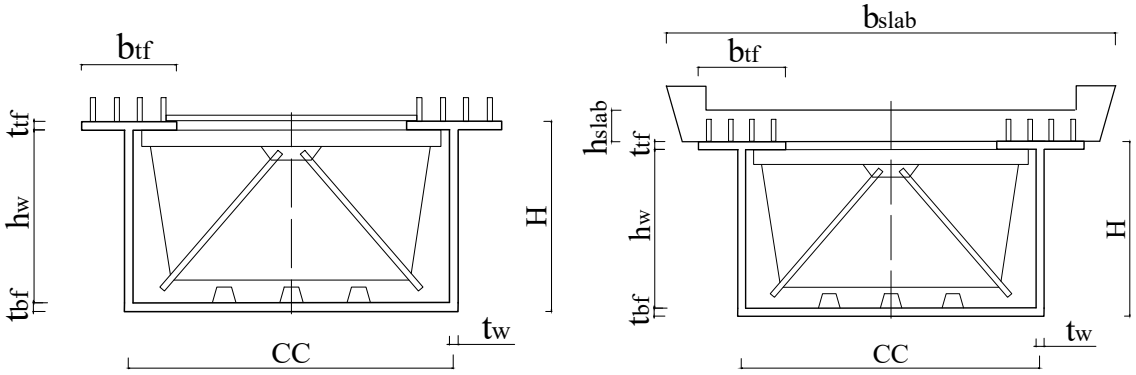

(a) During construction. **(b)** During service life.

Figure 3.3: Geometry of the box girder bridge's cross-section.

During the service life, the concrete is assumed fully cured and the composite action is active, which implies that the box and the I-section act as a closed section. The I-girder bridge can be considered closed as it is equipped with a lower horizontal bracing. As described in Table 3.1, only permanent loads are considered. Furthermore, it is assumed that the concrete slab is uncracked in every section of the bridge deck; this assumption is valid if the tensile stresses in the concrete do not exceed twice the value of f_{ctm} [1].

Table 3.1: Applied load for the idealised bridge.

Phase	**Load**
Construction	$G_{steel} + G_{c,uncured}$
Service life	$G_{steel} + G_{c,cured}$

Material properties of the steel and concrete used when modelling are summarised in Table 3.2. The long term response of the concrete during service life is regarded by applying an effective Young's modulus.

Table 3.2: Material properties for the idealised bridge.

Phase	**Material**	**Density** [kN/m^3]	**Young's modulus** [GPa]	**Poisson's ratio** [-]
Construction	Steel	78.5	210	0.3
	Concrete	26.0	-	-
Service life	Steel	78.5	210	0.3
	Concrete	25.0	13.3	0.2

The boundary conditions of the idealised bridge allow for movements caused by temperature changes and are presented in Figure 3.4. As the bridge is curved, temperature changes entail expansions in both the longitudinal and radial direction of the bridge [3], which is accounted for by these conditions. Rotations are considered free in all directions for every boundary node.

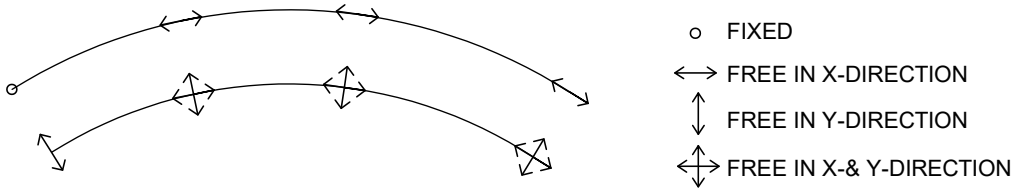

Figure 3.4: Boundary conditions of the idealised bridge.

In reality, the bearings will not posses an infinite stiffness, which is what is implied by these boundary conditions. The left-most boundary in Figure 3.4 is deemed too stiff and in order to avoid unwanted reaction forces, it is modelled with spring elements instead. The spring elements have a stiffness of 3.0 GN/m.

3.2 Finite element model

The idealised bridge described above is analysed with four different finite element models with varying degree of complexity. These models have been presented in Section 2.3.

3.2.1 Equivalent straight beam model

Two different FE-models have been set up for the equivalent straight beam model: one for the I-girder bridge and one for the box-girder bridge. The longitudinal elements consider a composite cross-section with the effective width of the slab set to the full tributary width. This assumption is accurate for bridges that are long and slender, for which the effect of shear lag is negligible [1]. The self-weight is distributed equally between the two main girders in the model of the I-girder bridge.

This assumption applies since a twin I-girder bridge is statically determinate in the transverse direction [18]. For the box girder bridge, all self-weight is instead applied to the main girder and the beam model captures the effect of curvature by an equivalent torque. The magnitude of this load depends on the bending moment, which implies that the modelling is performed in multiple steps for both cross-sections:

1. The analysis is performed on an equivalent straight bridge loaded by its self-weight, in order to get the distribution of bending moment.
2. This bending moment is in turn transformed to an equivalent torque and added to the model, as an anti-symmetric force couple for the I-girder bridge and as a torsion moment for the box girder bridge, see Figure 3.5a and 3.5b for the applied load in Brigade. Once the model is analysed a second time, the final distribution of bending moment is acquired.

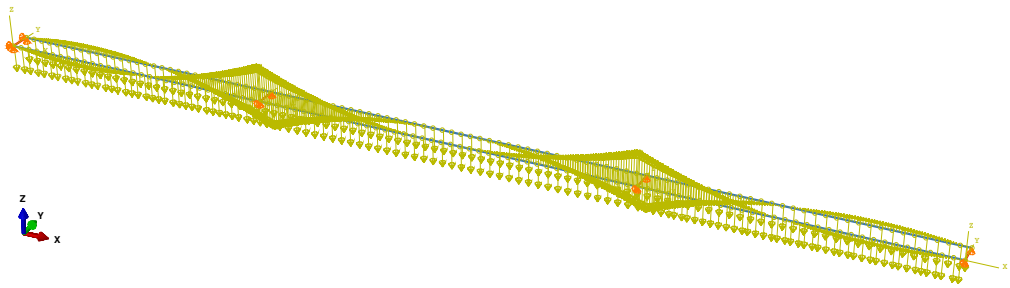

(a) Applied as an anti-symmetric force couple for the I-girder bridge.

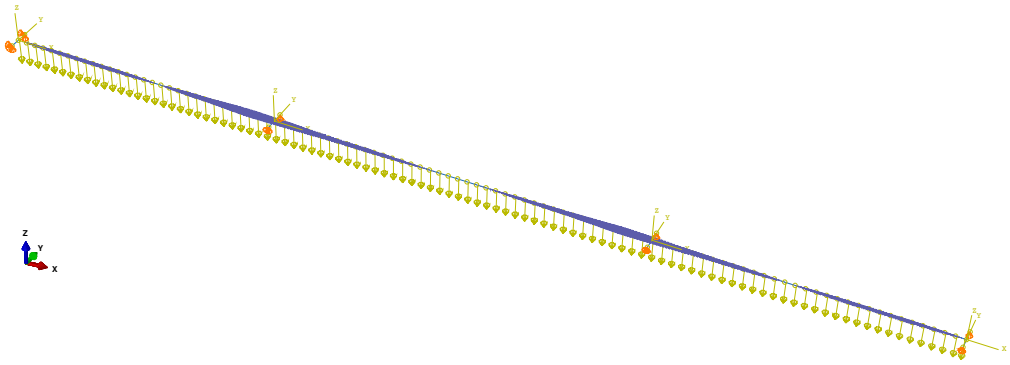

(b) Applied as a torsion moment for the box girder bridge.

Figure 3.5: Equivalent torque.

3.2.2 Grillage model

For the grillage model, the beams in the FE-model are straight elements placed in the same radius as the curved bridge. The curvature is more fully captured with smaller beam elements, and as spacing of the cross-bracing is small, one longitudinal beam element is placed between the cross-beams. As in the equivalent straight beam model, the longitudinal elements are modelled to capture the composite section, with the full tributary width of the concrete slab. Moreover, the self-weight is distributed

equally between the main girders for both the I- and the box girder bridge. The loading is illustrated in Figure 3.6.

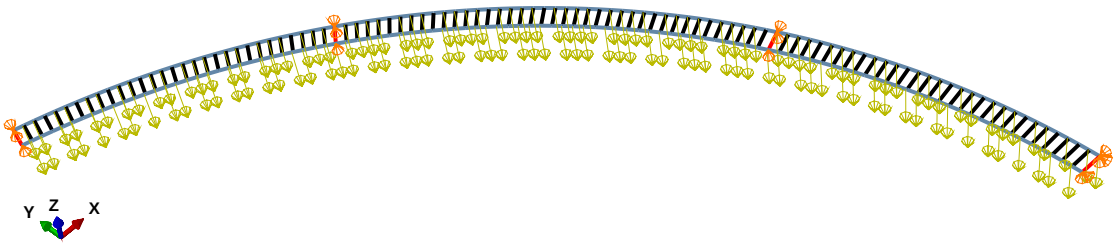

Figure 3.6: Grillage model with applied load.

3.2.3 Spatial beam model

The spatial beam model also consists of straight beam elements placed in a radius to reassemble the curvature, but with the addition of a central girder. As previously stated, the composite section is composed of the full width of the slab. This study emphasises only on the permanent vertical load, hence, the load is only applied along the axis of the MG-elements, distributed equally over the two elements, see Figure 3.7.

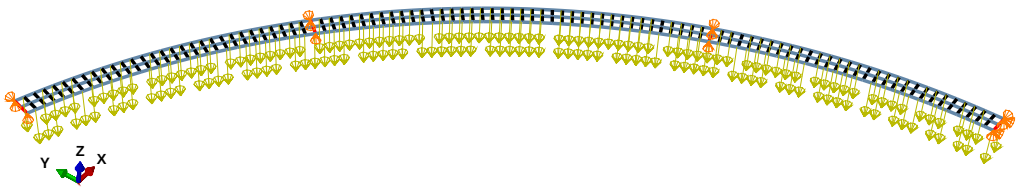

Figure 3.7: Spatial beam model with applied load.

3.2.4 3D shell model

The revised beam models are to be compared to a more complex shell model. Shell elements are chosen to represent the concrete slab and the steel web plate, as well as the bottom plate for the box girder bridge. The top flange, and the bottom flange for the I-girder bridge, are modelled as beam elements. This is a simplification of the geometry made to save modelling time, but implies an even distribution of stresses in the flanges according to Euler-Bernoulli beam theory. This assumption is deemed valid since the flanges are narrow. Furthermore, the cross-beams and the horizontal bracing are also modelled as beam elements. The shell models are illustrated in Figure 3.8 and 3.9.

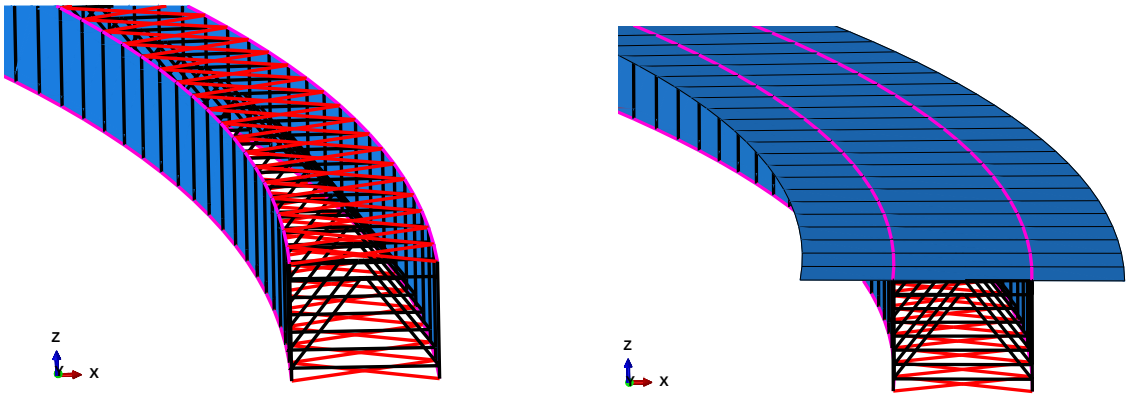

(a) During construction. **(b)** During service life.

Figure 3.8: Shell model for I-girder bridge.

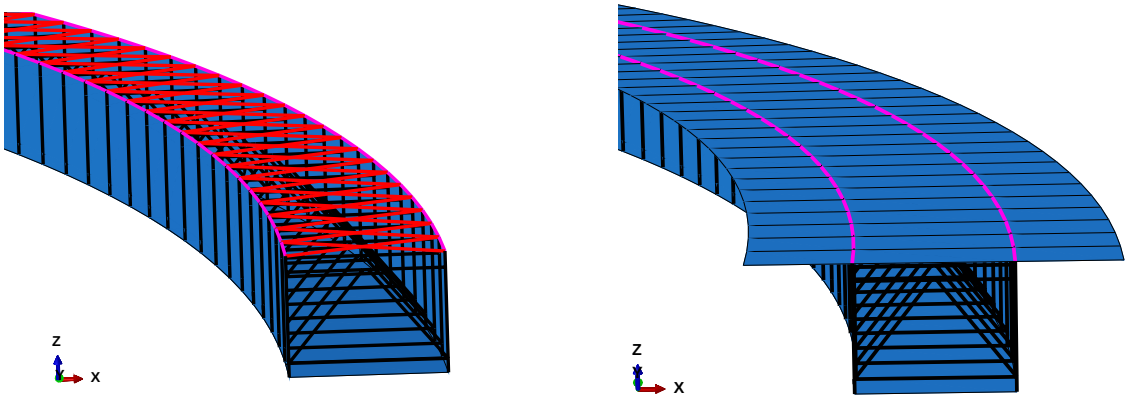

(a) During construction. **(b)** During service life.

Figure 3.9: Shell model for box girder bridge.

The elements in the shell model represent a specific part of the bridge, and are therefore assigned their geometry and material rather than the cross-sectional properties as in the revised beam models. The self-weight is applied as a gravity load, and the added weight of the unhardened concrete during construction is applied as a line load.

3.3 Results and discussion

Results obtained in the analysis of the idealised bridge are divided into a global study and an evaluation of the details. Firstly, the results are verified by considering the magnitude of the permanent load. The self-weight that is applied to the beam models should be equal to the gravity load of the shell model. This is verified by the total reaction force of each model, see Table 3.3. The difference compared to the shell model should be negligible, which it is deemed to be.

Table 3.3: Total vertical reaction force.

Section type	Phase	Shell model	Beam model	Difference
I-girder	Construction	21.74 MN	21.65 MN	0.4 %
	Service life	20.74 MN	20.88 MN	0.7 %
Box girder	Construction	20.29 MN	20.21 MN	0.4 %
	Service life	19.29 MN	19.43 MN	0.7 %

A convergence study is performed to verify the mesh of the shell model, see Table 3.4. The maximum displacement from the FE-model is determined for four different mesh types and the convergence error is calculated as the difference between two mesh refinements. This type of error is studied instead of the solution error, as it is difficult to find an analytical solution to curved continuous beams with varying span lengths. From the convergence study it is apparent that the mesh converges for a normal mesh type. However, the shell model will henceforth have a fine mesh, as the difference in computational time is trivial.

Table 3.4: Convergence study for shell model.

Mesh type	Element size [m]	Number of elements	Displacement [mm]	Convergence Error [%] [1)]
Very coarse	0.9	6 216	116.6	Unknown
Coarse	0.7	10 321	116.1	0.43 %
Normal	0.5	16 630	116.0	0.086 %
Fine	0.3	39 750	115.9	0.086 %

1) Convergence error: $|\frac{\text{Result(n)}-\text{Result(n-1)}}{\text{Result(n)}}|$ [15]

3.3.1 Global design

The results from the global analysis are presented as graphs of displacement for a bridge with a radius of 150 meters and 900 meters in Figure 3.11-3.14. To facilitate the comparability, the three beam models and the shell model are plotted in the same graphs. The values for the shell model have been retrieved along the lower flange at the inner and outer girder, see the paths in Figure 3.10. In addition to these results, an intermediate radius of 300 meters was also studied. However, as the results for this radius are consistent with that of 900 meters, they can be found in Appendix B instead.

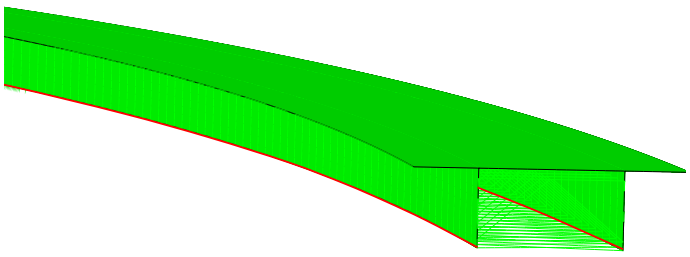

Figure 3.10: Paths for retrieving xy-data from shell model.

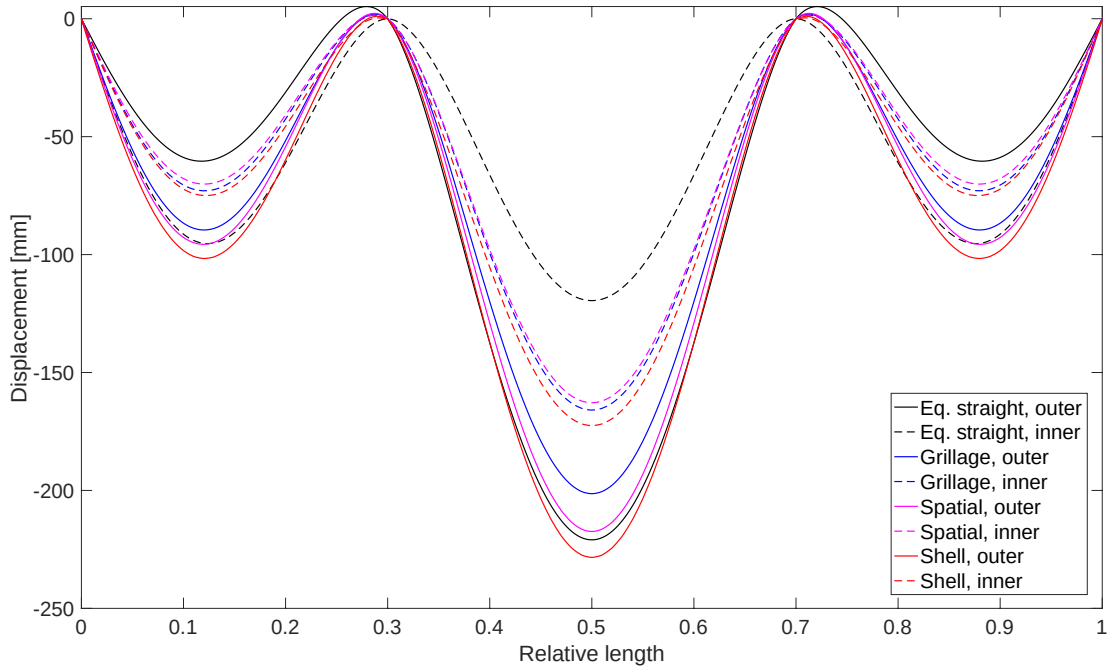

(a) Radius of 150 meter.

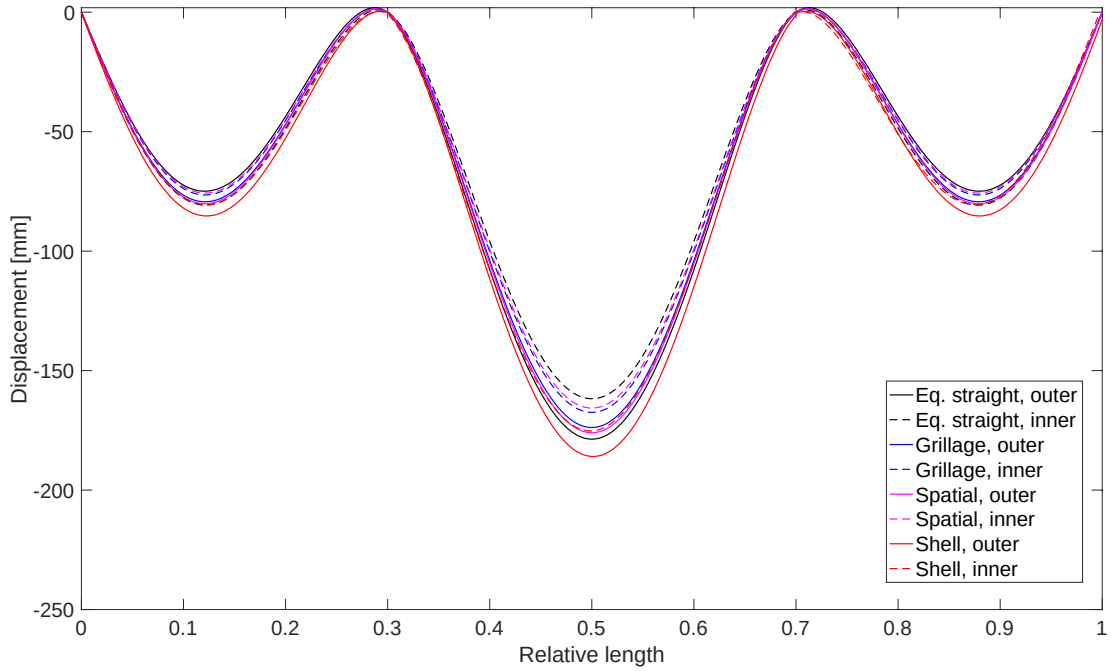

(b) Radius of 900 meter.

Figure 3.11: Displacement for I-girder bridge during construction.

Firstly, from Figure 3.11a and 3.11b it is clear that the displacement due to curvature increases as the radius decreases. In this case, the mid-span deflection changes from approximately 170 mm to 230 mm. Moreover, there is a visible spread between the results for the bridge with smaller curvature; a behaviour that is not apparent when the radius is increased to 900 meters.

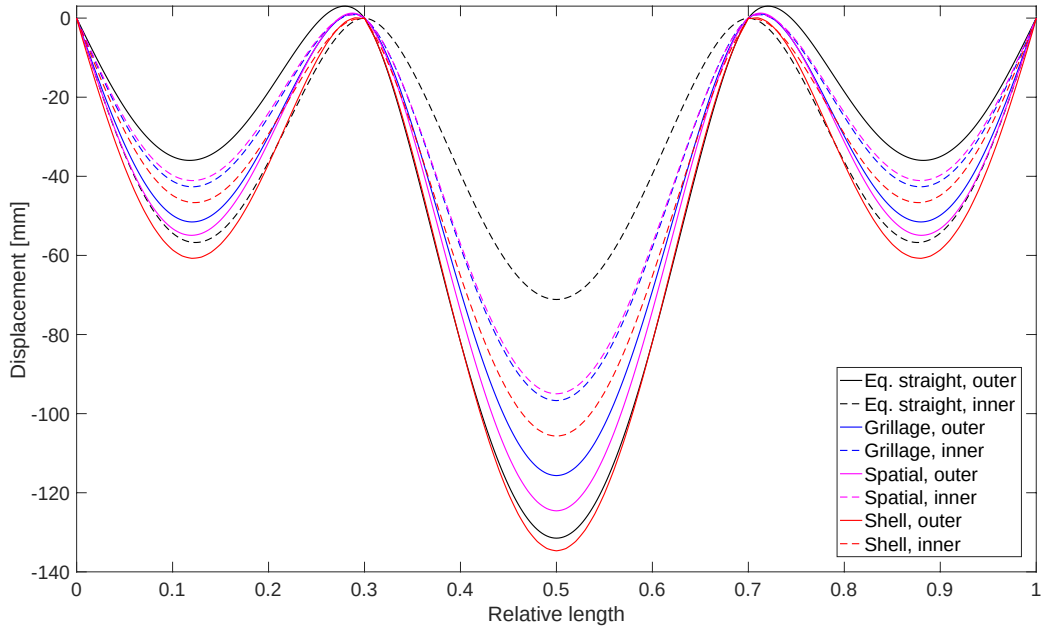

(a) Radius of 150 meter.

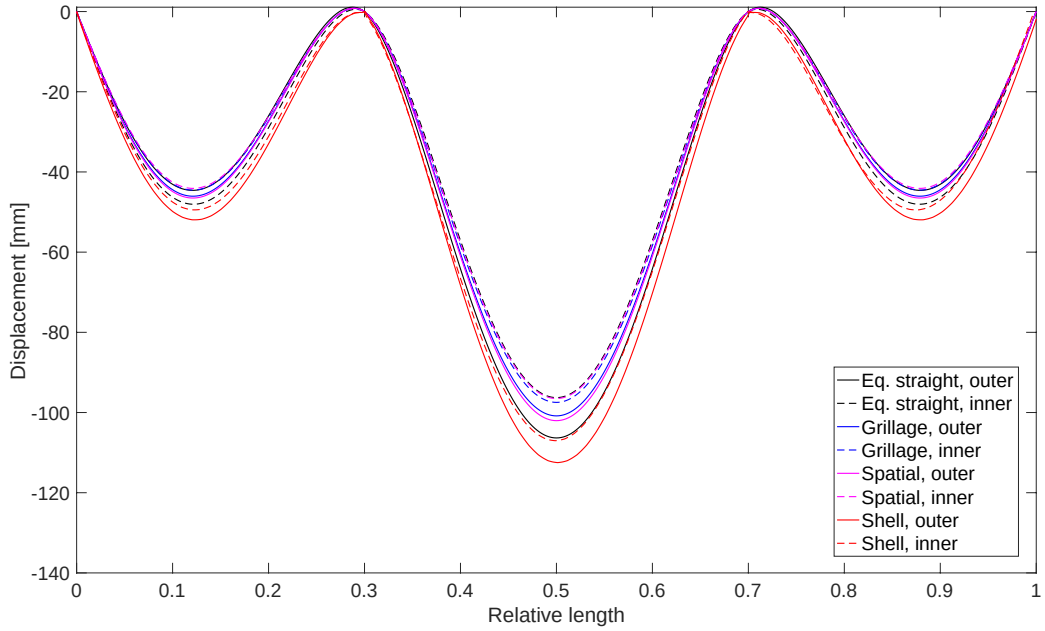

(b) Radius of 900 meter.

Figure 3.12: Displacement for I-girder bridge during service life.

During service life, a similar result spread as for the construction phase was detected for the I-girder bridge with a radius of 150 meters, seen Figure 3.12a. Above all, the equivalent straight beam model has difficulties capturing the individual behaviour of the inner and outer girder for smaller radii. The model underestimates the mid-span displacement for the inner girder, resulting in an overestimation of the end-span displacement. However, the opposite behaviour is seen for the outer girder. On the other hand, the grillage and the spatial beam model capture this behaviour to a larger extend even for the smaller curvature, although with magnitude differences.

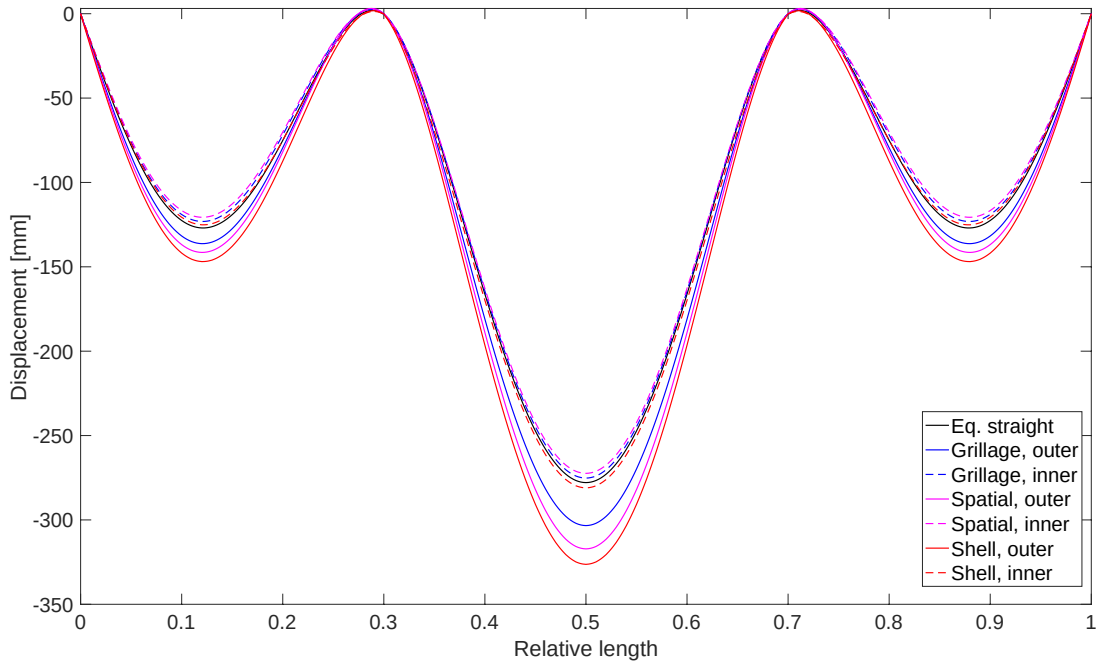

(a) Radius of 150 meter.

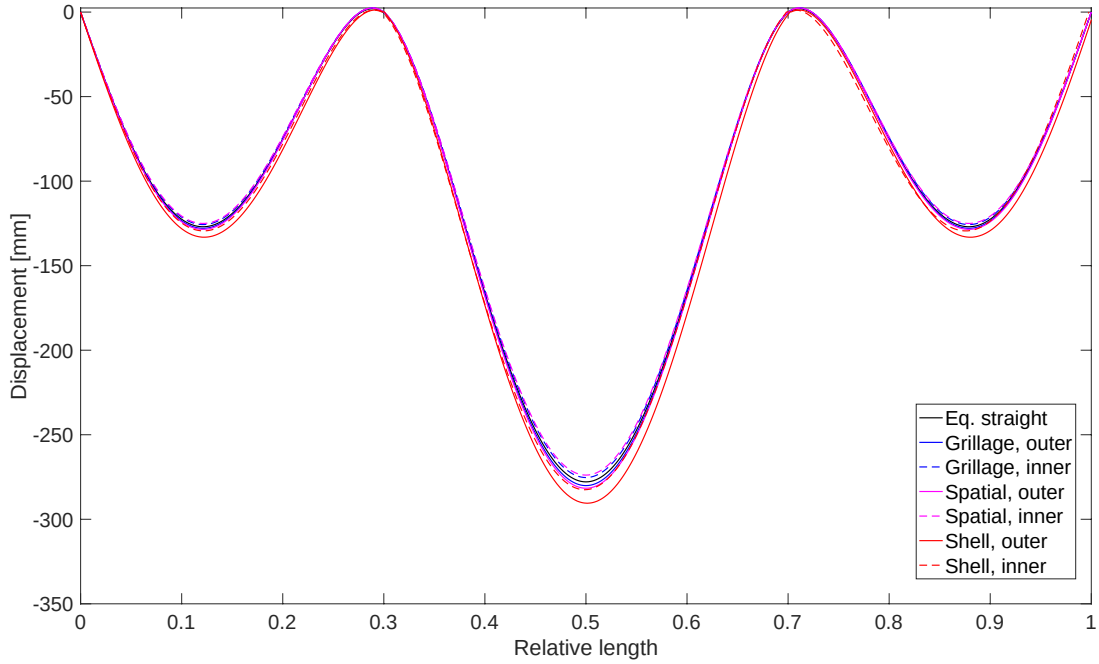

(b) Radius of 900 meter.

Figure 3.13: Displacement for box girder bridge during construction.

For the box girder bridge, the results are more uniform for smaller curvatures as seen in Figure 3.13a. It is also clear that the equivalent straight beam model does not capture the individual nature of the inner and outer web plates, as it is composed of one central beam element. When the radius is increased to 900 meters, the results of the beam models are inseparable and this can be observed in Figure 3.13b.

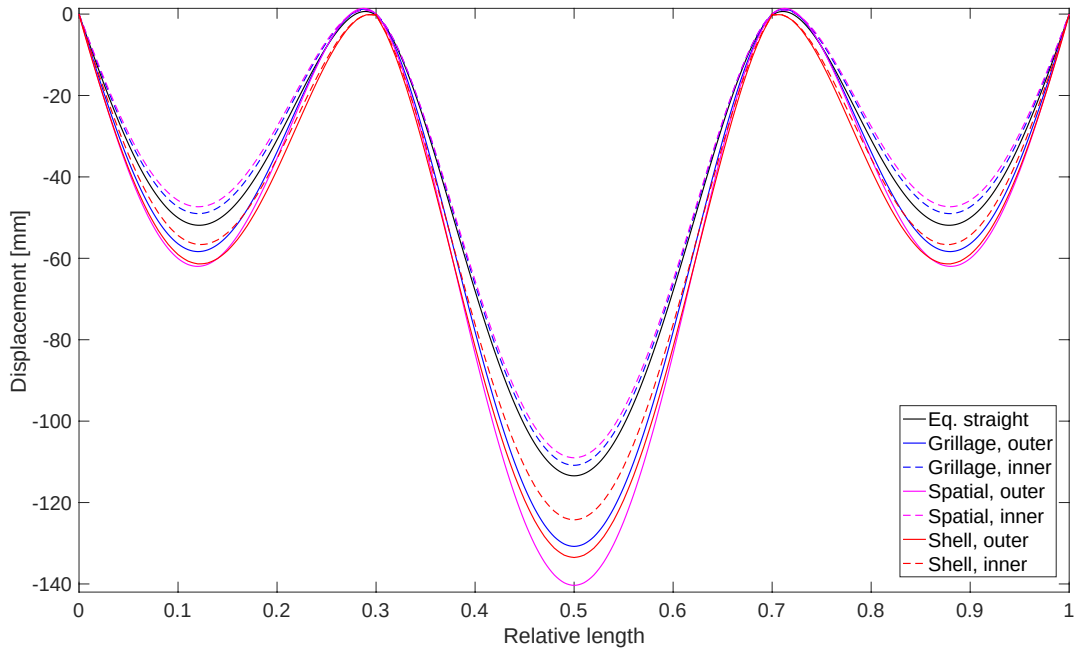

(a) Radius of 150 meter.

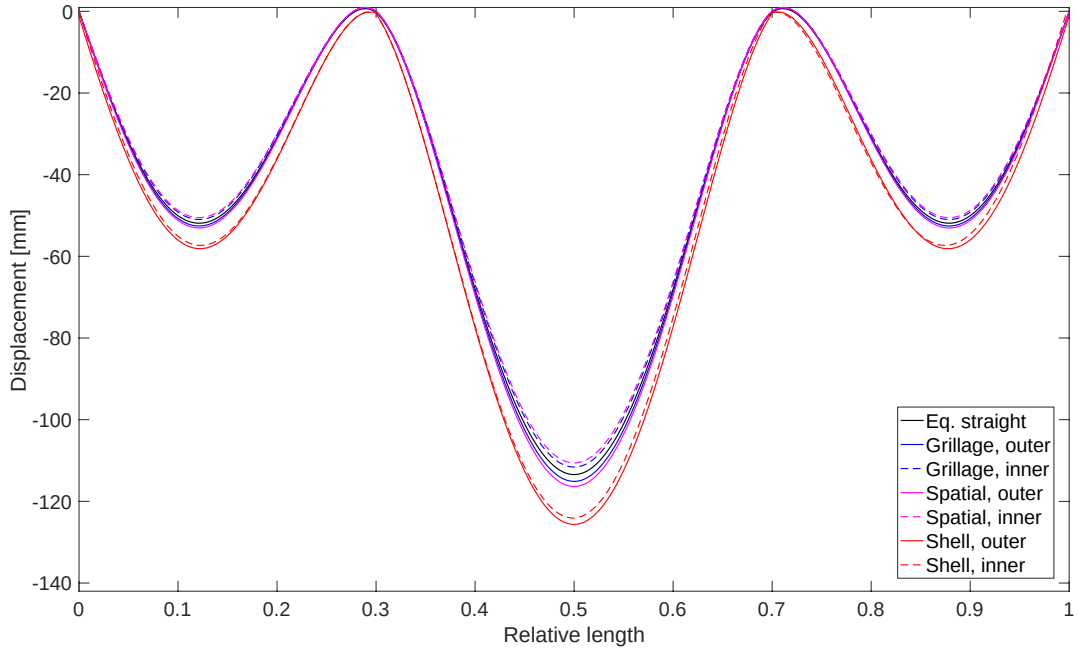

(b) Radius of 900 meter.

Figure 3.14: Displacement for box girder bridge during service life.

Figure 3.11 to 3.14 illustrate that the shell model, in general, demonstrates larger deformations than the three beam models do. This is expected since the shell model includes more parts and some of the distortional behaviours are not fully captured by the beam models. However, even though the magnitude differs, the main behaviour of both the outer and inner curve is at any rate captured for all beam models as the distribution is symmetrical with larger displacement in the mid-span than in the end-spans.

Furthermore, Table 3.5 to 3.6 exhibit how well the models conforms to the shell model. The difference considers the maximum field displacement, which is positioned in the mid-span of the outer girder. As previously mentioned, the equivalent straight beam model has difficulty capturing the difference between the inner and outer girder, thus the values in the tables can be misguiding for this model.

Table 3.5: Deviations from shell model[1)]: maximum field displacement for I-girder.

Beam model	**Radius of 150 meter**		**Radius of 900 meter**	
	Construction	Service life	Construction	Service life
Eq. straight	3.3 %	2.4 %	3.9 %	5.5 %
Grillage	11.8 %	14.1 %	6.5 %	10.4 %
Spatial	4.8 %	7.5 %	5.4 %	9.3 %

1) Deviations: $|\frac{\text{Shell model}-\text{Beam model}}{\text{Shell model}}|$

Table 3.6: Deviations from shell model: maximum field displacement for box girder.

Beam model	**Radius of 150 meter**		**Radius of 900 meter**	
	Construction	Service life	Construction	Service life
Eq. straight	14.8 %	15.0 %	4.3 %	9.7 %
Grillage	7.0 %	2.0 %	3.6 %	8.4 %
Spatial	2.8 %	5.1 %	3.0 %	7.4 %

From Table 3.5-3.6 it is clear that the deviations are larger for an I-girder bridge than a box girder, with the exception of the equivalent straight beam model. This is probably due to the difficulty of modelling the stiffness contributions from the lower plan bracing. For the beam models, the plan bracing is integrated as a torsional property, which is based on the assumption that it behaves as a steel plate. On the other hand, the shell model considers the plan bracing by an individual element and will therefore describe the component´s behaviour more accurately. It is worth noting that the stiffness of the plan bracing could be underestimated in the shell model, as it is modelled with beam elements. In reality, the bracing behaves more as bars and when substituting the beam elements with bar elements, a marginal difference is seen. Although the difference is small, it is something to keep in mind when considering the deviation in the tables.

As expected on beforehand, smaller radii are harder to capture for the beam models, since the effect of torsion, distortion and uneven loading is more distinct for highly curved bridges. Especially for the I-girder bridge, it is difficult to distinguish which model is most suitable for a radius of 150 meters, see Figure 3.11-3.12. In general, the spatial beam models have marginally smaller deviation than the grillage model for both bridge types, from 2.8 % to 9.3 % and from 2.0 % to 14.1 %. These results are consistent with the graphs in Figure 3.11 to 3.14, as both beam models follow the same behaviour as the shell model, but with the spatial beam model somewhat closer.

For both the I- and box section, the beam models show greater deviations during service life than during construction, see Table 3.5-3.6. The only difference between these phases is the concrete slab. Once the concrete slab is cured, it will influence the stiffness distribution of the structure and consequently the load distribution. Another possible explanation to the difference might be that the effect of shear lag has been neglected. However, this assumption holds according to Eurocode as the effective width is larger than the width of the slab [1].

Distributions of bending and shear stresses have also been studied. This result resemble the results that have already been presented in Figures 3.11 to 3.14 and therefore, the graphs are mainly found in Appendix C. However, one interesting point to allude is the fluctuating behaviour of the shell model that can be seen in Figure 3.15 and 3.16. This is a consequence of how the model is set up. In every node, stresses from both web and flange are registered, owing to the fact that the flanges are modelled as stringers attached to the web. It is, however, desirable to only show the stresses in the web and this should be avoided by analysing the axial forces acting on the web and not the stresses in these nodes. If the axial forces are retrieved instead, they would have to be divided by cross-sectional properties to get the stress distribution, and that would counteract the purpose of the shell model.

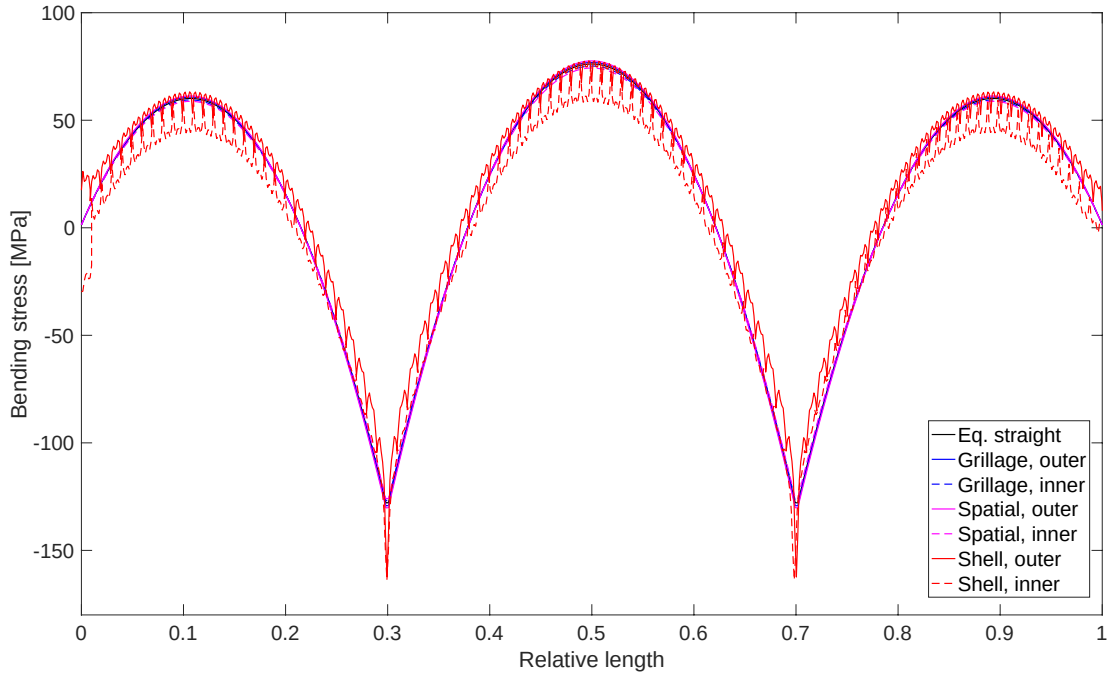

Figure 3.15: Bending stresses for the box girder bridge during service life and with a radius of 900 meters. Note the fluctuating behaviour of the shell model.

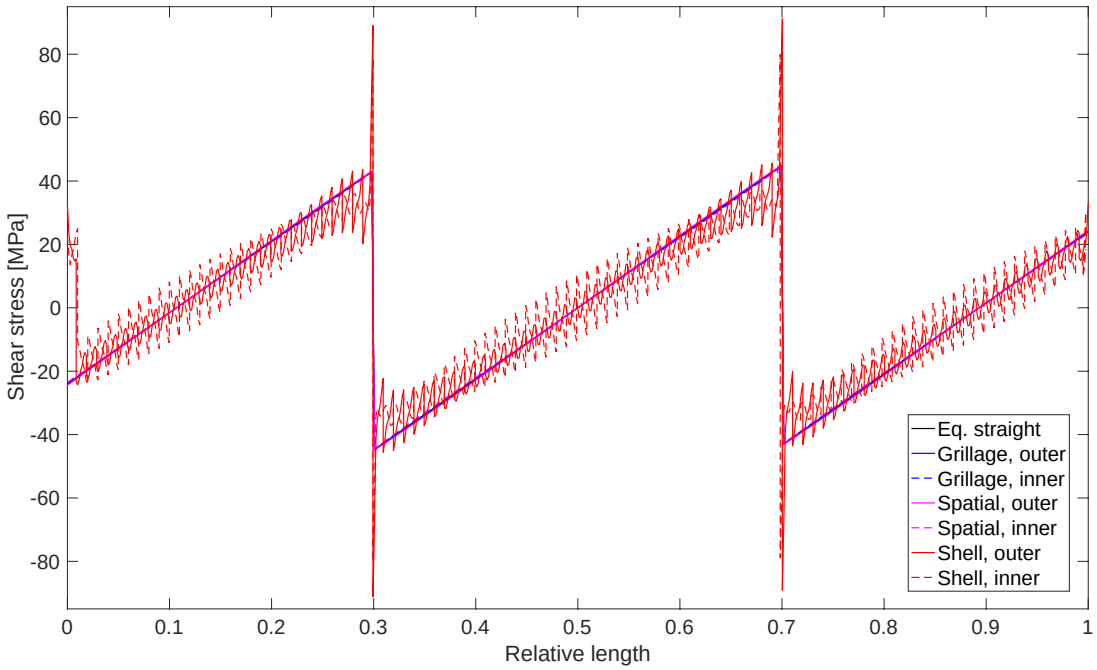

Figure 3.16: Shear stresses for the box girder bridge during service life and with a radius of 900 meters. Note the fluctuating behaviour of the shell model.

3.3.2 Details

The FE-models should also consider the design of details, which includes the cross-beams and, for the I-girder bridge, the plan bracing. The forces in these elements can be seen directly in the shell models, whereas a separate analysis has to be performed in order to determine the forces in the details from the beam models. Firstly, results for comparing forces in the most stressed cross-beam, namely at mid-span support, are presented. Figure 3.17 and Figure 3.18 illustrates these forces as evaluated in the shell model. The result is only retrieved for a bridge with a radius of 900 m during service life, since this is deemed sufficient to see how well the beam models capture the forces in details.

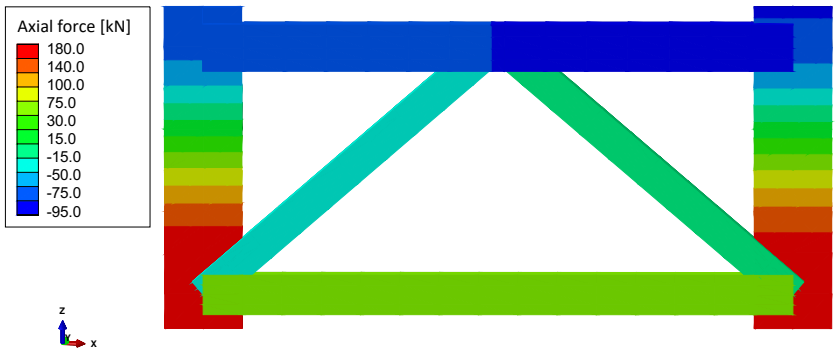

Figure 3.17: Axial force in cross-bracing from the shell model of the I-girder bridge.

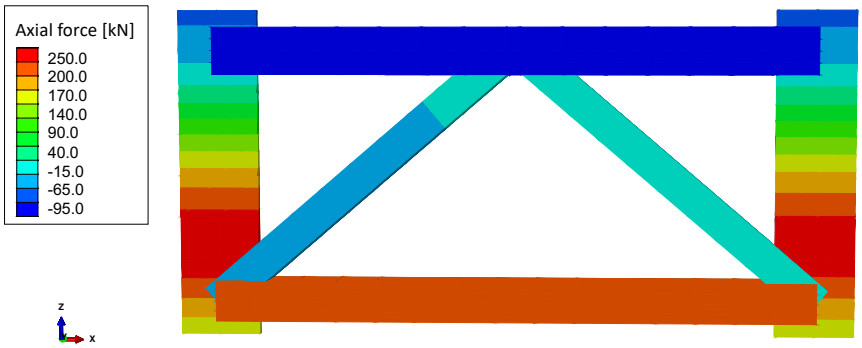

Figure 3.18: Axial force in cross-bracing from the shell model of the box girder bridge.

The local FE-analysis of the cross-bracing is performed using the *CALFEM* application to MatLab, where the bracing is modelled as a truss, see Figure 3.19. In this model, the effect of the curvature is captured by the distortional loads, H and V, which magnitude depends on to the bending moment. From the global result of the beam models, which was presented in Section 3.3.1, this bending moment is retrieved and used as input to Equation 3.1 and 3.2 [9], see Appendix D for the complete calculation. Table 3.7 presents the deviations between the internal forces from the local truss model to the ones obtained in the shell model.

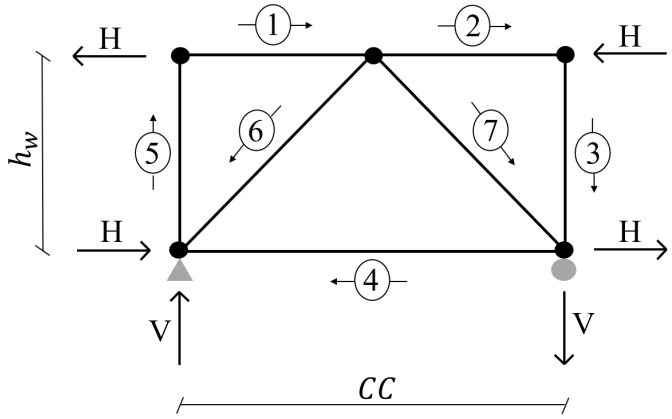

Figure 3.19: Truss model of cross-bracing [6].

$$V = \frac{C}{2 \cdot CC}\left(\frac{M_{Ed}}{R}\right) \text{ [N]} \tag{3.1}$$

$$H = \frac{C}{4 \cdot h_w}\left(\frac{M_{Ed}}{R}\right) \text{ [N]} \tag{3.2}$$

where M_{Ed} – Bending moment at support [Nm], h_w – Height of web[m],
R – Radius of curvature [m], CC – Distance between webs [m],
C – Distance between cross-bracing [m]

Table 3.7: Deviations from shell model: maximum axial forces in the diagonals, upper and lower chords of the cross-bracing.

Section type	Model	Diagonals	Upper chord	Lower chord
I-girder	Eq. straight	13.5 %	19.1 %	40.8 %
	Grillage	15.4 %	20.9 %	42.1 %
	Spatial beam	15.4 %	20.9 %	42.1 %
Box girder	Eq. straight	2.1 %	40.7 %	-
	Grillage	1.9 %	40.6 %	-
	Spatial beam	1.8 %	40.6 %	-

From Table 3.7 it is apparent that none of the beam models capture the forces in the cross-beams entirely. The closest match is for the diagonals of the box girder bridge, where all of the models have a deviation of 1.8 % to 2.1 % from the shell model. Overall, it can be said that all of the three beam models seem to follow the same coherent pattern for deviations from the shell model. Possibly, the equivalent straight beam model shows a closer behaviour to the shell model for the I-girder, but at the same time, the opposite is true for the box.

Furthermore, the I-girder bridge is equipped with a lower plan bracing in an X-shape. The forces in the bracing from the shell model are illustrated in Figure 3.20. The bracing that has the highest stresses is found at the position where the bending moment is equal to zero at the mid-span, as indicated in Figure 3.21.

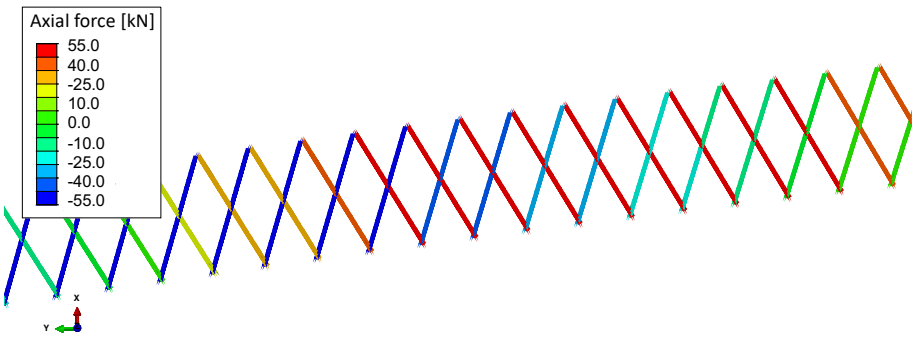

Figure 3.20: Axial force in lower plan bracing from the shell model.

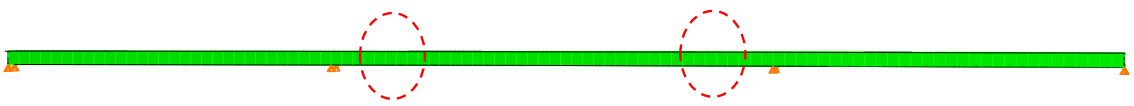

Figure 3.21: Position of the highest stressed lower plan bracing.

The torsion moment from the beam models can be transformed to axial forces in the diagonals of the plan bracing using Equation 3.3 [6]. The resulting maximum force in the diagonals of the plan bracing is found in Table 3.8.

$$F_{diagonal} = \frac{M_T}{2 \cdot CC \cdot h_w} \cdot \frac{d}{2} \text{ [N]} \tag{3.3}$$

where M_T – Torsion moment in cross-section [Nm], h_w – Height of web[m]
d – Length of diagonal truss [m], CC – distance between webs [m]

Table 3.8: Forces in lower plan bracing.

Model	**Maximum force** [kN]
Grillage	58.3 kN
Spatial beam	50.5 kN
Shell	55.2 kN

From Table 3.8 it is apparent that both the spatial beam and grillage model captures the forces in the lower bracing. This implies that the added central girder have little effect when it comes to capturing the magnitude of the forces on a local level, however, as seen in the previous chapter it does have an effect on a global level.

4

Case study

The second objective of the thesis has been formulated as follows: When is it advantageous or disadvantageous to use an I- or a box girder system for a curved composite bridge? This question will be investigated in the second study, which is based on a case study. One major difference between the first and second study is that variable loads will now be considered. Up until now, they have been excluded for the benefit of distinguishing the effects of the curvature from effects coming from other loads. Furthermore, the case study will solely focus on the service life of the bridge. Based on the outcome of the idealised bridge study, which was put forward in the discussion in Section 3.3, the spatial beam model will be used to perform this second part of the work.

4.1 Bridge description

Solvalla Bridge is the subject for the case study and it is located in Stockholm, Sweden. It has been designed by ELU Konsult AB and is at the time of writing under construction [20]. The bridge has a total length of approximately 700 meters divided into different segments of both concrete and composite bridges, with the composite segment of interest in this thesis. The study emphasises on the conceptual design phase and Figure 4.1 illustrates the geometry of the bridge. It consists of continuous girder(s) in three spans, where the cross-sectional dimensions varies for the end-, field- and support-section, see Figure 4.2 for their respective geometrical values.

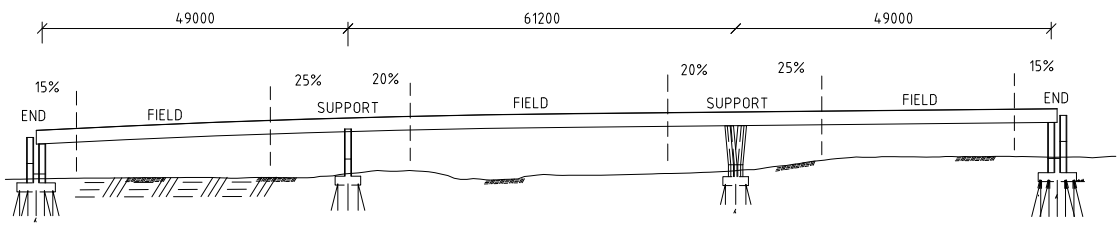

Figure 4.1: Geometry of Solvalla Bridge.

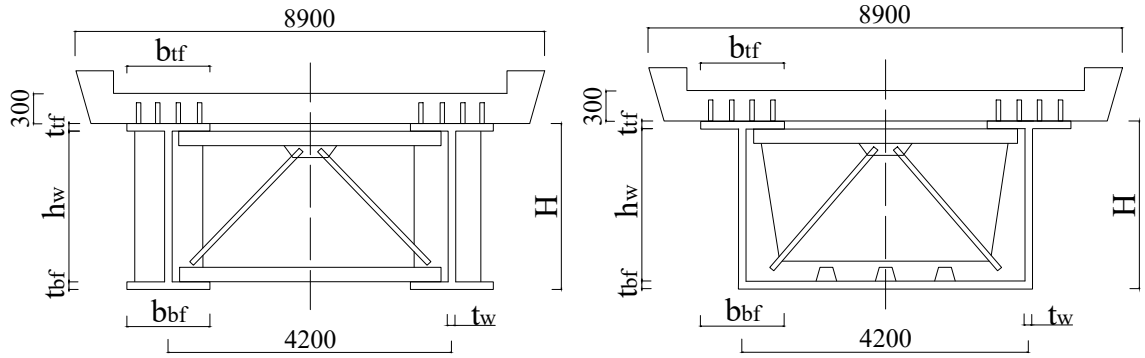

(a) I-girder bridge. **(b)** Box girder bridge.

Figure 4.2: Cross-section of Solvalla bridge.

As indicated in Figure 4.2, fixed geometries for the cross-sections include the area of the concrete slab and the centre-to-centre distance between webs. The distance between the webs is chosen so that the tracks are centred above the webs, in order to avoid any eccentricities in the overhang of the deck. Furthermore, the spacing of the cross-beams is set to approximately seven meters for the box girder bridge and five meters for the I-girder bridge. The cross-beams are consistent for all sections of the bridge and are assumed sufficiently stiff to transfer the torque to the main girders. The dimensions of the cross-bracing, as well as the geometry of the plan bracing for the I-girder bridge, can be found in Appendix E.

The bridge is made with steel quality S355 and concrete C35/45, which material properties are given in Table 4.1. For the boundary conditions, the ones applicable for the idealised bridge is assumed for the case study as well, see Figure 3.4.

Table 4.1: Material properties for the Solvalla Bridge.

Material	**Density** [kN/m^3]	**Young's modulus** [GPa]	**Poisson's ratio** [-]
Steel	78.5	210.0	0.3
Concrete (short term)	25.0	34.0	0.2
Concrete (long term)	25.0	13.3	0.2

4.1.1 Loads

The loads applied on the Solvalla Bridge are listed in Table 4.2 and Figure 4.3 illustrates how they act on the structure. The bridge is in reality used by tram traffic, however, in this thesis it is assumed to be loaded by railway traffic in order to generalise the bridge description. The railroad traffic is defined according to Eurocodes traffic model LM71 and the horizontal loads are the common ones associated with rail road action: centrifugal, nosing, traction and breaking force [21]. Wind load is also considered according to Eurocode [22]. Temperature and accidental loads, however, are excluded from the analysis with the motivation that only loads that

significantly influence the design of the bridge should be considered. The most conservative application of the horizontal forces is assumed to be when they act in the same direction as the centrifugal force i.e. outwardly.

Table 4.2: Loads that act on Solvalla Bridge.

Load		Description
Permanent	G_s [N/m]	Weight of the steel work
	G_c [N/m]	Weight of the slab
	G_{rail} [N/m]	Weight of the rails
	$G_{railing}$ [N/m]	Weight of the railing
	G_{cable} [N/m]	Weight of the cables
Variable	Q_{vk} [N]	Rail traffic load
	q_{vk} [N/m]	Rail traffic load
	Q_{lk} [N/m]	Traction and breaking force
	Q_{sk} [N]	Nosing force
	Q_{tk} [N/m]	Centrifugal force
	Q_w [N/m]	Wind load

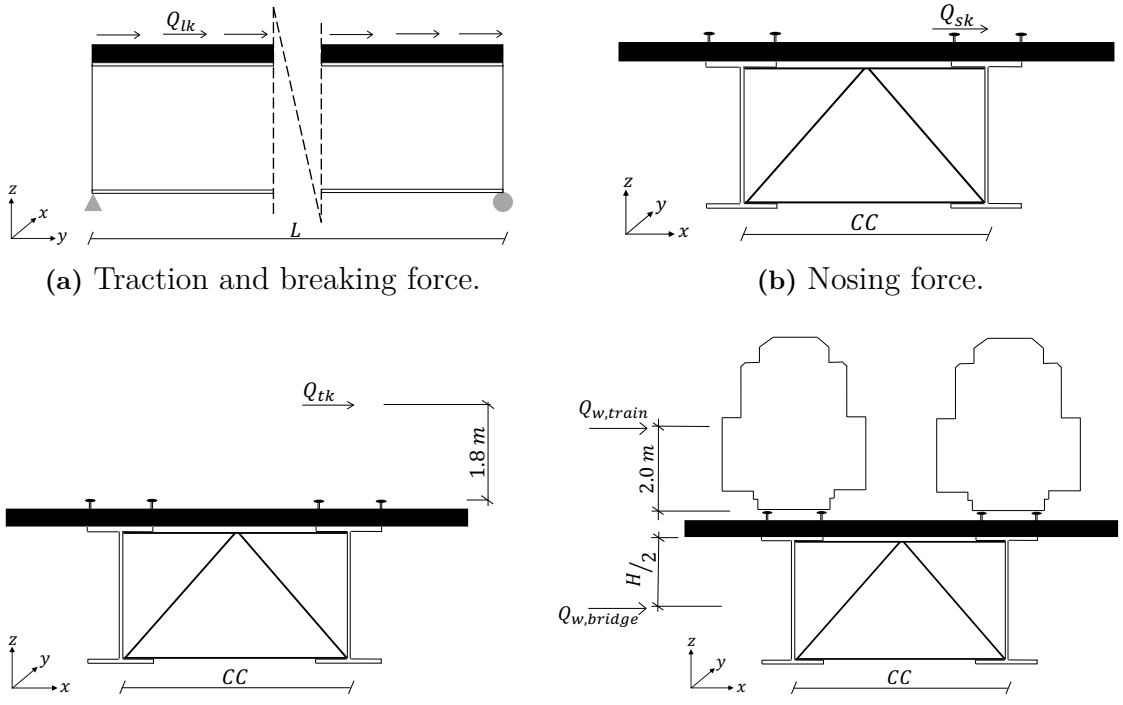

(a) Traction and breaking force.

(b) Nosing force.

(c) Centrifugal force.

(d) Wind load.

Figure 4.3: Illustration of how the forces act on Solvalla Bridge.

The variable loads illustrated in Figure 4.3 act with some eccentricity to the bridge deck, which, with the exception of the traction force, induces torsion in the structure. All the horizontal forces and the torsional moments are applied along the fictitious

central girder that in the spatial beam model handles torsion, whereas the vertical loads such as traffic and self-weight are divided equally between the two main girders.

Concerning the vertical loading, the worst position of the traffic load can be determined in Brigade by running a traffic simulation. However, this simulation is time consuming and thus, not desirable for this analysis. The traffic load is therefore applied in two configurations: one for the worst case scenario with regard to bending moment and to displacement, and one for the worst case scenario with regard to shear force, see illustrations in Figure 4.4. For the bending moment, this occurs when the train is placed solely at the outer curve, with the point loads placed in mid span, whereas for the displacement, the train is placed at both tracks. For the shear force, however, the worst case is instead when a train is placed at both the outer and the inner curve, and the point loads are placed above the second support.

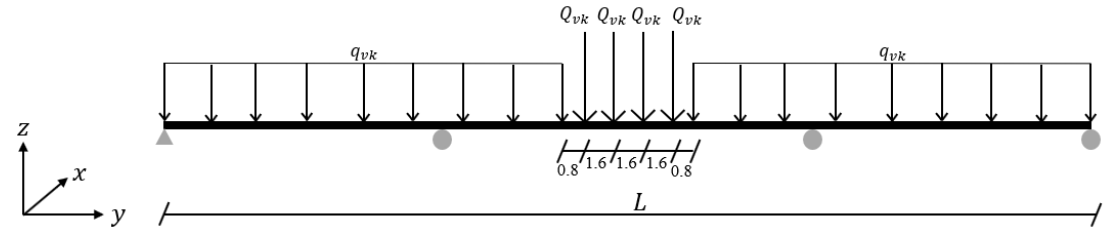

(a) Worst case with regard to bending moment and to displacement.

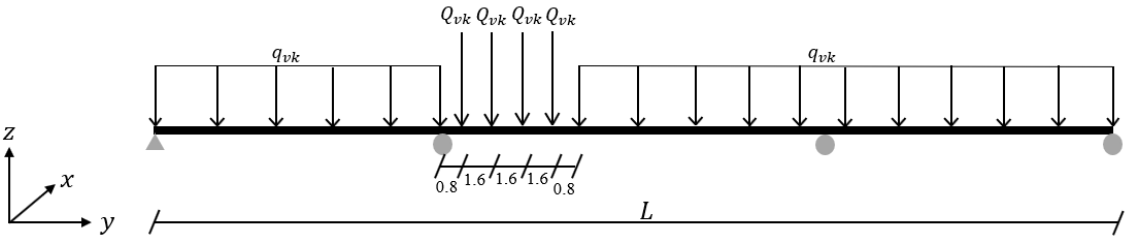

(b) Worst case with regard to shear force.

Figure 4.4: Traffic load model LM71 for the dimensioning cases.

4.1.2 Load combinations

The loads listed in Table 4.2 are combined according to Equation 4.1-4.3 and are thereafter utilised when ensuring the requirements listed in Section 4.1.3. The loads are combined for a strength control in ultimate limit state, which is governed by equation 6.10a and 6.10b in Eurocode Annex A2 [23]. In this annex it is also specified that the verification of displacements should solely consider the traffic load for railway bridges. For composite bridges, the load combination for fatigue is governed by Eurocode 2 [24], where the fatigue load includes rail traffic according to traffic model LM71 and the centrifugal force [21].

$$\text{Strength} : \begin{cases} 6.10\text{ a}) \sum_{i=1} 1.35 \cdot G_{k,i} + \sum_{i=1} 1.5 \cdot \psi_{0,i} \cdot Q_{k,i} \\ 6.10\text{ b}) \sum_{i=1} 1.202 \cdot G_{k,i} + 1.5 \cdot Q_{k,1} + \sum_{i=1} 1.5 \cdot \psi_{0,i} \cdot Q_{k,i} \end{cases} \tag{4.1}$$

$$\text{Displacement} : 1.0 \cdot Q_{vk} \tag{4.2}$$

$$\text{Fatigue} : \sum_{i=1} G_{k,i} + \psi_{1,1} \cdot Q_{k,1} + \sum_{i=1} \psi_{2,i} \cdot Q_{k,i} + Q_{fat} \tag{4.3}$$

Table 4.3: ψ-factor for load combination [23].

Load action	ψ_0	ψ_1	ψ_2
Rail traffic load	0.8	0.7	0
Traction and breaking force	0.8	0.7	0
Nosing force	1.0	0.8	0
Centrifugal force	0.8	0.7	0
Wind load [1)]	1.0	0	0

1) ψ-factors for wind load acting simultaneously as traffic load.

4.1.3 Requirements

When designing a composite bridge, its performance has to satisfy requirements governed by Eurocode and stated in the national annex *TRVINFRA-00227: Bro och broliknande konstruktion* [25]. The following requirements are relevant for the case study of Solvalla Bridge:

- Total vertical displacement should be limited to $\delta \leq \frac{L}{600}$ for railway bridges considering solely the characteristic value of the traffic load [23].
- Normal stresses, including the influence of warping, should be limited by the capacity: $\frac{N_{Ed}}{A} + \frac{M_{Ed}}{I} \leq \sigma_{Rd}$. [26]
- Shear stresses, including the influence of warping and torsion, should be limited by the capacity: $\frac{\tau_{Ed}}{\tau_{Rd}} \leq 1$. [26]
- Interaction of normal stress and shear stress should also be verified against capacities [26].
- Lastly, fatigue stresses should be verified for the design situation of 100 years [27]: $\frac{\Delta\sigma_E \cdot \gamma_{Ff}}{\Delta\sigma_R / \gamma_{Mf}} \leq 1$, where $\Delta\sigma_E = \lambda \cdot \Phi \cdot \Delta\sigma_{Ed}$ is the difference in normal stress during one cycle of loading [28].

It is assumed that lateral torsional buckling is prevented through bracing of the elements during construction, and therefore, no particular requirement concerning that is applicable. Furthermore, for an elastic analysis, the capacity, σ_{Rd}, is set to the yielding strength. Determination of the normal stress is made according to Navier's formula, which is consistent for I- and box girder bridges. However, for the load effect of shear stress, different methods are applicable for the two cross-section types due to the way torsion is introduced to the bridge. For the I-girder bridge, warping is seen as a part of the shear forces, whereas for the box girder bridge,

torsion will appear as a shear flow. This shear flow is transformed to a shear force according to Equation 4.4 [29].

$$V_{MT.Ed} = \frac{M_{T.Ed}}{2 \cdot A_0} \cdot l \text{ [N]} \tag{4.4}$$

where $M_{T.Ed}$ – Torsion moment in cross-section [Nm], l – Length of segment [m]
A_0 – Enclosed area between webs [m^2]

The shear flow will increase the shear force of the outer web plate, but decrease it of the inner web plate, as illustrated in Figure 4.5. It will also be apparent at the bottom plate of the box girder and in the slab, however, due to the moderate thickness of the slab, no verification of its shear strength is made.

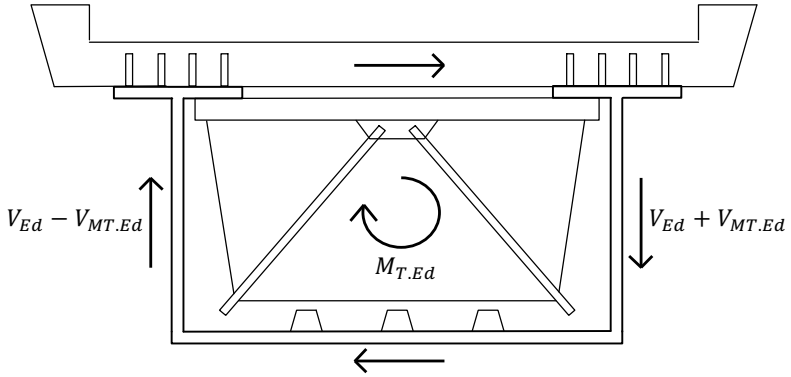

Figure 4.5: Shear force due to torsion.

Regarding fatigue verification, the detail category of 80 MPa, marked as 1) in Figure 2.6 in Section 2.2.2, is assumed applicable for the entire bridge. It is deemed to be the worst loaded one and will thereby govern the design. The detail category of the gusset plate, marked as 3) in 2.6, is assumed to have smooth edges, which implies a detail category of 90 MPa. Moreover, the but welds which connects the girders to one another are assumed to be positioned where the normal stresses are low. Therefore, no fatigue control of these details is performed.

4.2 Optimisation

To answer the objective in question and distinguish when an I- or a box section is more advantageous, the volume of the steel work is used as comparative parameter. The volume considered has to be optimised with regard to performance requirements listed in the previous Section 4.1.3. The optimisation is performed with the MatLab application *Global Optimisation toolbox*, which has a genetic algorithm as a built-in function handle. The genetic algorithm will test the performance of some predefined parameters against an objective function and choose the most optimal combination based on natural selection. How well the algorithm will perform depends on the settings, which have mostly been chosen according to the default values set in MatLab,

see Table 4.4. The optimisation is performed with a large amount of variables and therefore a low value has been chosen for the population size to limit the maximum number of iterations.

Table 4.4: Settings for the genetic algorithm.

Setting	Value
Generation	100 · Number of variables
Population size	50
Number of iterations	Population · Generation
Time limit	20 000 s
Tolerance	$1 \cdot 10^{-5}$
Elite count	0.05 · Population size

The optimisation will be performed for varying radii of the bridge for the purpose of distinguishing if a cross-section is more or less optimal for smaller curvatures. In Figure 4.6, the procedure of the analysis is illustrated.

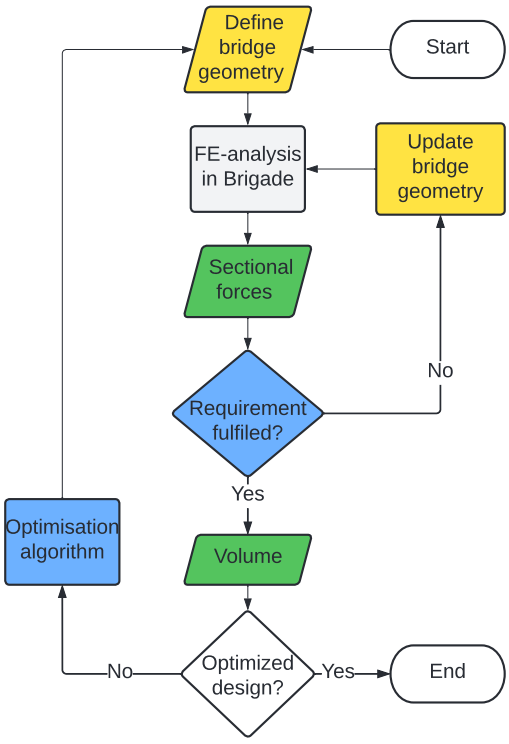

Figure 4.6: Flowchart over the analysis of the case study. Color code: Inputs, Outputs, Calculations

In order to carry through with the purpose of the case study, the cross-sectional dimensions of the bridge will be altered to optimise the volume of the steel work. The cross-sectional parameters that were presented in Figure 4.2 in Section 4.1 are defined as discrete variables and may vary according to specific values given in Table 4.5 and 4.6 below. The choice of lower and upper limit is based on the theory presented in Table 2.1 of typical geometrical values for I- and box girder bridges, see

Section 2.1.1. The variables are limited to four values per investigated radii, due to the computational effort of performing this optimisation. All combinations of the flanges are in cross-section class 4, since an elastic analysis is performed.

Table 4.5: Varying geometrical parameters in [mm] for the I-girder bridge.

Variable	Cross-section	Lower limit	Upper limit	Increment
H	End	2300	3000	100
	Field			
	Support			
b_{tf}	End	350	500	50
	Field			
	Support	450	600	50
t_{tf}	End	25	40	5
	Field			
	Support	30	60	10
t_w	End	14	20	2
	Field	12	18	2
	Support	16	22	2
b_{bf}	End	600	900	100
	Field			
	Support	600	1200	100
t_{bf}	End	40	55	5
	Field			
	Support	45	60	5

Table 4.6: Varying geometrical parameters in [mm] for the box girder bridge.

Variable	Cross-section	Lower limit	Upper limit	Increment
H	End	2200	2700	100
	Field			
	Support			
b_{tf}	End	250	400	50
	Field			
	Support	300	450	50
t_{tf}	End	20	32	4
	Field			
	Support	28	40	4
t_w	End	14	20	2
	Field	12	18	2
	Support	18	24	2
t_{bf}	End	10	25	5
	Field			
	Support	15	30	5

The result will be determined by running two different optimisations: one with regard to stresses and one with regard to displacement. This division is made to save computational time. In the first optimisation, the sectional forces are computed only for the first configuration of parameters listed in Table 4.5-4.6 and thereafter the optimisation is performed based on these results. As there are a total of 13 parameters for the box girder bridge and 16 for the I-girder bridge, the optimisation will be performed in 65 000-80 000 iterations. After the first optimisation is complete, the sectional forces are computed for the optimised combination of parameters and the utilisation ratios are determined.

In the second optimisation, the FE-analysis is performed for each iteration in order to updated the sectional forces and displacement for all combinations of parameters. The communication between MatLab and Brigade Plus is time consuming, which implies that a limited number of parameters can be altered. Therefore, solely the height of the cross-section, as well as, the width of the bottom flange for the I-girder bridge and the thickness of the bottom plate for the box girder bridge, are the parameters to be optimised. These have been chosen since they have the largest affect on the magnitude of the displacement.

4.3 Results and discussion

Firstly, the results are verified by considering the configurations of the rail traffic load. The assumed worst case with regard to moment, shear and displacement for one example is compared to a traffic simulation performed with Brigade Plus. This example is summarised in Table 4.7. It can be observed that the deviations for the bending moment and shear force is between six and eight percent, which is deemed negligible. However, the assumed configuration of the traffic load for the displacement is underestimated throughout the analysis. Even though this does not directly affect the comparability, it is something to keep in mind when assessing the results of the optimisation.

Table 4.7: Verification of the rail traffic load position.

Output	**Evaluated in Brigade**	**Assumed**	**Difference**
Bending moment	28.0 MNm	29.8 MNm	6.2 %
Shear force	3.6 MN	3.9 MN	7.7 %
Displacement	180 mm	150 mm	16.7 %

4.3.1 Global design

The result is presented in the form of tables and graphs, and one illustrative example of the complete calculation can be found in Appendix F. Table 4.8 displays the utilisation ratios for curved bridges of different radii after the first optimisation. Seeing that only requirements regarding stresses are considered in this first part, the utilisation rations for displacement generally exceeds 100% here. The same

applies for fatigue, due to that the sectional forces are not continuously evaluated throughout the first optimisation. Moreover, attention should be given to the fact that the I-girder bridge is evaluated both with, and without a lower plan bracing system throughout the case study. All cross-sectional parameters that were chosen after both the first and the second optimisation is found in Appendix F.

Table 4.8: Utilisation ratios for all studied radii from the first optimisation.

Section type	**Radius**	**Displacement**	**Fatigue**	**Moment**[1)]	**Shear**[1)]
I-girder with plan bracing	150 m	124.1 %	101.8 %	67.2 %	74.4 %
	300 m	115.1 %	105.1 %	69.3 %	81.7 %
	500 m	108.6 %	103.5 %	68.1 %	82.3 %
	700 m	115.3 %	108.3 %	71.0 %	86.1 %
	900 m	114.8 %	108.2 %	70.8 %	86.2 %
I-girder without plan bracing	150 m	128.8 %	103.7 %	68.9 %	67.9 %
	300 m	113.9 %	106.8 %	70.3 %	78.7 %
	500 m	113.1 %	107.8 %	70.8 %	82.5 %
	700 m	109.6 %	106.3 %	69.7 %	82.6 %
	900 m	107.9 %	105.5 %	69.2 %	82.6 %
Box girder	150 m	136.1 %	102.7 %	71.8 %	96.5 %
	300 m	114.7 %	99.6 %	67.7 %	90.2 %
	500 m	111.1 %	99.7 %	66.6 %	100.2 %
	700 m	109.6 %	99.9 %	66.1 %	98.2 %
	900 m	110.0 %	101.7 %	67.1 %	99.1 %

1) Considers the maximum utilisation ratio with regard to bending moment and shear.

All utilisation ratios are found in Appendix G.

All the more interesting is the results from the second optimisation that can be observed in Table 4.9, from which it becomes clear what the design criteria are. On this basis, the design of the I-girder bridge with a radius of 150 meters will be governed by the displacement, whereas when the radii increases, both the displacement and the fatigue will be design criteria, see examples in the table highlighted in green. Instead looking at the box section and the areas highlighted in yellow, the utilisation ratios for fatigue are not as high as for the I-girder bridge and this implies that the latter one is more susceptible to fatigue stresses. However, just as for the I-girder bridge, displacement is the governing design factor for the box.

In addition, it can be observed that the shear utilisation is very high for the box section, and in hindsight, the same would be apparent for the I-girder bridge if a different choice of parameters had been made for the second optimisation, see values highlighted in blue. The parameters that would be the most influential for the I-girder bridge are the height and width of the webs, as shear buckling should have been controlled for this cross-section type as well. This implies that the result for the I-girder bridge might be underestimated, since altering these parameters would probably make the webs more stocky.

Table 4.9: Final utilisation ratios for all studied radii.

Section type	Radius	Displacement	Fatigue	Moment	Shear
I-girder with plan bracing	150 m	99.5%	87.4%	58.1 %	64.6 %
	300 m	96.9 %	99.8 %	65.8 %	72.5 %
	500 m	99.4 %	97.0 %	63.9 %	70.0 %
	700 m	98.3 %	98.5 %	64.6 %	78.9 %
	900 m	97.4%	98.4%	64.5 %	79.0 %
I-girder without plan bracing	150 m	97.4 %	76.1 %	50.7 %	61.8 %
	300 m	98.9 %	99.0 %	64.9 %	72.6 %
	500 m	96.9%	99.6 %	65.1 %	75.9 %
	700 m	93.8 %	98.1 %	64.1 %	76.0 %
	900 m	99.6 %	101.3 %	66.3 %	79.2 %
Box girder	150 m	99.5 %	77.0 %	53.9 %	94.3 %
	300 m	97.8 %	90.4 %	61.7 %	88.7 %
	500 m	94.7 %	90.2 %	60.5 %	98.7 %
	700 m	93.3 %	90.4 %	60.0 %	96.6 %
	900 m	94.2 %	86.0 %	56.8 %	97.9 %

For the final result of the case study, the graph in Figure 4.7 illustrates a comparison between amount of steel needed to produce the optimised solution for all three cross-sections. Foremost, the graph shows that a decreased radius of curvature increases the steel mass, something that is evident for both of the I-girder bridges and the box girder bridge.

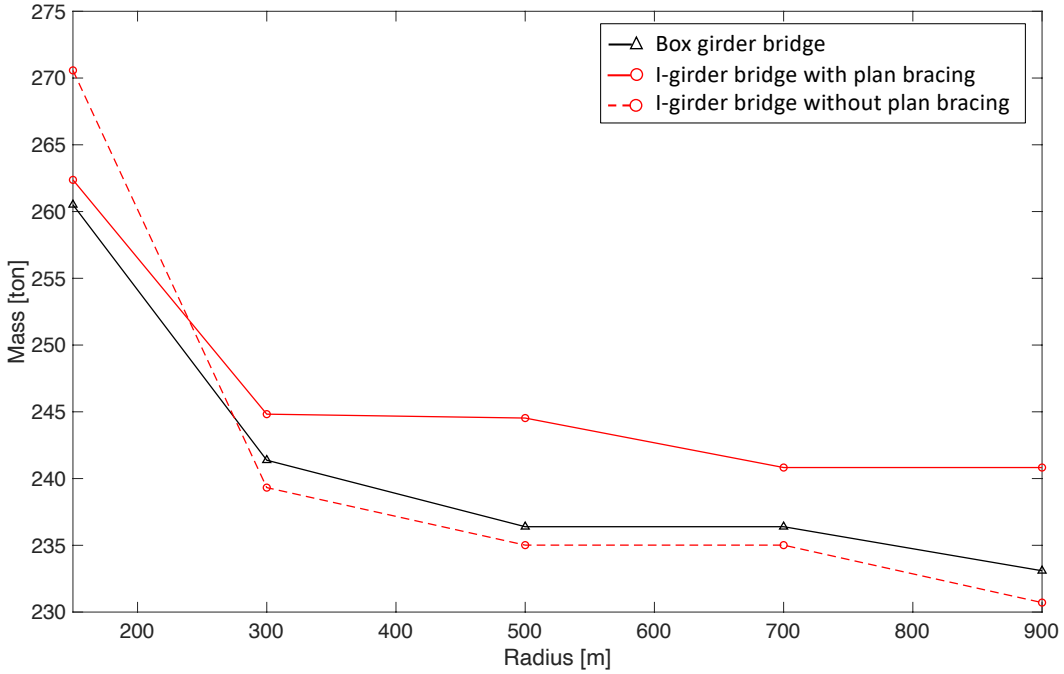

Figure 4.7: Final results of case study: Steel masses for optimised cross-sections at different radii.

Furthermore, regarding the compelling question of which cross-section that gives the most optimal solution, it can be observed that for a radius of curvature down to 300 meters, the I-girder bridge without a plan bracing system performs best in regard to required steel volume. Thereafter, an intersection of the curves suggests that the box girder bridge is more material-efficient. This is expected from study of the idealised bridge, as the result of 300 meters and 900 meters radii was coherent, whilst in the result of 150 meters radius, the effect of torsion was more apparent. To give it a context, bridges with a radius below 300 meters is not uncommon; for instance Solvalla Bridge has a radius of 240 meters. Although, it is important to remember that the y-axis only varies from 230 to 275 ton and the differences between the cross-sections are in other words quite small.

In addition, a sensitivity regarding the upper and lower boundaries of the parameters was recognised when performing the optimisation. It proved that the span of the parameters needed to be well estimated on beforehand, otherwise the result would be very different.

4.3.2 Details

Compared to the study of the idealised bridge, the discussion of the details are based on the global optimisation, since a separate local optimisation has not been performed. Throughout the case study, the spacing of cross-beams is chosen to five meters for the I-girder bridge and seven meters for the box girder bridge. From Figure 4.7 it is apparent that the I-girder bridge without lower plan bracing is the most optimised solution for radii above 300 meters. However, this is based on the assumption that the cross-beams can handle the horizontal force couple, which magnitude depends on the centre-to-centre distance of the cross-bracing. It is not obvious that the chosen dimensions of the cross-beams are robust enough to take this force couple, since they have been kept constant in the global optimisation. If a separate optimisation that included the dimensions and the spacing of cross-beams where to be performed, it might result in an increase of the total amount of steel work.

Moreover, the form of the plan bracing has been chosen to an X-shape, but other configurations also exists, see Section 2.1.2. For railway bridges, the secondary effects due to the traffic load can be significant, which implies that the form of plan bracing becomes an important design feature. The result of this study indicates that the I-girder bridge with plan bracing has a higher volume than the two other cross-section types for radii above 300 meters. However, if another shape of the plan bracing was chosen, its dimensions might decrease, which ultimately would alter the total volume of the bridge.

As previously discussed in the global design, the I-girder bridge is sensitive to fatigue, which confirms the theory mentioned in Section 2.2.2. The plan bracing results in additional details, and the chosen detail category is dependent on whether or not careful attention has been made during the construction of these details. For instance, the gusset plate might have a detail category of 40 MPa if made with harsh edges and this would in turn alter the results seen in Figure 4.7.

5
Conclusion

This thesis set out to investigate the modelling and design of horizontally curved composite bridges with the intention of summarising the lessons learned in a practical design guide. Firstly, the accuracy of simplified modelling strategies was evaluated by comparing three published beam models to a 3D shell model. From this study, it is concluded that the grillage model and the spatial beam model both exhibit similar behaviour to that of the shell model for the examined cross-section types. In particular, the result indicates that for smaller radii, where the effect of curvature is more advanced, the spatial beam model is more efficient. These findings are limited to a curved bridge loaded by its self-weight and thus the results does not reflect the influence of curvature coming from horizontal loads. The research further shows that the expected torsional behaviour of the curved bridge is not observed with the equivalent straight beam model, especially regarding the difference of the inner and outer girder.

Secondly, design of curved composite bridges was investigated through a case study of Solvalla bridge. The results from the first study is further confirmed by the findings here, which indicates that for bridges with a radius smaller than 300 meters, the influence of curvature becomes far more apparent. From a material-efficiency point of view, the study has found that an I-girder bridge is to be advantageous over box girder bridge when the radius of curvature is greater than 300 meters. On the contrary, the result suggests that a box section requires less steel for more curved bridges. The exclusion of details from the case study makes these findings less general, but despite this limitation, the study offers some insight into the advantageous cross-section type with regard to required amount of steel.

5.1 Design guide

The design guide in Figure 5.1 concludes the findings of the thesis, with the ambition of it serving as a practical tool for the industry when designing curved composite bridges. It presents the optimal cross-section type depending on the radius of curvature, along with the recommended modelling strategy for each respective section.

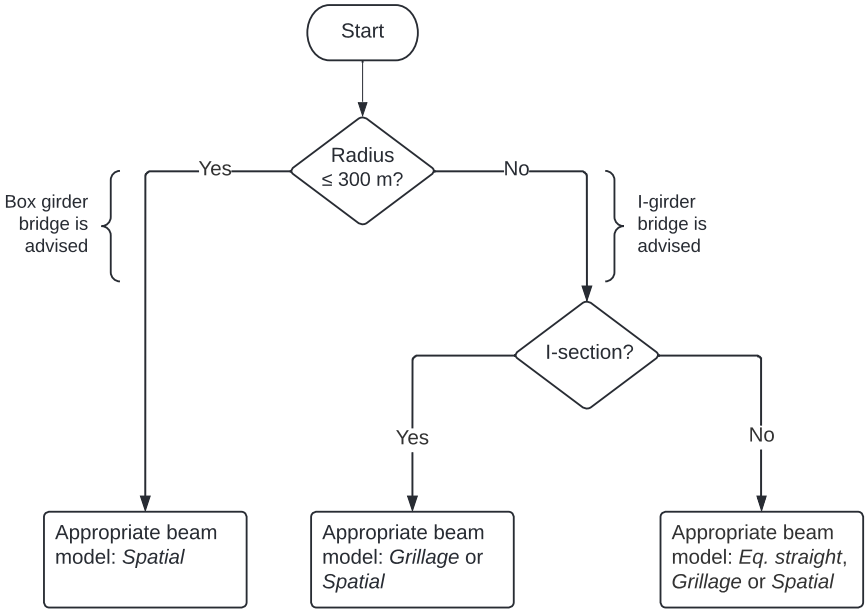

Figure 5.1: Developed flowchart over modelling approach and design procedure for curved composite bridges with a radius of curvature up to 900 meters.

5.2 Further research

During the process of answering the thesis aim, some questions have arisen that would be interesting for further research. Firstly, during the assessment of the accuracy of the beam models compared to the shell model, the concrete slab was found influential on the stiffness distribution of the whole structure. Unfortunately, there is not much research on exactly why this behaviour can be observed for curved bridges. The studies that do exist mention that the I-girder bridge will in reality exhibit a torsional resistance that also includes a modified uniform torsion contributed by the slab [5]. Nonetheless, seeing that a shell element has no thickness, it cannot possibly capture this effect. In a further research, the shell model could be complimented by a plate element for the concrete slab. This way, shear stresses in this model could be compared to the ones in the beam models in order to investigate how the slab contributes to the overall stiffness distribution of the structure.

Secondly, this thesis have focused on the influence of curvature on mainly the global behaviour of composite bridges. When performing the optimisation of the I-girder bridge equipped with a lower plan bracing, a high detail category was assumed for the gusset plate. In a further research, the effect of having harsher edges on the gusset plate could be studied, as the fatigue criterion would probably become the decisive design factor. Furthermore, the spacing and form of the cross-bracing have been excluded from this thesis. Current literature exist on the spacing of cross-beams [30] [31], however, it would be interesting to perform an optimisation that included these factors as parameters and investigate the variation in steel volume. All in all, these investigations of the details of the I-girder bridge would probably influence the global design and result in changes of the optimised solution.

Bibliography

[1] Eurocode 4: Design of composite steel and concrete structures - Part 2: General rules and rules for bridges, Swedish Standard SS-EN-1994-2:2005, 2009

[2] M.A. Hirt and J. Lebet, "Bridge description" in *Steel Bridges*, M.A. Hirt and J. Lebet, Lausanne Switzerland: EPFL Press, 2013, pp. 13-27.

[3] M.A. Hirt and J. Lebet, "Structural Forms for Bridges" in *Steel Bridges*, M.A. Hirt and J. Lebet, Lausanne Switzerland: EPFL Press, 2013, pp. 73-100.

[4] N.E. Shanmugam and C.M. Wang, "Interaction of curvature on the stability and design of curved plate girders" in *Analysis and Design of Plated Structures*, J.S. Davidson, Cambridge England: Woodhead Publishing Limited, 2006, pp. 382-421.

[5] M.A. Hirt and J. Lebet, "Internal Moments and Forces in Beam Bridges" in *Steel Bridges*, M.A. Hirt and J. Lebet, Lausanne Switzerland: EPFL Press, 2013, pp. 221-278.

[6] M.A. Hirt and J. Lebet, "Cross-bracing and Plan bracing" in *Steel Bridges*, M.A. Hirt and J. Lebet, Lausanne Switzerland: EPFL Press, 2013, pp. 377-400.

[7] M.A. Hirt and J. Lebet, "Fabrication and Erection of the Steel Structure" in *Steel Bridges*, M.A. Hirt and J. Lebet, Lausanne Switzerland: EPFL Press, 2013, pp. 125-146.

[8] I. Vayas and A. Iliopoulos, "Types of steel–concrete composite bridges" in *Design of Steel-Concrete Composite Bridges to Eurocodes*. Taylor & Francis Group, LLC: Boca Raton. FL, 2013, pp. 13-66.

[9] Z. Fan, T.A. Helwig, Distortional Loads and Brace Forces in Steel Box Girders. Journal of structural engineering, 128(6): 710-718, 2002.

[10] H. Unterweger, Global analysis of steel and composite highway bridges - Developement if improved spatial beam models.

[11] M. Al-Emrani and B. Åkesson, Steel Structures course literature VSM 191, Gothenburg, Sweden: Chalmers University of Technology, 2020.

[12] Y. Wang, et al., Cracking reasons and features of fatigue details in the diaphragm of curved steel box girder. Engineering structures 201, 2019.

[13] M. Hossain, M.B. Zisan, M.N. Haque, Analysis of Distortion-Induced Stress and Retrofitting Technique of Curved Twin I-Girder Composite Bridge. Arabian Journal for Science and Engineering 44:4395-4404, 2019.

[14] Eurocode 3: Design of steel structures - Part 1-9: Fatigue, Swedish Standard SS-EN-1993-1-9:2005, 2008

[15] P.M Kurowski, *Finite Element Analysis for Design Engineers*, USA: SAE, 2004

[16] S.J. Fatemi, A.H. Sheikh, M.S. Mohamed Ali, Development and Application of an Analytical Model for Horizontally Curved Bridge Decks. Advances in Structural Engineering Vol. 18 No. 1, 2015.

[17] J.F. Hajjar, D. Krzmarzick, L. Pallarés, Development and Measured behaviour of a curved composite I-girder bridge. Journal of Constructional Steel Research 66 351-368, 2010.

[18] I. Vayas and A. Iliopoulos, "Modeling and methods for global analysis" in *Design of Steel-Concrete Composite Bridges to Eurocodes*. Taylor & Francis Group, LLC: Boca Raton. FL, 2013, pp. 183-252.

[19] C-J. Chang, D.W. White, An assessment of modeling strategies for composite curved steel I-girder bridges. Engineering structures 30 2991-3002, 2008.

[20] Region Stockholm. (2022, Apr. 21). *Solvalla*[online]. Avaiable: `https://www.regionstockholm.se/verksamhet/kollektivtrafik/aktuella-projekt/Tvarbanan-Kista-Helenelund/solvalla/`

[21] Eurocode 1: Actions on structures - Part 2: Traffic loads on bridges, Swedish Standard SS-EN-1991-2:2003, 2010

[22] Eurocode 1: Actions on structures - Part 1-4: General actions - Wind actions, Swedish Standard SS-EN-1991-1-4:2005, 2008

[23] Eurocode: Basis of structural design, Swedish Standard SS-EN-1990-A1:2005, 2006

[24] Eurocode 2: Design of concrete structures - Part 1-1: General rules and rules for buildings, Swedish Standard SS-EN 1992-1-1:2005, 2008

[25] Krav: Bro och broliknande konstruktion, TRVINFRA-00227, 2021

[26] Eurocode 3: Design of steel structures - Part 1-1: General rules and rules for buildings, Swedish Standard SS-EN-1993-1-1:2005, 2008

[27] Eurocode: Basis of structural design, Swedish Standard SS-EN-1990, 2010

[28] Eurocode 3: Design of steel structures – Part 2: Steel bridges, Swedish Standard SS-EN-1993-2:2006, 2009

[29] I. Vayas and A. Iliopoulos, "Ultimate limit state" in *Design of Steel-Concrete Composite Bridges to Eurocodes*. Taylor & Francis Group, LLC: Boca Raton. FL, 2013, pp. 341-416.

[30] L. Jeonghwa, et al., *Effect of cross-sectional rigidity on intermediate diaphragm spacing of steel-box girder bridges*. Journal of Construction Steel Research, 2022.

[31] H. Maneetes, D.G. Linzell, *Cross-frame and lateral bracing influence on curved steel bridge free vibration response*. Journal of Construction Steel Research, 2003.

A

Cross-section of idealised bridge design

Table A.1: Geometries of the I- and box girder cross-sections

Variable	**I-girder section**	**Box section**	**Unit**
Height of cross section, H	2.5	2.37	m
Height of web, h_w	2400	2300	mm
Thickness of web, t_w	18	18	mm
Width of top flange, b_{tf}	1250	500	mm
Thickness of top flange, t_{tf}	40	40	mm
Width of bottom flange, b_{bf}	1200	CC	mm
Thickness of bottom flange, t_{bf}	60	30	mm
Width of concrete slab, b_{slab}	8.5	8.5	m
Thickness of concrete slab, t_{slab}	300	300	mm
Length of spans, L_n	60, 80, 60	60, 80, 60	m
Spacing between cross-bracing, C	3	3	m
Spacing between webs, CC	4.5	4.5	m

B

Supplementary results: radius of 300 meters

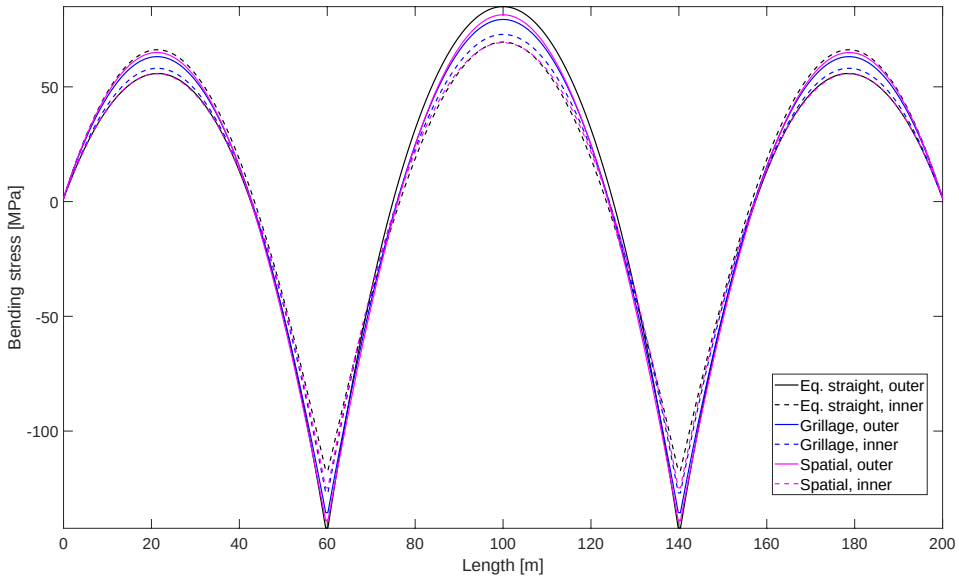

(a) Construction.

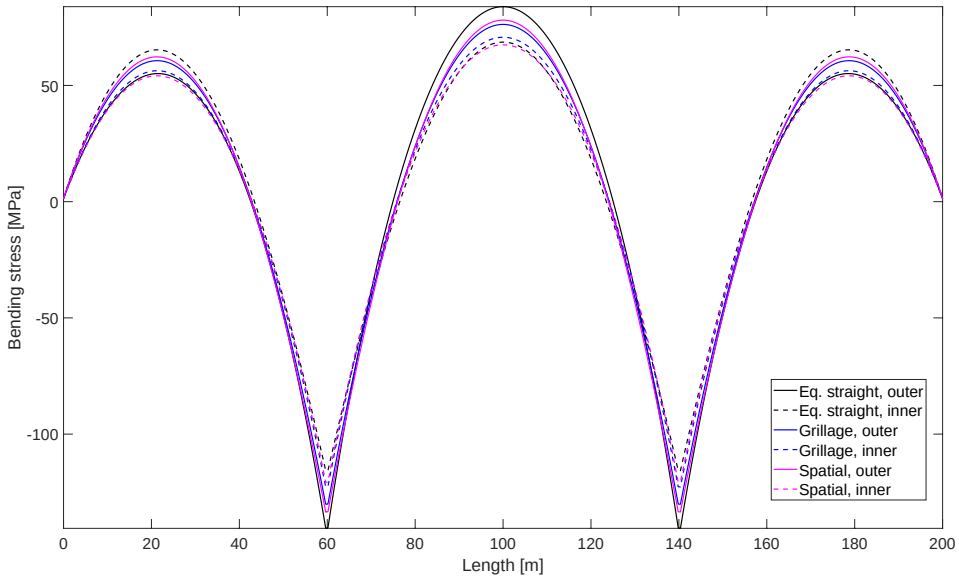

(b) Service life.

Figure B.1: Bending stress for I-girder bridge with radius of 300 meters.

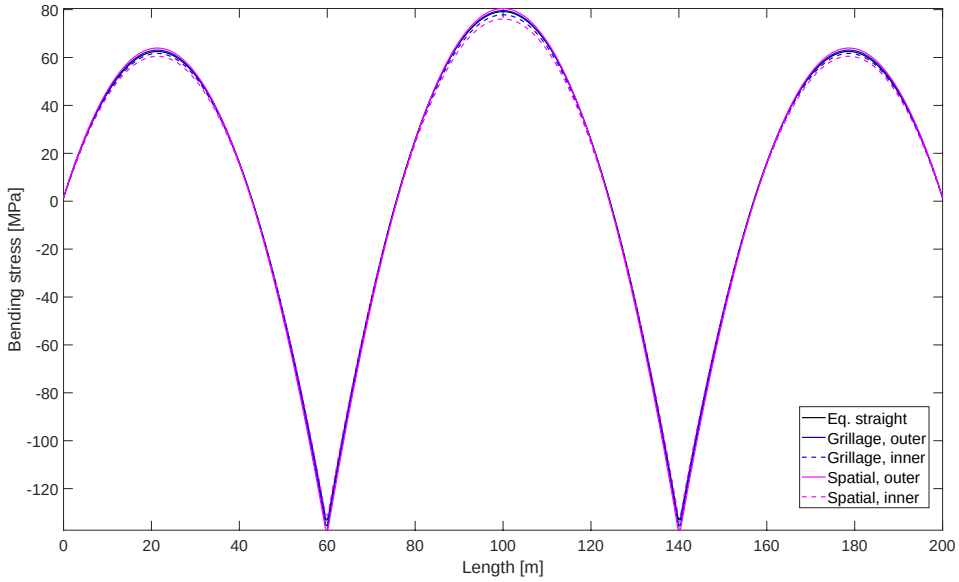

(a) Construction.

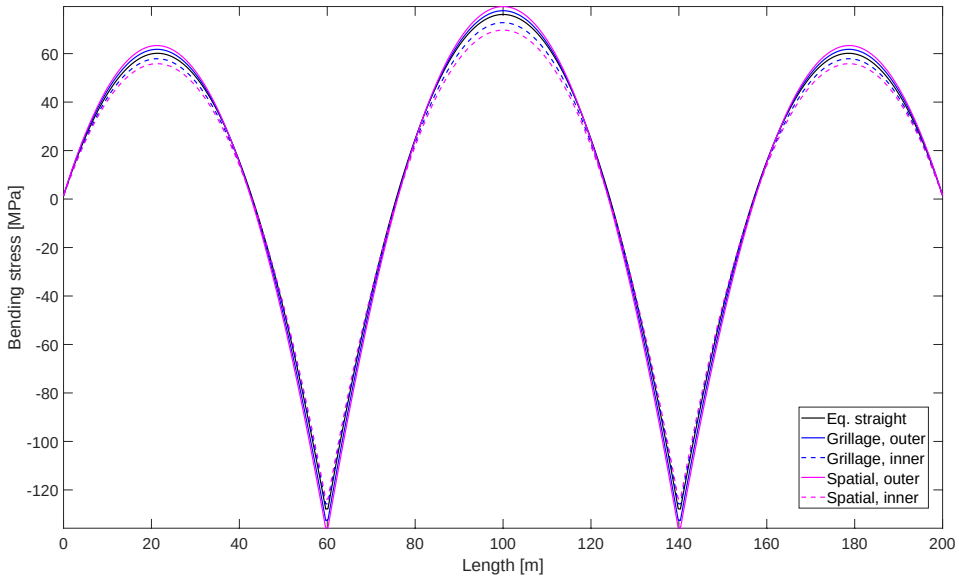

(b) Service life.

Figure B.2: Bending stress for box girder bridge with radius radius of 300 meters.

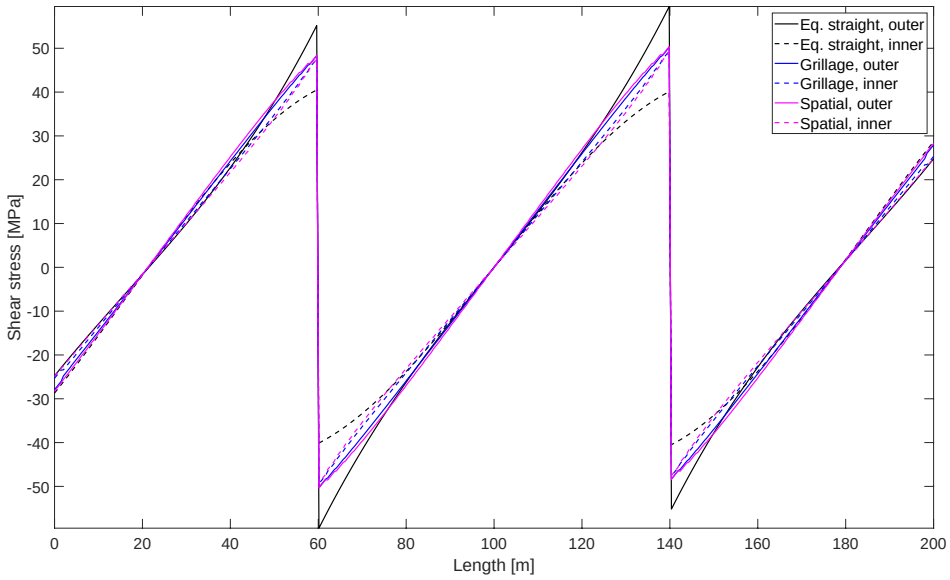

(a) Construction.

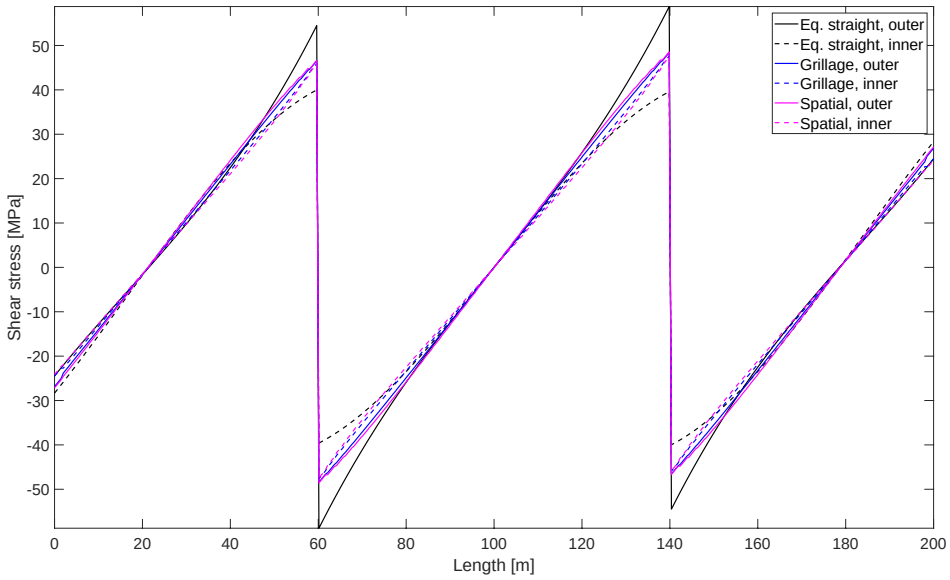

(b) Service life.

Figure B.3: Shear stress for I-girder bridge with radius of 300 meters.

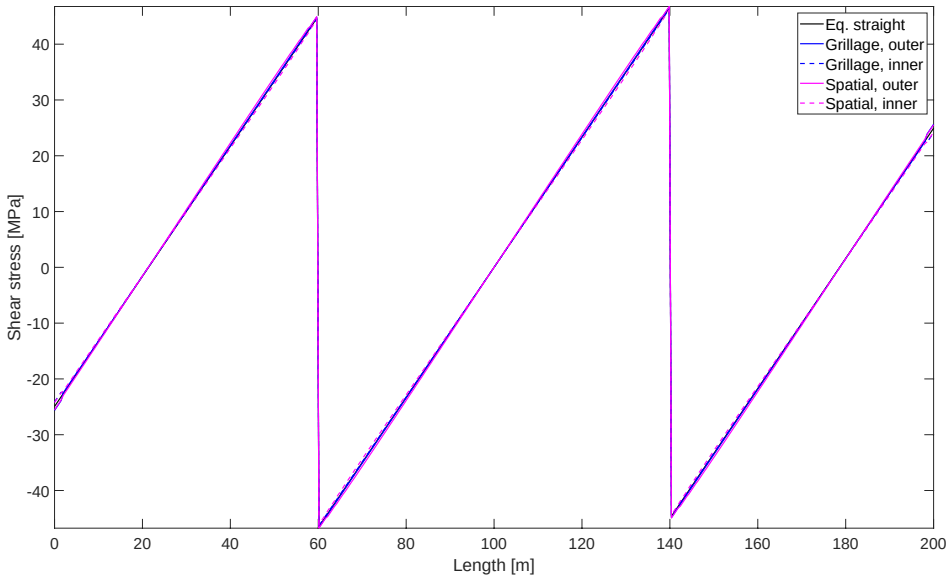

(a) Construction.

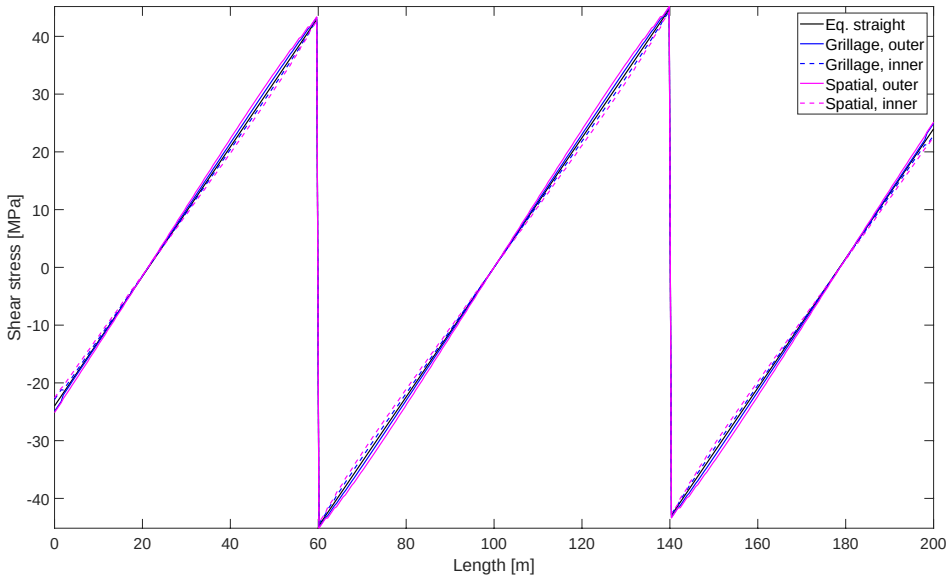

(b) Service life.

Figure B.4: Shear stress for box girder bridge with radius of 300 meters.

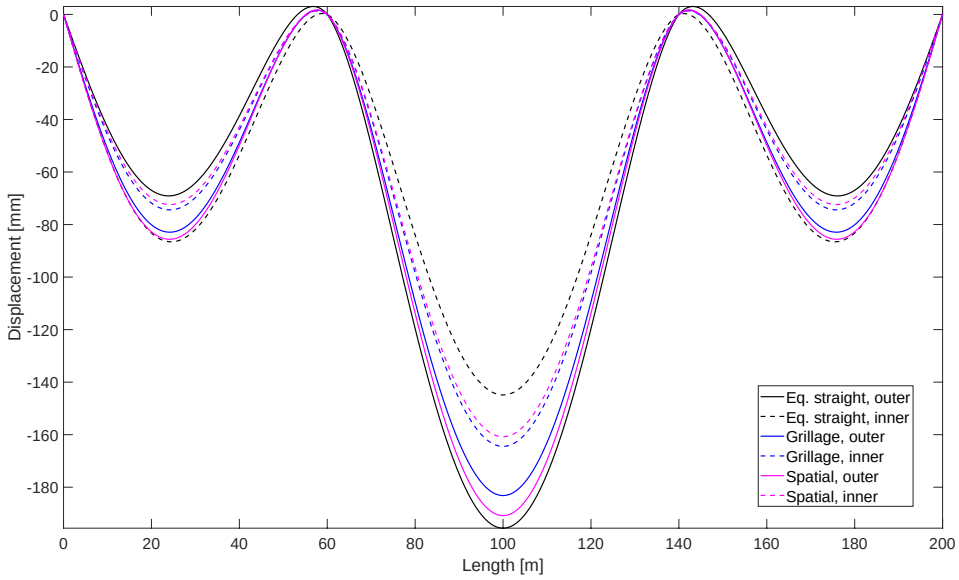

(a) Construction.

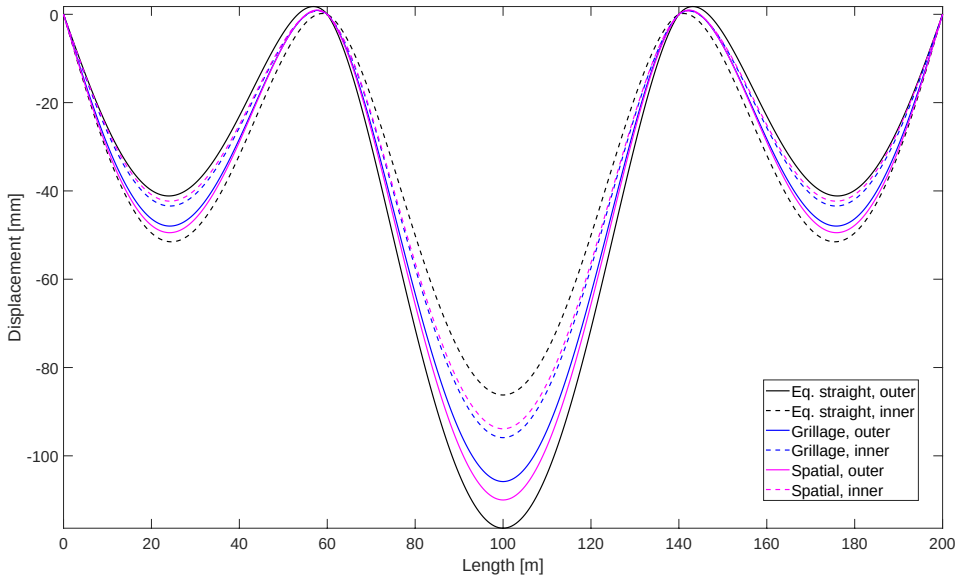

(b) Service life.

Figure B.5: Displacement for I-girder bridge with radius of 300 meters.

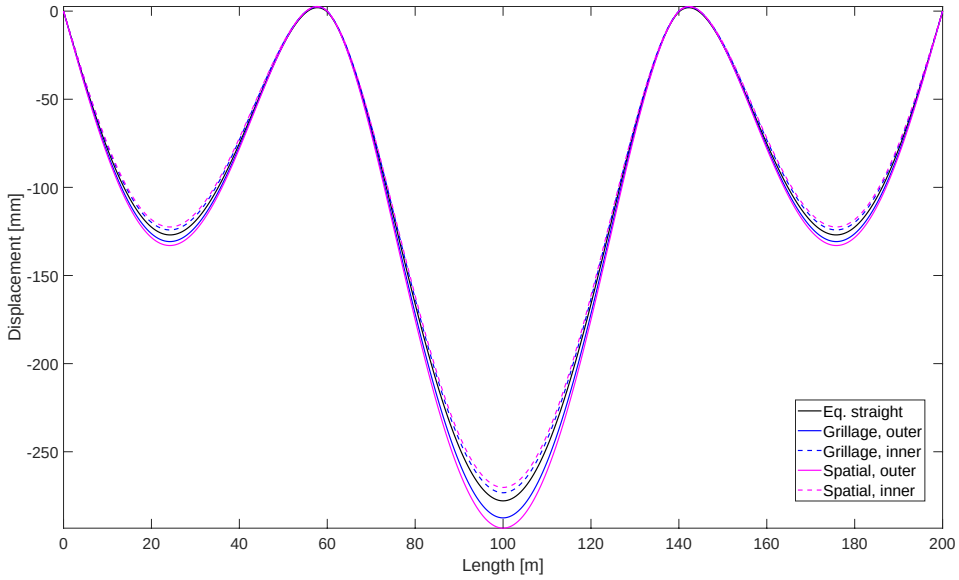

(a) Construction.

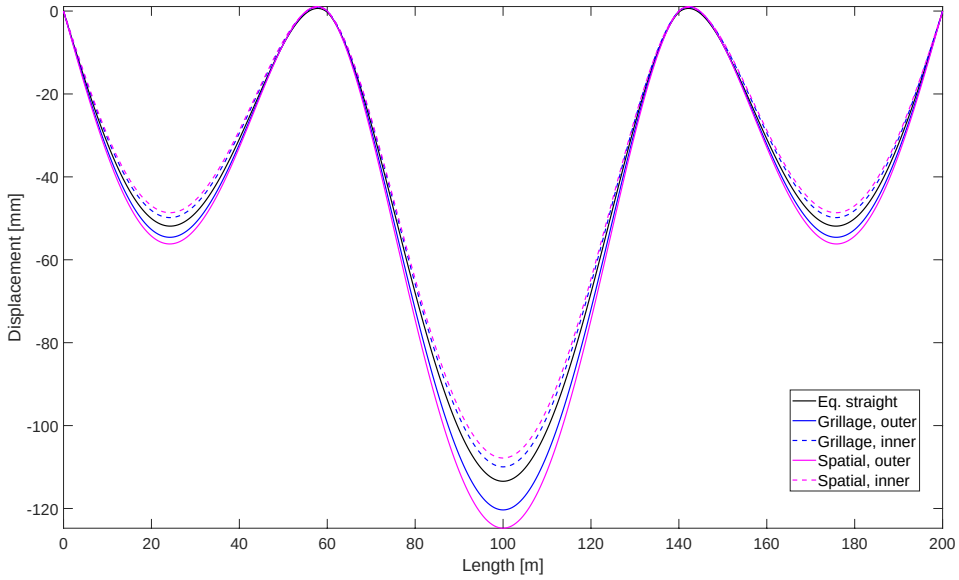

(b) Service life.

Figure B.6: Displacement for box girder bridge with radius of 300 meters.

C

Supplementary results: bending and shear stresses

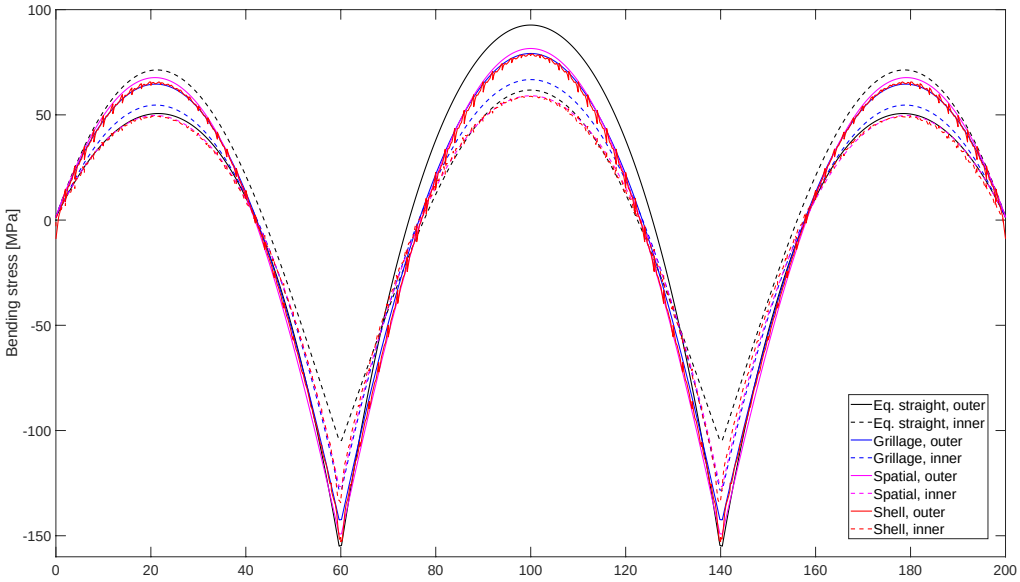

(a) Radius of 150 meters.

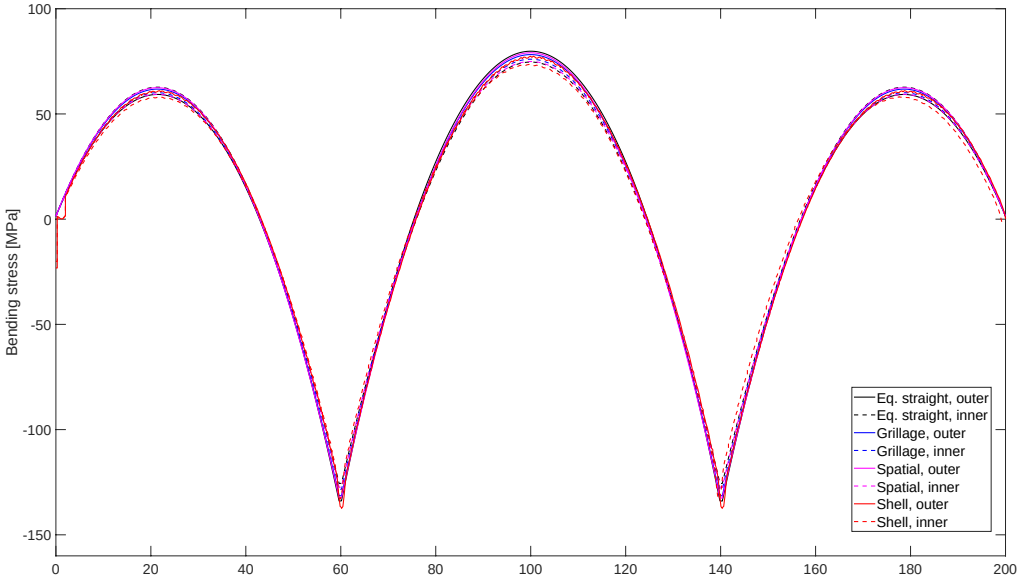

(b) Radius of 900 meters.

Figure C.1: Bending stress for I-girder bridge during construction.

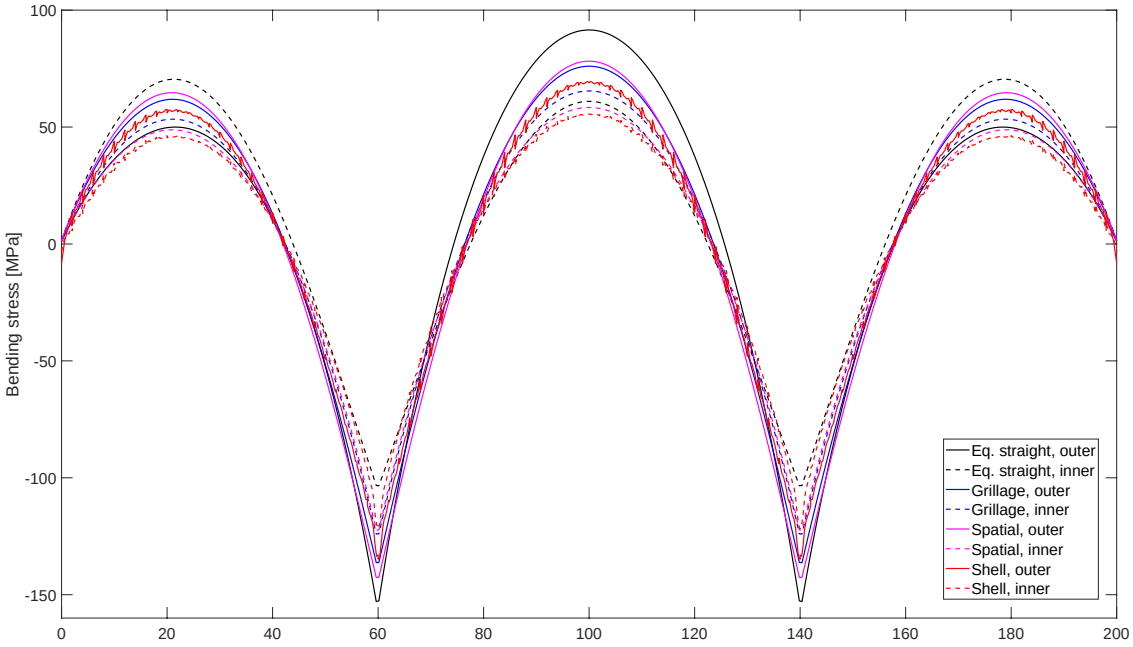

(a) Radius of 150 meters.

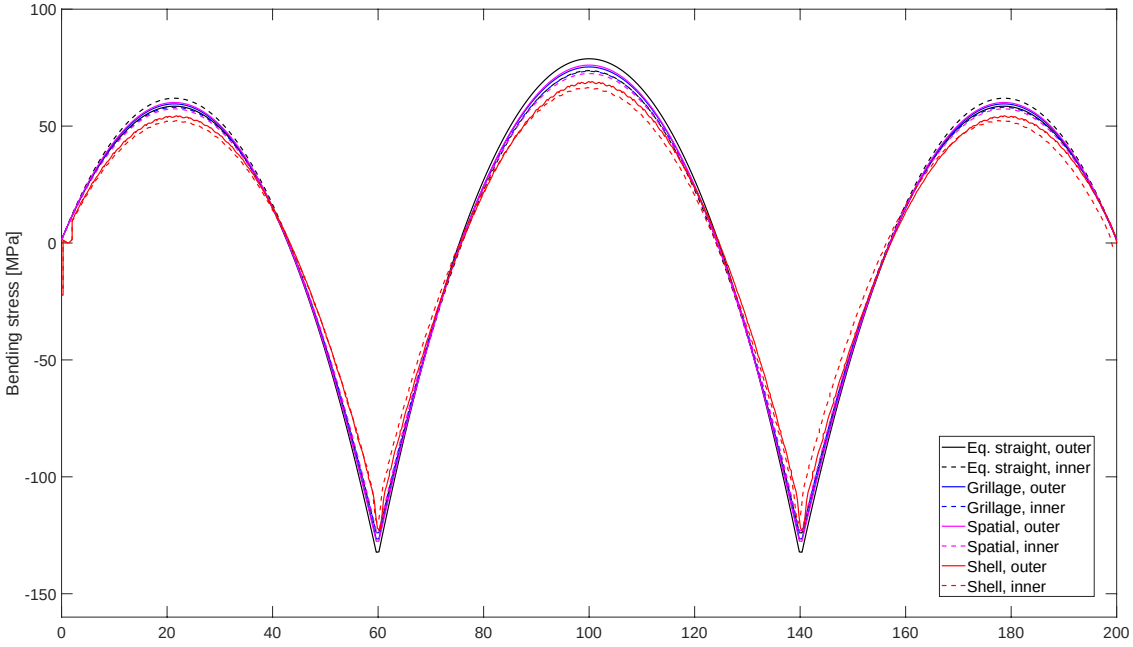

(b) Radius of 900 meters.

Figure C.2: Bending stress for I-girder bridge during service life.

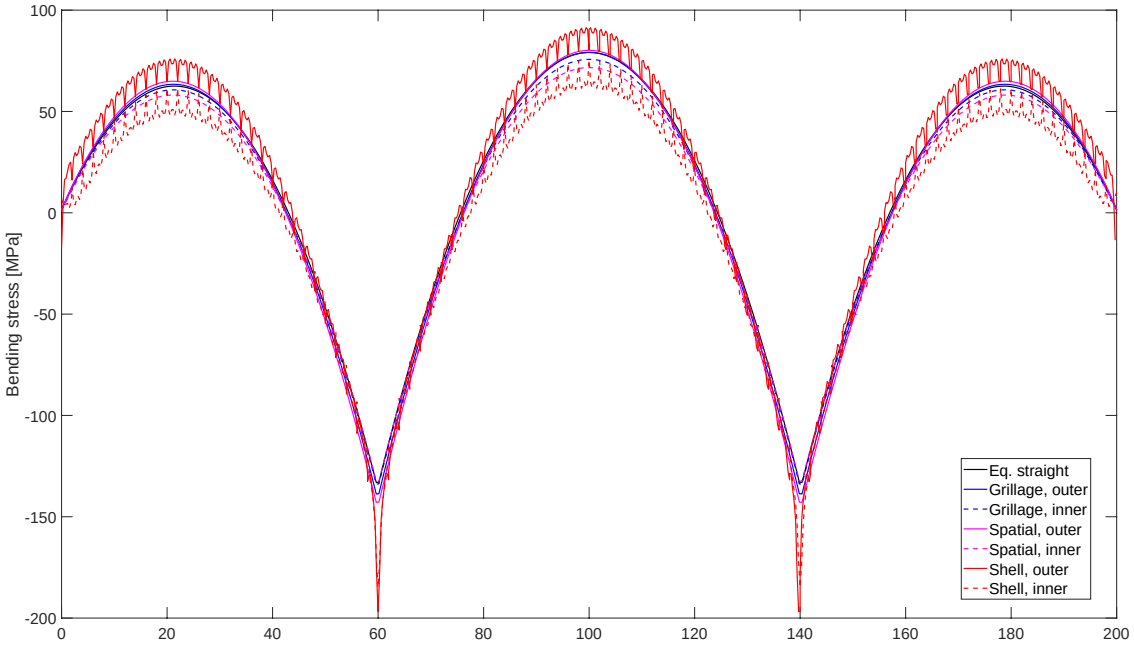

(a) Radius of 150 meters.

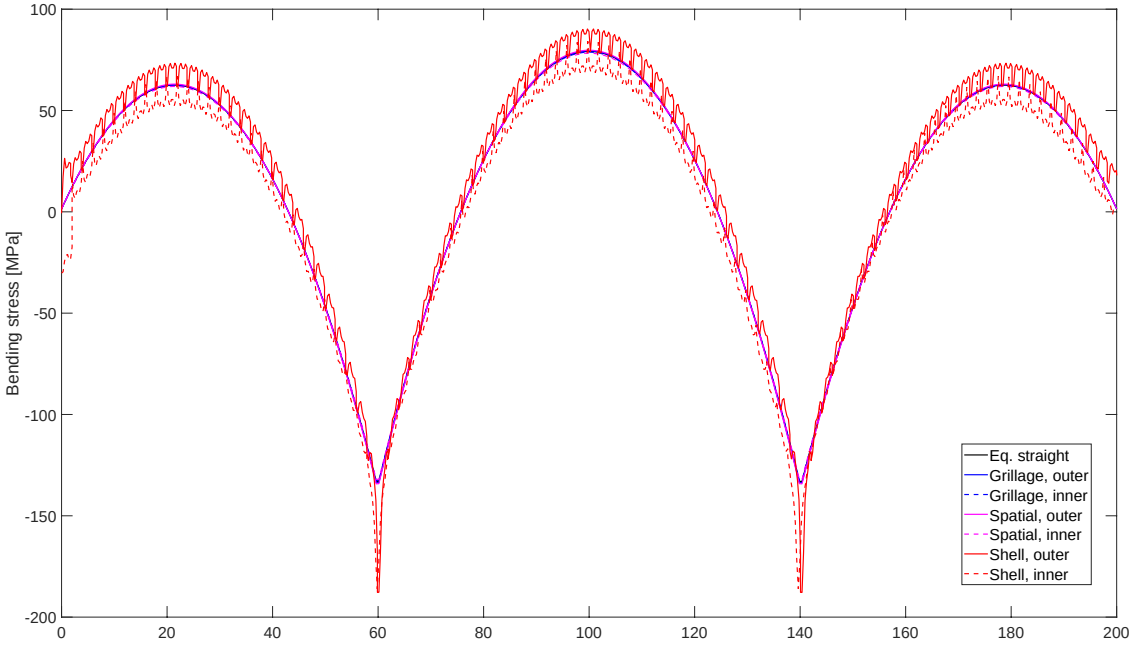

(b) Radius of 900 meters.

Figure C.3: Bending stress for box girder bridge during construction.

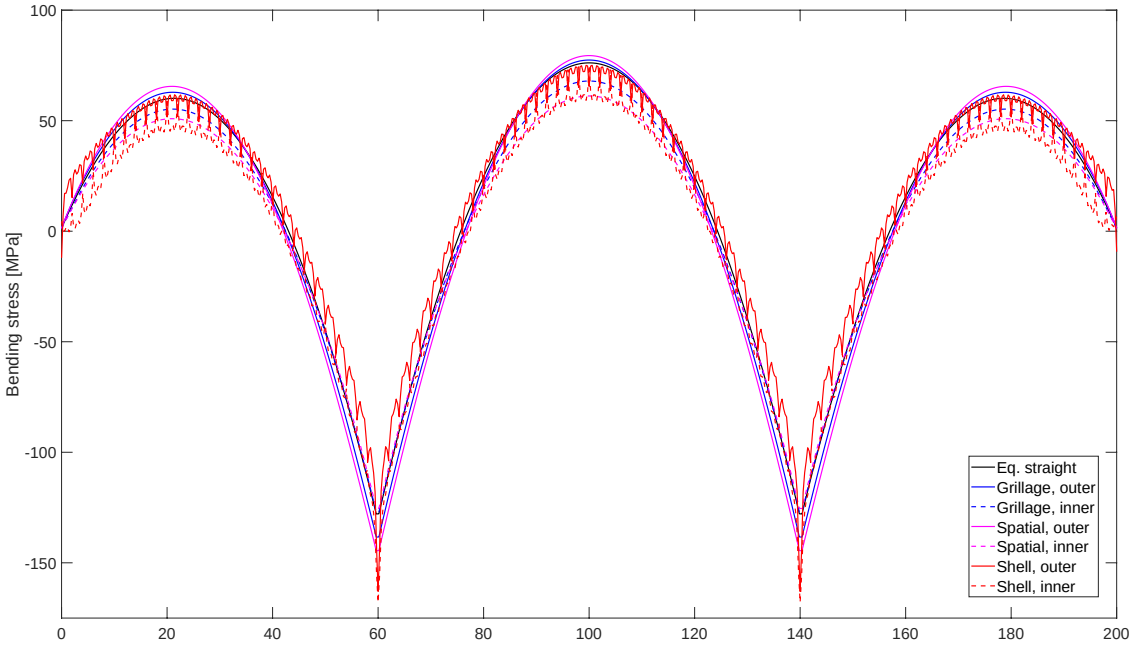

(a) Radius of 150 meters.

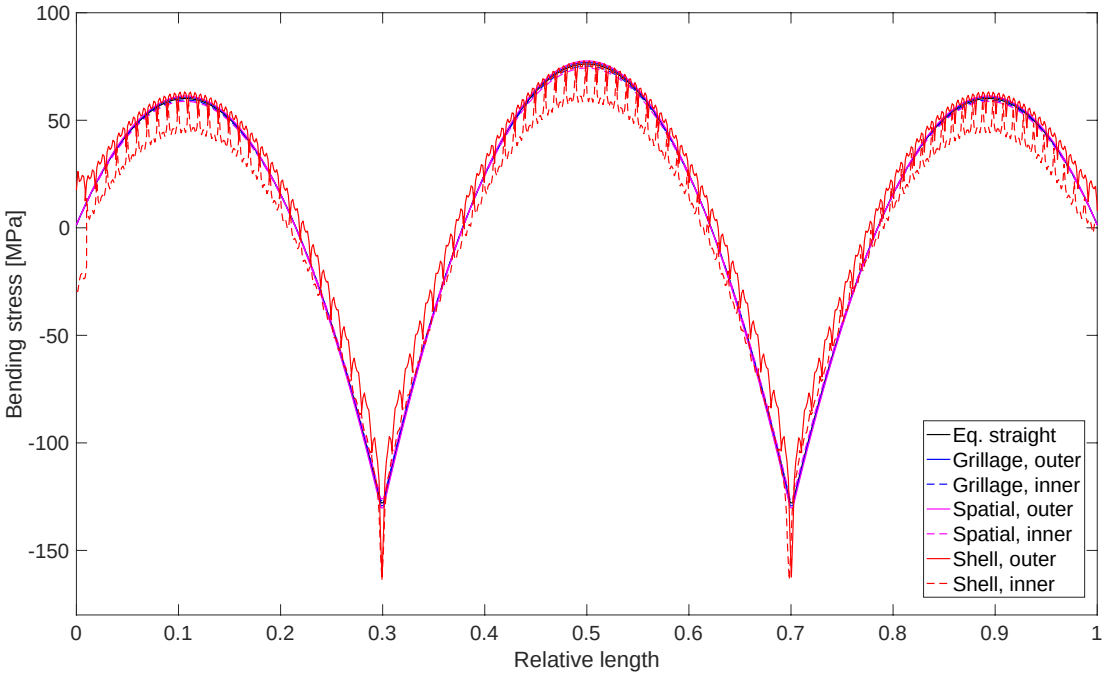

(b) Radius of 900 meters.

Figure C.4: Bending stress for box girder bridge during service life.

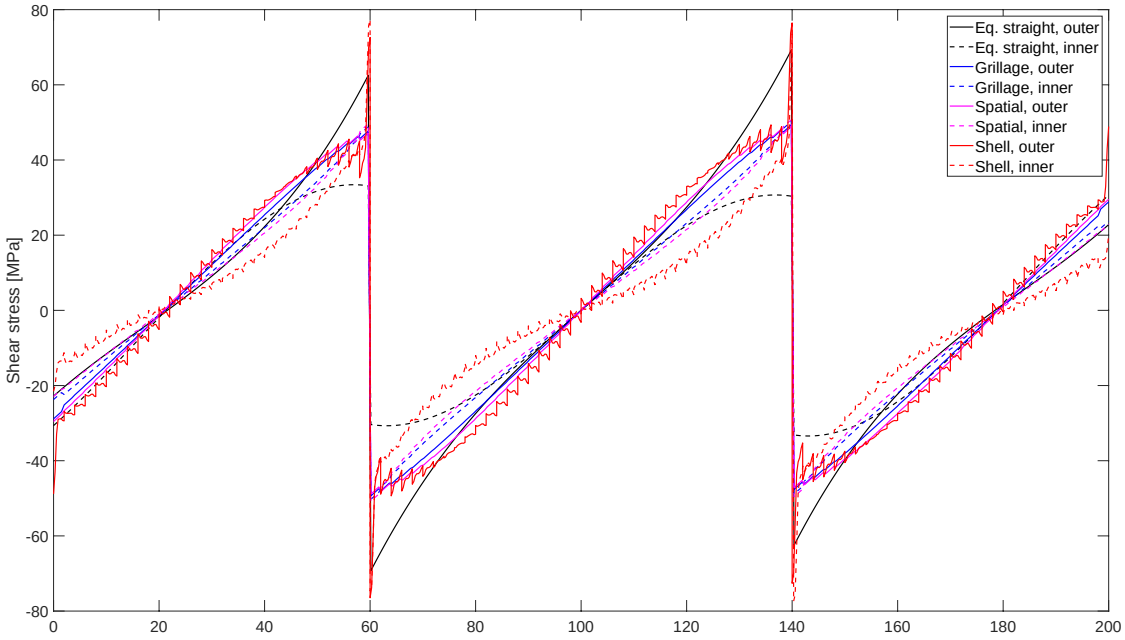

(a) Radius of 150 meters.

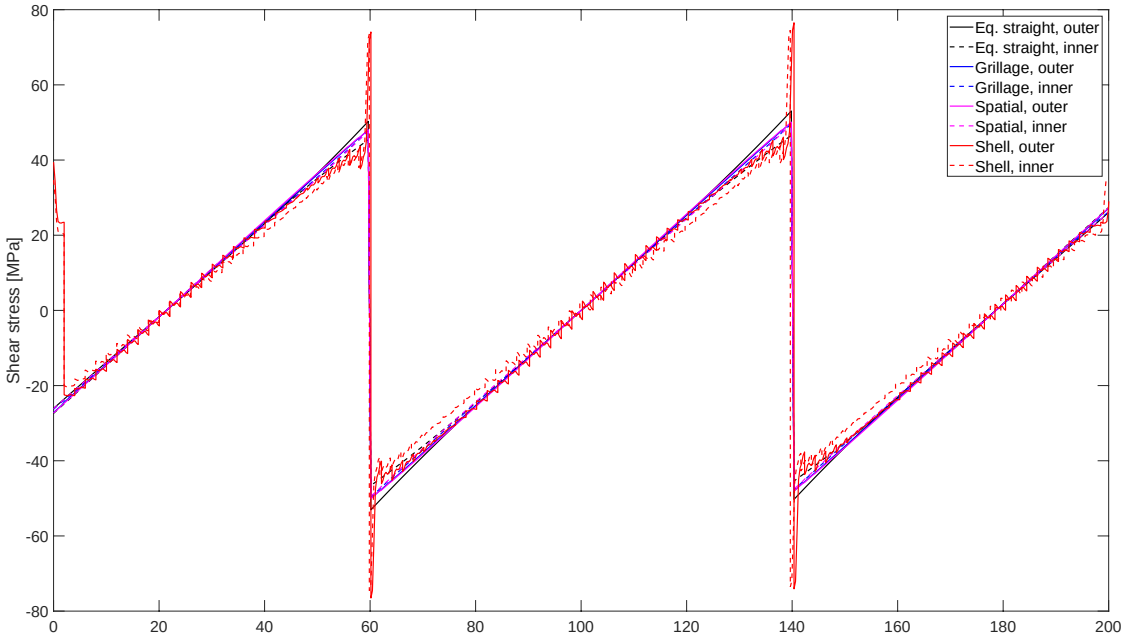

(b) Radius of 900 meters.

Figure C.5: Shear stress for I-girder bridge during construction.

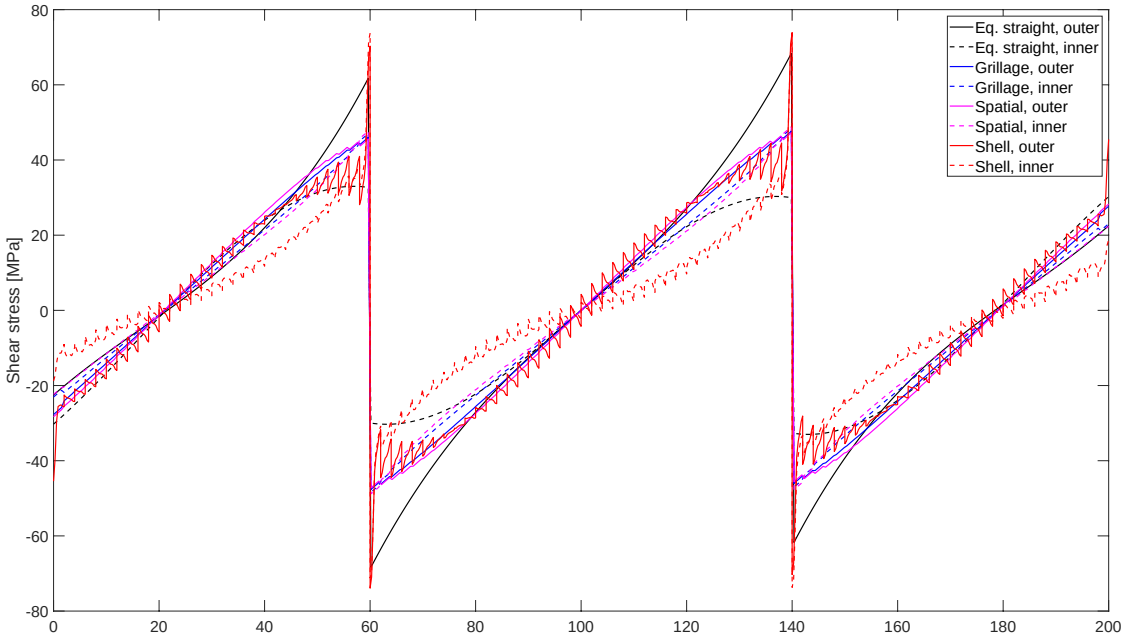

(a) Radius of 150 meters.

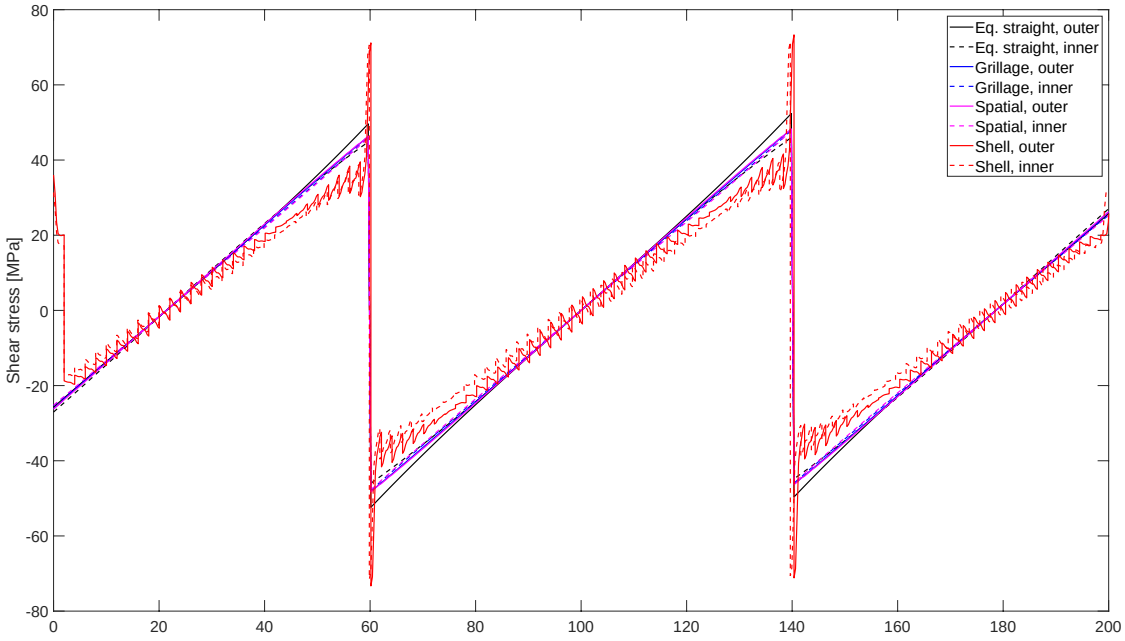

(b) Radius of 900 meters.

Figure C.6: Shear stress for I-girder bridge during service life.

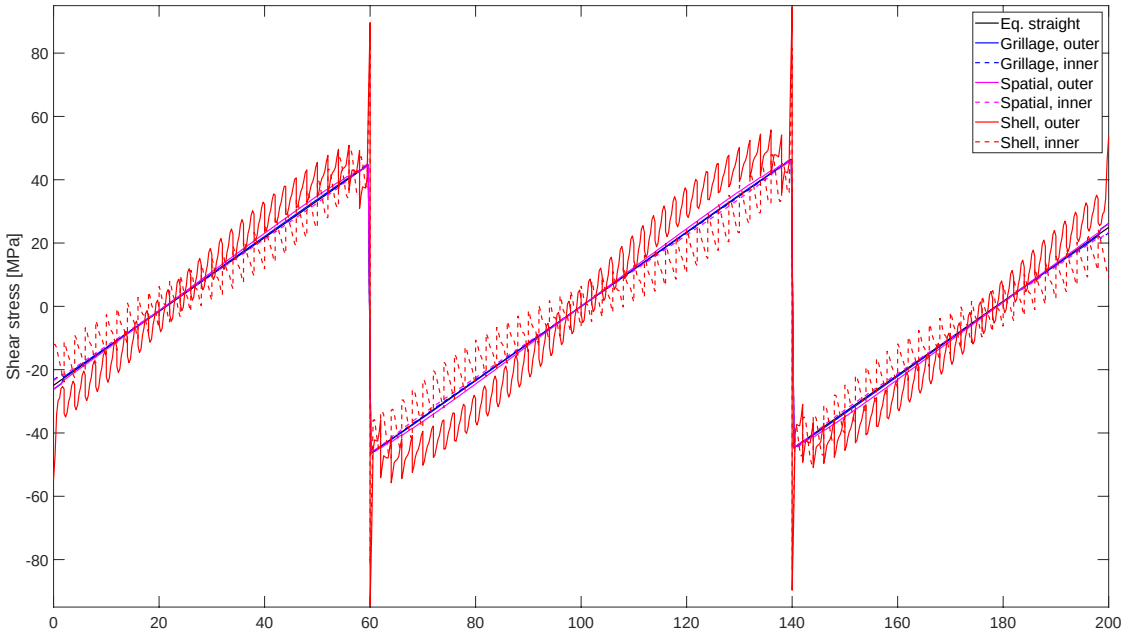

(a) Radius of 150 meters.

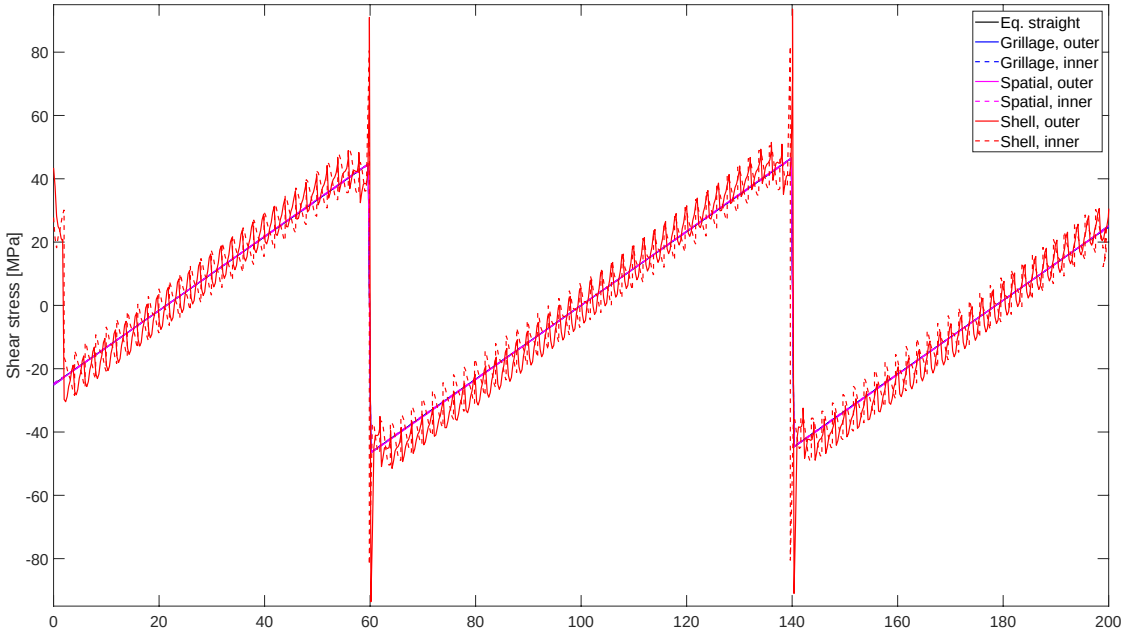

(b) Radius of 900 meters.

Figure C.7: Shear stress for box girder bridge during construction.

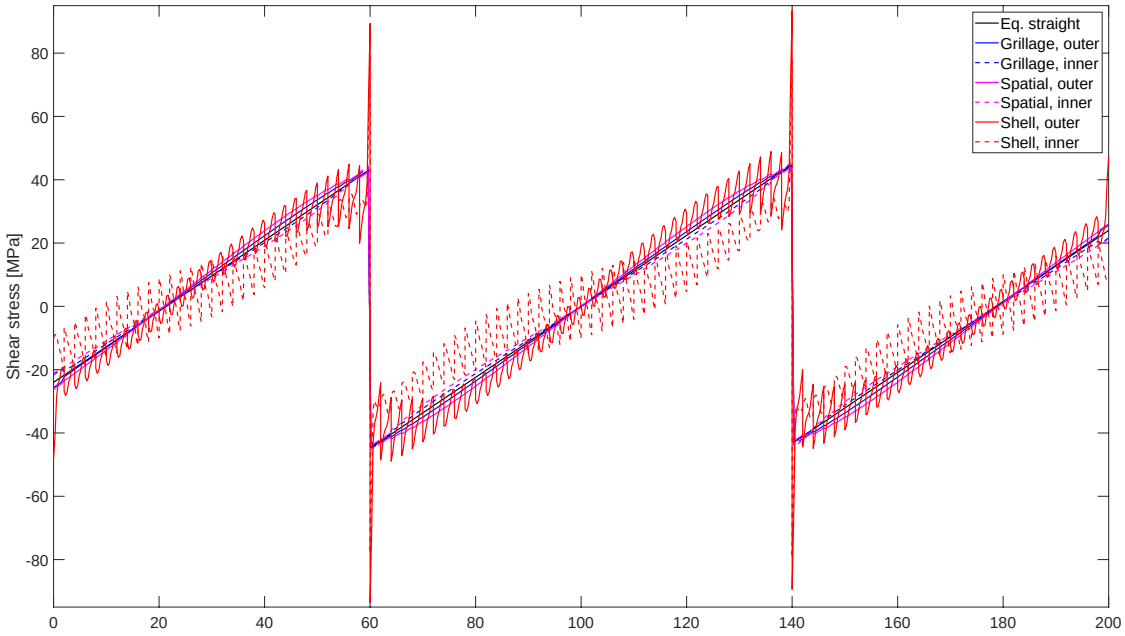

(a) Radius of 150 meters.

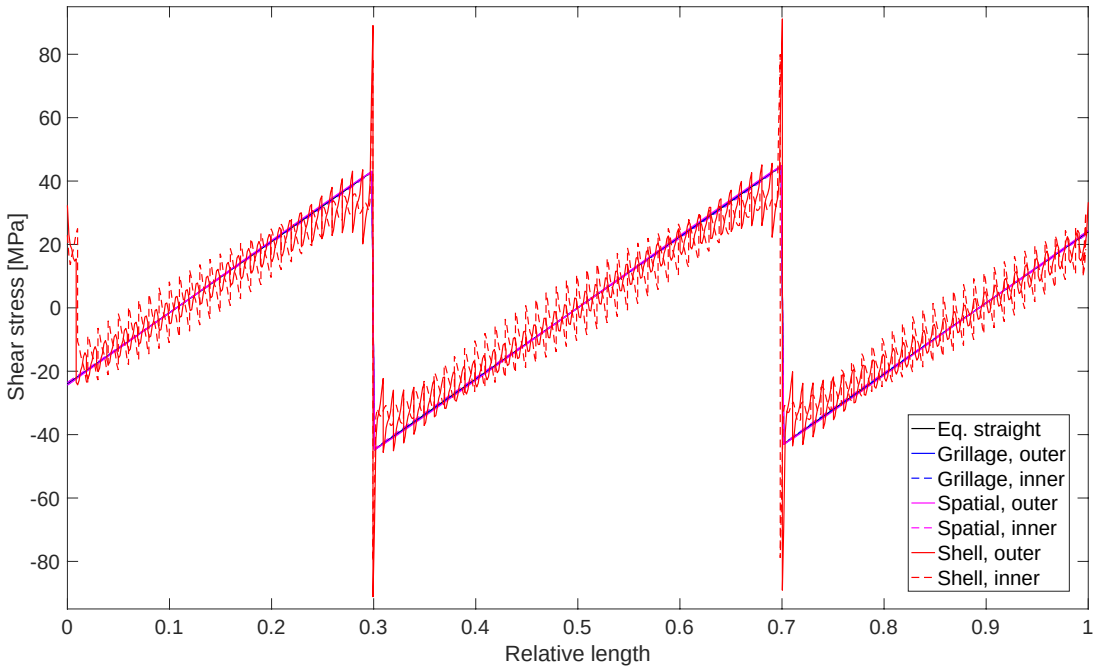

(b) Radius of 900 meters.

Figure C.8: Shear stress for box girder bridge during service life.

D

Calculation of internal forces of cross-bracing

D.1 Bridge description

The calculations of internal forces in cross-bracing is performed for a I- and box girder bridge during service life.

Centre-to centre distance of webs: $CC := 4.5 \cdot m$

Spacing of cross-bracing: $C := 3 \cdot m$

Radius of curvature: $R := 900m$

D.1.1 Box girder bridge

Height of web: $h_{w.B} := 2300 \cdot mm$

Bending moment over mid-span support is retrieved from the FE-analysis performed in Brigade Plus.

Eq. straight beam model $M_{support.1B} := 48.09 \cdot MN \cdot m$

Grillage model: $M_{support.2B} := (23.87 + 24.32) \cdot MN \cdot m = 48.19 \cdot MN \cdot m$

Spatial beam model: $M_{support.3B} := (23.7 + 24.5) \cdot MN \cdot m = 48.2 \cdot MN \cdot m$

D.1.2 I-girder bridge

Height of web: $h_{w.I} := 2400 \cdot mm$

Bending moment over mid-span support is retrieved from the FE-analysis performed in Brigade Plus.

Eq. straight beam model $M_{support.1I} := (27.34 + 25.62) \cdot MN \cdot m = 52.96 \cdot MN \cdot m$

Grillage model: $M_{support.2I} := (25.62 + 26.17) \cdot MN \cdot m = 51.79 \cdot MN \cdot m$

Spatial beam model: $M_{support.3I} := (25.44 + 26.38) \cdot MN \cdot m = 51.82 \cdot MN \cdot m$

D.2 Internal forces

The distortional loads acting on the cross-bracing is determined from ther article *Distortional loads and Brace Forces in Steel Box Girders* by Fan Z.T, Helwig T.A. (2002). The internal forces are then computed by setting up a local FE-model in MatLab using *CALFEM,* where the cross-bracing is modeled with 2D bar elements. This local model can be set up in any software that can model truss elements.

D.2.1 Forces in box girder bridge

The internal forces can be seen directly from the shell model.

Force in upper chord: $F_{chord.shell.B} := 117.59 \cdot kN$

Force in diagonals: $F_{diagonal.shell.B} := 50.88 \cdot kN$

Equivalent straight beam model

Firstly, the bending moments results in horizontal and vertical distortional loads.

Horizontal force: $H_{1B} := \frac{C}{2 \cdot h_{w.B}} \cdot \frac{M_{support.1B}}{R} = 34.848 \cdot kN$

Vertical force: $V_{1B} := \frac{C}{2 \cdot CC} \cdot \frac{M_{support.1B}}{R} = 17.811 \cdot kN$

Therafter, the internal forces in the chords and diagonals are determined.

Force in upper chord: $F_{upper.1B} := 2 \cdot 34.85 \cdot kN$

Force in diagonal: $F_{diagonal.1B} := 49.83 \cdot kN$

Deviations from shell model: $D_{upper.1B} := \frac{F_{chord.shell.B} - F_{upper.1B}}{F_{chord.shell.B}} = 40.726 \cdot \%$

$D_{diagonal.1B} := \frac{F_{diagonal.shell.B} - F_{diagonal.1B}}{F_{diagonal.shell.B}} = 2.064 \cdot \%$

Grillage model

Firstly, the bending moments results in horizontal and vertical distortional loads.

Horizontal force: $H_{2B} := \frac{C}{2 \cdot h_{w.B}} \cdot \frac{M_{support.2B}}{R} = 34.92 \cdot kN$

Vertical force: $V_{2B} := \frac{C}{2 \cdot CC} \cdot \frac{M_{support.2B}}{R} = 17.848 \cdot kN$

Therafter, the internal forces in the chords and diagonals are determined.

Force in upper chord: $F_{upper.2B} := 2 \cdot 34.92 \cdot kN$

Force in diagonal: $F_{diagonal.2B} := 49.936 \cdot kN$

Deviations from shell model: $D_{upper.2B} := \frac{F_{chord.shell.B} - F_{upper.2B}}{F_{chord.shell.B}} = 40.607 \cdot \%$

$D_{diagonal.2B} := \frac{F_{diagonal.shell.B} - F_{diagonal.2B}}{F_{diagonal.shell.B}} = 1.855 \cdot \%$

Spatial beam model

Firstly, the bending moments results in horizontal and vertical distortional loads.

Horizontal force: $H_{3B} := \frac{C}{2 \cdot h_{w.B}} \cdot \frac{M_{support.3B}}{R} = 34.928 \cdot kN$

Vertical force: $V_{3B} := \frac{C}{2 \cdot CC} \cdot \frac{M_{support.3B}}{R} = 17.852 \cdot kN$

Therafter, the internal forces in the chords and diagonals are determined.

Force in upper chord: $F_{upper.3B} := 2 \cdot 34.93 \cdot kN$

Force in diagonal: $F_{diagonal.3B} := 49.948 \cdot kN$

Deviations from shell model: $D_{upper.3B} := \frac{F_{chord.shell.B} - F_{upper.3B}}{F_{chord.shell.B}} = 40.59 \cdot \%$

$D_{diagonal.3B} := \frac{F_{diagonal.shell.B} - F_{diagonal.3B}}{F_{diagonal.shell.B}} = 1.832 \cdot \%$

D.2.1 Forces in I-girder bridge

The internal forces can be seen directly from the shell model.

Force in upper chord: $F_{upper.shell.I} := 90.93 \cdot kN$

Force in lower chord: $F_{lower.shell.I} := 95.32 \cdot kN$

Force in diagonal $F_{diagonal.shell.I} := 60.81 \cdot kN$

Equivalent straight beam model

Firstly, the bending moments results in horizontal and vertical distortional loads.

Horizontal force: $H_{1I} := \frac{C}{2 \cdot h_{w.I}} \cdot \frac{M_{support.1I}}{R} = 36.778 \cdot kN$

Vertical force: $V_{1I} := \frac{C}{2 \cdot CC} \cdot \frac{M_{support.1I}}{R} = 19.615 \cdot kN$

Therafter, the internal forces in the chords and diagonals are determined.

Force in upper chord: $F_{upper.1I} := 2 \cdot 36.778 \cdot kN = 73.556\,kN$

Force in lower chord: $F_{lower.1I} := 56.39 \cdot kN$

Force in diagonal: $F_{diagonal.1I} := 52.59 \cdot kN$

Deviations from shell model:

$$D_{upper.1I} := \frac{F_{upper.shell.I} - F_{upper.1I}}{F_{upper.shell.I}} = 19.107 \cdot \%$$

$$D_{lower.1I} := \frac{F_{lower.shell.I} - F_{lower.1I}}{F_{lower.shell.I}} = 40.841 \cdot \%$$

$$D_{diagonal.1I} := \frac{F_{diagonal.shell.I} - F_{diagonal.1I}}{F_{diagonal.shell.I}} = 13.518 \cdot \%$$

Grillage model

Firstly, the bending moments results in horizontal and vertical distortional loads.

Horizontal force: $$H_{2I} := \frac{C}{2 \cdot h_{w.I}} \cdot \frac{M_{support.2I}}{R} = 35.965 \cdot kN$$

Vertical force: $$V_{2I} := \frac{C}{2 \cdot CC} \cdot \frac{M_{support.2I}}{R} = 19.181 \cdot kN$$

Therafter, the internal forces in the chords and diagonals are determined.

Force in upper chord: $F_{upper.2I} := 2 \cdot 35.965 \cdot kN = 71.93\,kN$

Force in lower chord: $F_{lower.2I} := 55.15 \cdot kN$

Force in diagonal: $F_{diagonal.2I} := 51.43 \cdot kN$

Deviations from shell model:

$$D_{upper.2I} := \frac{F_{upper.shell.I} - F_{upper.2I}}{F_{upper.shell.I}} = 20.895 \cdot \%$$

$$D_{lower.2I} := \frac{F_{lower.shell.I} - F_{lower.2I}}{F_{lower.shell.I}} = 42.142 \cdot \%$$

$$D_{diagonal.2I} := \frac{F_{diagonal.shell.I} - F_{diagonal.2I}}{F_{diagonal.shell.I}} = 15.425 \cdot \%$$

Spatial beam model

Firstly, the bending moments results in horizontal and vertical distortional loads.

Horizontal force: $$H_{3I} := \frac{C}{2 \cdot h_{w.I}} \cdot \frac{M_{support.3I}}{R} = 35.986 \cdot kN$$

Vertical force: $V_{3I} := \frac{C}{2 \cdot CC} \cdot \frac{M_{support.3I}}{R} = 19.193 \cdot kN$

Therafter, the internal forces in the chords and diagonals are determined.

Force in upper chord: $F_{upper.3I} := 2 \cdot 35.986 \cdot kN = 71.972\,kN$

Force in lower chord: $F_{lower.3I} := 55.18 \cdot kN$

Force in diagonal: $F_{diagonal.3I} := 51.46 \cdot kN$

Deviations from shell model:

$$D_{upper.3I} := \frac{F_{upper.shell.I} - F_{upper.3I}}{F_{upper.shell.I}} = 20.849 \cdot \%$$

$$D_{lower.3I} := \frac{F_{lower.shell.I} - F_{lower.3I}}{F_{lower.shell.I}} = 42.111 \cdot \%$$

$$D_{diagonal.3I} := \frac{F_{diagonal.shell.I} - F_{diagonal.3I}}{F_{diagonal.shell.I}} = 15.376 \cdot \%$$

E

Geometrical values for Solvalla bridge

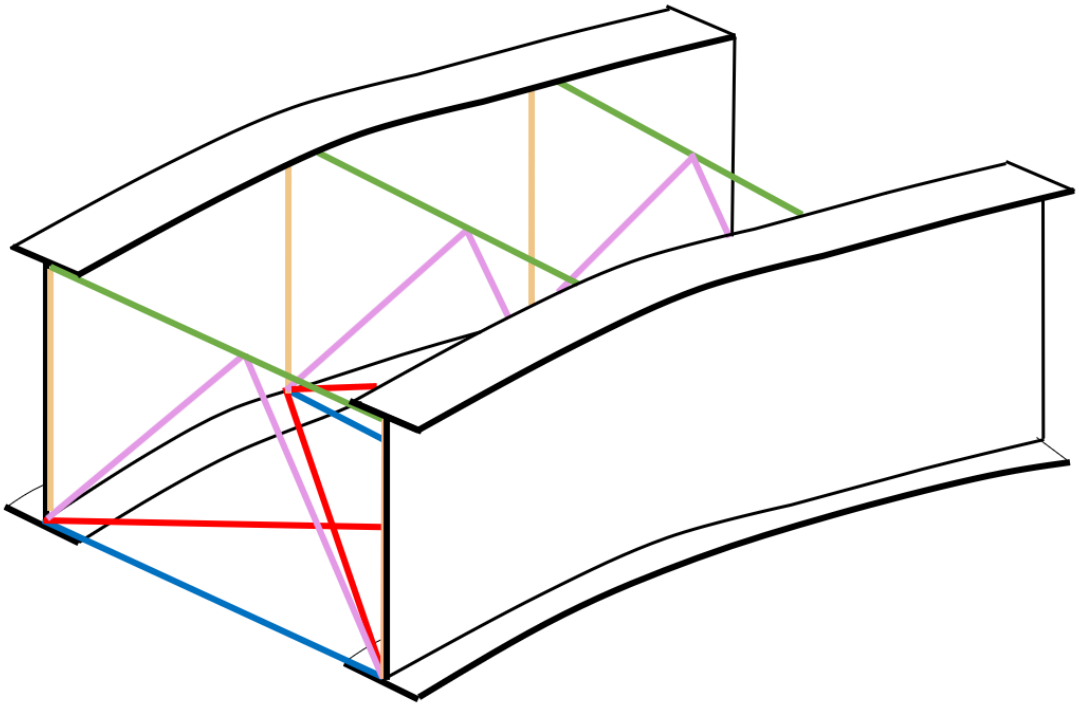

Figure E.1: Positions of the parts that constitutes the cross-bracing and the plan bracing.

Table E.1: Measurements of the parts that constitutes the cross-bracing and the plan bracing.

Bracing type	**Part**	**Shape**	**Measurements [mm]**
Plan bracing	Lower	L-beam	$130 \times 12 \quad l = \sqrt{CC^2 + C^2}$
Cross-bracing	Upper	Quadratic tube	$160 \times 160 \quad t = 6.3 \quad l = CC$
	Lower	Quadratic tube	$200 \times 200 \quad t = 12.5 \quad l = CC$
	Diagonal	Quadratic tube	$160 \times 160 \quad t = 6.3 \quad l = \sqrt{\left(\frac{CC}{2}\right)^2 + hw^2}$
	Stiffener	I-beam	flange: $b = 10 \quad t = 25 \quad l = hw$
			web: $b = \frac{0.9 - tw}{2} \quad t = 25 \quad l = hw$

F

Calculations for one cross-section in the case study

F.1 Bridge description

The chosen values of the bridge geometry is an example from one of the iterations. These calculations are performed for both I- and box girder bridges with varying radius.

F.1.1 Constant bridge geometry

These geometrical values are constant for all iterations and both the I- and box girder bridge.

Span length: $L_1 := 49.0 \cdot m$

$L_2 := 61.2 \cdot m$

$L_3 := 49.0 \cdot m$

Total length: $L_{tot} := L_1 + L_2 + L_3 = 159.2\,m$

Width of bridge: $CC := 4.2 \cdot m$

Thickness of slab: $t_{slab} := 0.3 \cdot m$

Width of slab: $b_{slab} := CC + 2 \cdot 2.35 \cdot m = 8.9\,m$

F.1.2 Varying bridge geometry

These geometrical values will vary for different radius and depending on if it is an I- or a box girder bridge.

Radius: $R := 900 \cdot m$

Spacing of cross-beams: $C := \begin{pmatrix} 4.9 \cdot m \\ 5.1 \cdot m \\ 4.9 \cdot m \end{pmatrix}$

Height of bridge: $H := 2.5 \cdot m$

	Field section	**Support section**	**End section**
Thickness of web:	$t_{w.f} := 12 \cdot mm$	$t_{w.s} := 16 \cdot mm$	$t_{w.e} := 14 \cdot mm$
Thickness of top flange:	$t_{tf.f} := 25 \cdot mm$	$t_{tf.s} := 30mm$	$t_{tf.e} := 25 \cdot mm$
Width of top flange:	$b_{tf.f} := 350 \cdot mm$	$b_{tf.s} := 450 \cdot mm$	$b_{tf.e} := 350 \cdot mm$
Thickness of bottom flange:	$t_{bf.f} := 40 \cdot mm$	$t_{bf.s} := 60 \cdot mm$	$t_{bf.e} := 40 \cdot mm$
Width of bottom flange:	$b_{bf.f} := 600 \cdot mm$	$b_{bf.s} := 900 \cdot mm$	$b_{bf.e} := 600 \cdot mm$

F.1.3 Material properties

For steel qulity S355 the material properties are:

Yield strength: $f_{yk} := 355MPa$

Young's modulus: $E_s := 210 \cdot GPa$

Poissions ratio: $\nu := 0.3$

Shear modulus: $G_s := \frac{E_s}{2 \cdot (1 + \nu)} = 80.769 \cdot GPa$

Safety factor: $\gamma_{M0} := 1.0$

$\gamma_{Ff} := 1.0$

$\gamma_{Mf} := 1.15$

For concrete C35/45 the material properties are:

Young's modulus: $E_{cm} := 34 \cdot GPa$

Creep coefficent: $\varphi_{creep} := 1.55$

Effective E-modulus: $E_{c.eff} := \frac{E_{cm}}{1 + \varphi_{creep}} = 13.333 \cdot GPa$

Transformed section: $\alpha_c := \frac{E_s}{E_{cm}} = 6.176$ (Short term response)

$\alpha_{c.eff} := \frac{E_s}{E_{c.eff}} = 15.75$ (Long term response)

Note. All cross-sectional properties are determined for both long term and short term response, depending on if permanent or variable loads are considered. The calculations in this Appendix is solely for short term respons as the procedure is repetitive.

F.2 Cross-sectional properties

The cross-sectional properties that is determined includes the area and volume of the bridge, as well as, the bending and torsion stiffness.

F.2.1 Cross-section class

The control of cross-section class (CSC) is according to SS-EN 1993-1-1, Table 5.2. The top flange have to be above CSC 3, as an elastic analysis is performed to determine the sectional forces. The field- and support-section is soley checked, as the end-section is an intermidiate section.

$\varepsilon := \sqrt{\frac{235MPa}{f_{yk}}} = 0.814$

$$CSC_{tf.f} := \begin{cases} 1 \text{ if } \dfrac{\left(\dfrac{b_{tf.f} - t_{w.f}}{2}\right)}{t_{tf.f}} \le 9\cdot\varepsilon \\ 2 \text{ if } \dfrac{\left(\dfrac{b_{tf.f} - t_{w.f}}{2}\right)}{t_{tf.f}} \le 10\cdot\varepsilon \\ 3 \text{ if } \dfrac{\left(\dfrac{b_{tf.f} - t_{w.f}}{2}\right)}{t_{tf.f}} \le 14\cdot\varepsilon \\ 4 \text{ otherwise} \end{cases} = 3 \qquad CSC_{tf.s} := \begin{cases} 1 \text{ if } \dfrac{\left(\dfrac{b_{tf.s} - t_{w.s}}{2}\right)}{t_{tf.f}} \le 9\cdot\varepsilon \\ 2 \text{ if } \dfrac{\left(\dfrac{b_{tf.s} - t_{w.s}}{2}\right)}{t_{tf.f}} \le 10\cdot\varepsilon \\ 3 \text{ if } \dfrac{\left(\dfrac{b_{tf.s} - t_{w.s}}{2}\right)}{t_{tf.f}} \le 14\cdot\varepsilon \\ 4 \text{ otherwise} \end{cases} = 3$$

Thereafter, the cross-section class of the web plate is check, which is allowed to be in CSC4.

$$CSC_{w.f} := \begin{cases} 1 \text{ if } \dfrac{\left(H - t_{tf.f} - t_{bf.f}\right)}{t_{w.f}} \le 72\cdot\varepsilon \\ 2 \text{ if } \dfrac{\left(H - t_{tf.f} - t_{bf.f}\right)}{t_{w.f}} \le 83\cdot\varepsilon \\ 3 \text{ if } \dfrac{\left(H - t_{tf.f} - t_{bf.f}\right)}{t_{w.f}} \le 124\cdot\varepsilon \\ 4 \text{ otherwise} \end{cases} = 4 \qquad CSC_{w.s} := \begin{cases} 1 \text{ if } \dfrac{\left(H - t_{tf.s} - t_{bf.s}\right)}{t_{w.s}} \le 72\cdot\varepsilon \\ 2 \text{ if } \dfrac{\left(H - t_{tf.s} - t_{bf.s}\right)}{t_{w.s}} \le 83\cdot\varepsilon \\ 3 \text{ if } \dfrac{\left(H - t_{tf.s} - t_{bf.s}\right)}{t_{w.s}} \le 124\cdot\varepsilon \\ 4 \text{ otherwise} \end{cases} = 4$$

F.2.2 Area of cross-section

Area of end-section:

$$A_{tf.e} := t_{tf.e}\cdot b_{tf.e} = 8.75 \times 10^{3}\cdot mm^{2}$$

$$A_{bf.e} := t_{bf.e}\cdot b_{bf.e} = 2.4 \times 10^{4}\cdot mm^{2}$$

$$A_{w.e} := \left(H - t_{tf.e} - t_{bf.e}\right)\cdot t_{w.e} = 3.409 \times 10^{4}\cdot mm^{2}$$

$$A_{e} := 2\left(A_{tf.e} + A_{bf.e} + A_{w.e}\right) = 0.134\,m^{2}$$

Area of support-section:

$$A_{tf.s} := t_{tf.s}\cdot b_{tf.s} = 1.35 \times 10^{4}\cdot mm^{2}$$

$$A_{bf.s} := t_{bf.s}\cdot b_{bf.s} = 5.4 \times 10^{4}\cdot mm^{2}$$

$$A_{w.s} := \left(H - t_{tf.s} - t_{bf.s}\right)\cdot t_{w.s} = 3.856 \times 10^{4}\cdot mm^{2}$$

$$A_{s} := 2\left(A_{tf.s} + A_{bf.s} + A_{w.s}\right) = 0.212\,m^{2}$$

Area of field-section:

$$A_{tf.f} := t_{tf.f} \cdot b_{tf.f} = 8.75 \times 10^{3} \cdot mm^{2}$$

$$A_{bf.f} := t_{bf.f} \cdot b_{bf.f} = 2.4 \times 10^{4} \cdot mm^{2}$$

$$A_{w.f} := \left(H - t_{tf.f} - t_{bf.f}\right) \cdot t_{w.f} = 2.922 \times 10^{4} \cdot mm^{2}$$

$$A_{f} := 2\left(A_{tf.f} + A_{bf.f} + A_{w.f}\right) = 0.124\,m^{2}$$

Area of concrete slab:

$$A_{slab} := \frac{b_{slab} \cdot t_{slab}}{\alpha_{c}} = 0.432\,m^{2}$$

The dimension of the cross- and plan bracing is fixed for all iterations. For the box girder bridge, the plan bracing is excluded.

Area of one diagonal in plan bracing:

$$A_{truss} := 2 \cdot 130 \cdot mm \cdot 12 \cdot mm = 3.12 \times 10^{-3}\,m^{2}$$

Length of one diagonal in plan bracing:

$$d_{truss} := \sqrt{CC^{2} + \left(C_{0}\right)^{2}} = 6.454\,m$$

Area of cross-bracing:

The cross-bracing consists of one upper chord, one lower chord, as well as, two diagonals with an hollow box-section. It is connected to two stiffners with an

$$A_{upper} := 2[160 \cdot mm \cdot 6.3 \cdot mm + (160 - 6.3) \cdot mm \cdot 6.3 \cdot mm] = 3.953 \times 10^{-3}\,m^{2}$$

$$A_{lower} := 2[200 \cdot mm \cdot 12.5 \cdot mm + (200 - 12.5) \cdot mm \cdot 12.5 \cdot mm] = 9.688 \times 10^{-3}\,m^{2}$$

$$A_{diagonal} := 2 \cdot 2 \cdot [160 \cdot mm \cdot 6.3 \cdot mm + (160 - 6.3) \cdot mm \cdot 6.3 \cdot mm] = 7.905 \times 10^{-3}\,m^{2}$$

$$A_{stiffener} := 2 \cdot 25 \cdot mm \cdot 10 \cdot mm + 25 \cdot mm \cdot \frac{\left(1.2 \cdot m - t_{w.f}\right)}{2} = 0.015\,m^{2}$$

Note. The area of the stiffener is overestimated. Instead of 1.2 m the value should be that of the width of the bottom flange. The difference is minimal, but should be kept in mind.

F.2.3 Volume of the bridge

Number of cross-beams:

$$n_{cross} := \frac{L_{1}}{C_{0}} + \frac{L_{2}}{C_{1}} + \frac{L_{3}}{C_{2}} + 1 = 33$$

Volume of cross-bracing:

$$V_{cross} := n_{cross} \cdot \left[\begin{array}{l} A_{upper} \cdot CC + A_{diagonal} \cdot \sqrt{\left(\frac{CC}{2}\right)^{2} + \left(H - t_{tf.f} - t_{bf.f}\right)^{2}} \ \ldots \\ + 2A_{stiffener} \cdot \left(H - t_{tf.f} - t_{bf.f}\right) + A_{lower} \cdot CC \end{array} \right] = 5.196 \cdot m^{3}$$

Number of diagonals in plan bracing:

$$n_{truss} := \left(n_{cross} - 1\right) = 32$$

Volume of plan bracing: $V_{truss} := 2A_{truss} \cdot d_{truss} \cdot n_{truss} = 1.289 \cdot m^3$

How the devition of end-, field- and support-section is made is illustrated in Chapter 4.

Total length of end-section: $L_e := 0.15 \cdot L_1 + 0.15 \cdot L_3 = 14.7\,m$

Total length of support-section: $L_s := 0.40 \cdot L_2 + 0.25 \cdot L_1 + 0.25 \cdot L_3 = 48.98\,m$

Total length of field-section: $L_f := L_{tot} - L_e - L_s = 95.52\,m$

Volume of the steel structure: $V_{steel} := A_f \cdot L_f + A_s \cdot L_s + A_e \cdot L_e + V_{truss} + V_{cross} = 30.678 \cdot m^3$

F.2.4 Moment of inertia

The determination of the sectional properties are solely presented for the support cross-section. The same is procedure is applied to the field- and end-section in the iterative process.

Centre of gravity in the vertical direction:

$$z_{bf} := \frac{t_{bf.s}}{2} = 0.03\,m$$

$$z_w := t_{bf.s} + \frac{\left(H - t_{tf.s} - t_{bf.s}\right)}{2} = 1.265\,m$$

$$z_{tf} := t_{bf.s} + \left(H - t_{tf.s} - t_{bf.s}\right) + \frac{t_{tf.s}}{2} = 2.485\,m$$

$$z_{slab} := t_{bf.s} + \left(H - t_{tf.s} - t_{bf.s}\right) + t_{tf.s} + \frac{t_{slab}}{2} = 2.65\,m$$

$$z_{tp} := \frac{\left(2A_{tf.s} \cdot z_{tf} + 2A_{w.s} \cdot z_w + 2A_{bf.s} \cdot z_{bf} + A_{slab} \cdot z_{slab}\right)}{2A_{tf.s} + 2 \cdot A_{w.s} + 2 \cdot A_{bf.s} + A_{slab}} = 2.038\,m$$

Centre of gravity in the horizontal direction:

$$y_{bf} := \frac{CC}{2} = 2.1\,m$$

$$y_w := \frac{CC}{2} = 2.1\,m$$

$$y_{tf} := \frac{CC}{2} = 2.1\,m$$

$$y_{slab} := 0 \cdot m = 0$$

$$y_{tp} := \frac{A_{slab} \cdot y_{slab}}{2A_{tf.s} + 2 \cdot A_{w.s} + 2 \cdot A_{bf.s} + A_{slab}} = 0$$

Moment of inertia in the vertical direction:

$$I_{z1} := 2\cdot\left[\frac{b_{tf.s}\cdot t_{tf.s}^{3}}{12} + \frac{t_{w.s}\cdot\left(H - t_{tf.s} - t_{bf.s}\right)^{3}}{12} + \frac{b_{bf.s}\cdot t_{bf.s}^{3}}{12}\right] + \frac{b_{slab}\cdot t_{slab}^{3}}{12\cdot\alpha_c} = 0.041\,m^4$$

$$I_{z2} := 2\cdot\left[A_{bf.s}\cdot\left(z_{tp} - z_{bf}\right)^2 + A_{w.s}\cdot\left(z_{tp} - z_w\right)^2 + A_{tf.s}\cdot\left(z_{tp} - z_{tf}\right)^2\right] \ldots = 0.649\,m^4$$
$$+ A_{slab}\cdot\left(z_{tp} - z_{slab}\right)^2$$

$$I_z := I_{z1} + I_{z2} = 0.689\,m^4$$

Moment of inertia in the horizontal direction:

$$I_{y1} := 2\cdot\left[\frac{t_{tf.s}\cdot b_{tf.s}^{3}}{12} + \frac{\left(H - t_{tf.s} - t_{bf.s}\right)\cdot t_{w.f}^{3}}{12} + \frac{t_{bf.s}\cdot b_{bf.s}^{3}}{12}\right] + \frac{t_{slab}\cdot b_{slab}^{3}}{12\cdot\alpha_c} = 2.861\,m^4$$

$$I_{y2} := 2\cdot\left[A_{bf.s}\cdot\left(y_{tp} - y_{bf}\right)^2 + A_{w.s}\cdot\left(y_{tp} - y_w\right)^2 + A_{tf.s}\cdot\left(y_{tp} - y_{tf}\right)^2\right] \ldots = 0.935\,m^4$$
$$+ A_{slab}\cdot\left(y_{tp} - y_{slab}\right)^2$$

$$I_y := I_{y1} + I_{y2} = 3.797\,m^4$$

Sectional modulus for top and bottom fibre:

$$W_{el.top} := \frac{I_z}{H + \frac{t_{slab}}{2} - z_{tp}} = 1.127\cdot m^3$$

$$W_{el.bottom} := \frac{I_z}{-z_{tp}} = -0.338\cdot m^3$$

F.2.5 Torsion stiffness

The torsion stiffness is presented for solely the field section, but is calculated for end- and support section as well. The equivalent thickness of the fictious steel sheet is determined from Table 7.2 in *Design of Steel-Concrete Composite Bridges to Eurocode*.

Equivalent thickness:

$$t_{eq} := \frac{E_s}{G_s}\cdot\frac{C_0\cdot CC}{\frac{d_{truss}^{3}}{2\cdot A_{truss}} + \frac{\left(C_0\right)^3}{24\cdot 2\cdot A_{tf.s}}} = 1.237\cdot mm$$

Torsion stiffness using Bredt's second formula:

$$I_t := \frac{4\cdot CC^2\left[\left(H - t_{tf.s} - t_{bf.s}\right) + \frac{0.5\cdot t_{slab}}{\alpha_c}\right]^2}{2\frac{\left(H - t_{tf.s} - t_{bf.s}\right)}{t_{w.s}} + \frac{CC}{t_{eq}} + \frac{CC}{\frac{t_{slab}}{\alpha_c}}} + \frac{b_{slab}\cdot t_{slab}^{3}}{3\alpha_c} = 0.123\,m^4$$

F.3 Loads

F.3.1 Permanent loads

Density of steel: $\gamma_s := 78.5 \cdot \frac{kN}{m^3}$ (SS-EN 1991-1-1 Table A.4)

Self-weight of steel structure: $g_s := \gamma_s \cdot \frac{V_{steel}}{L_{tot}} = 15.127 \cdot \frac{kN}{m}$

Density of concrete: $\gamma_c := 25 \cdot \frac{kN}{m^3}$ (SS-EN 1991-1-1 Table A.1)

Self-weight of the slab: $g_c := \gamma_c \cdot A_{slab} = 10.807 \cdot \frac{kN}{m}$

Weight of railing for railway bridge: $g_{railing} := 1.0 \cdot \frac{kN}{m}$ (TDOK 2016:0204 section G.10)

Area of concrete for the slab-track system: $A_{TS} := 2.064 \cdot m^2$ (From client of Solvalla Bridge)

Density of asphaltic concrete: $\gamma_{ac} := 24 \cdot \frac{kN}{m^3}$ (SS-EN 1991-1-1 Table A.3)

Weight of rails: $g_{rail} := \gamma_{ac} \cdot A_{TS} = 49.536 \cdot \frac{kN}{m}$

Weight of cables: $g_{cable} := 5.2 \cdot \frac{kN}{m}$ (Specific to Solvalla Bridge)

F.3.2 Traffic load

Rail traffic

Defined accoring to SS-EN 1991-2 Chapter 6. *Rail traffic actions and other actions specifically for railway bridges*.

Average span length: $L_m := \frac{1}{3} \cdot (L_1 + L_2 + L_3) = 53.067\,m$

Determinante length: $L_\Phi := \max(1.3 \cdot L_m, L_2) = 68.987\,m$

Dynamic factor: $\Phi := \frac{1.44}{\sqrt{\frac{L_\Phi}{m}} - 0.2} + 0.82 = 0.998$

Amplification factor: $\alpha := 1.33$ (TDOK 2016:0204 section B.3.2.1.4)

Load according to LM71: $Q_{vk} := 250 \cdot kN = 250 \cdot kN$

$$q_{vk} := 80 \cdot \frac{kN}{m} = 80 \cdot \frac{kN}{m}$$

The load should be multipled by the dynamic factor and the amplification factor.

$Q_{vd} := \Phi \cdot \alpha \cdot Q_{vk} = 331.719 \cdot kN$

$q_{vd} := \Phi \cdot \alpha \cdot q_{vk} = 106.15 \cdot \frac{kN}{m}$

The eccentricity of the vertical traffic load, due to the position of the rail, can be neglected. This assumption is valid since the eccentric load acts in a favourable direction compared to the centrifugal force.

Nosing force

$Q_{sk} := \alpha \cdot 100 \cdot kN = 133 \cdot kN$

The concentrated force acts horizontally at the top of the rail. (6.5.2(1))

Traction and breaking force

The traction and breaking force acts in the longitudinal direction over the bridge length, resulting in an influence length equal to each span length.

Traction force: $Q_{lak} := \alpha \cdot 33 \cdot \frac{kN}{m} = 43.89 \cdot \frac{kN}{m}$ but no larger than 1000 kN

Breaking force: $Q_{lbk} := \alpha \cdot 20 \cdot \frac{kN}{m} = 26.6 \cdot \frac{kN}{m}$ but no larger than 6000 kN

The bridge consists of two tracks with opposite direction of travel. The combined action of traction and breaking will therefore not be the most conservative case. Therefore, the applied force is either the traction or the breaking force, depending on which is larger for each span.

Centrifugal force

The centrifugal force is an outwardly acting horizontal load, position 1.8 meters over the top surface.

Highest train speed: $v := 200kph$

Reduction factor: $$f := \max\left[0.35 , 1 - \frac{\frac{v}{kph} - 120}{1000} \cdot \left(\frac{814}{\frac{v}{kph}} + 1.75\right) \cdot \left(1 - \sqrt{\frac{2.88}{\frac{L_{tot}}{m}}}\right)\right] = 0.597$$

Which results in a centrifugal force, for a horizontal radius of R = 900 m,

$$Q_{tk} := \alpha \cdot \frac{\left(\frac{v}{kph}\right)^2}{127\left(\frac{R}{m}\right)} \cdot f \cdot Q_{vk} = 69.47 \cdot kN$$

$$q_{tk} := \alpha \cdot \frac{\left(\frac{v}{kph}\right)^2}{127\left(\frac{R}{m}\right)} \cdot f \cdot q_{vk} = 22.23 \cdot \frac{kN}{m}$$

F.3.3 Wind load

The wind load is determined according to SS-EN 1991-4 Chapter 8. *Wind load on bridges.*

Reference wind speed: $v_b := 24 \cdot \frac{m}{s}$ (Appendix D3 for Stockholm, Sweden)

Density of air: $\rho_{air} := 1.25 \cdot \frac{kg}{m^3}$

Total height of bridge: $d_{tot.bridge} := H + t_{slab} + 0.6 \cdot m = 3.4\,m$ (Tab. 8.1)

Height of train: $d_{tot.train} := 4m = 4\,m$ (Ch. 8.3.1 (4) b))

Shape factor: $C_{bridge} := \frac{6.7 - 3.6}{0.5 - 4.0} \cdot \frac{b_{slab}}{d_{tot.bridge}} + 7.143 = 4.825$ (Linear interpolation Tab. 8.2)

Shape factor: $C_{train} := \frac{6.7 - 3.6}{0.5 - 4.0} \cdot \frac{b_{slab}}{d_{tot.train}} + 7.143 = 5.172$ (Linear interpolation Tab. 8.2)

Reference area: $A_{refx.bridge} := d_{tot.bridge} \cdot L = 3.4 \times 10^{-3}\,m^4$

Reference area: $A_{refx.train} := d_{tot.train} \cdot L = 4 \times 10^{-3}\,m^4$

Results in a wind load of: $F_{w.bridge} := \frac{1}{2} \cdot \rho_{air} \cdot v_b^{\,2} \cdot C_{bridge} \cdot A_{refx.bridge} = 5.905 \times 10^{-3}\,m^2 \cdot kN$

$$F_{w.train} := \frac{1}{2} \cdot \rho_{air} \cdot v_b^{\,2} \cdot C_{train} \cdot A_{refx.train} = 7.448 \times 10^{-3}\,m^2 \cdot kN$$

F.4 Requirements

The sectional forces and displacements are determined by running the analysis in Brigade. The resulting values are then combined according to the load combinations listed in Chapter 4. *Case study.* In order to illustrate the requirments that are checked, the values from the FE-analysis is written in after the load combination have been performed. The requirments are checked for end-, field- and support-section, however, only the support section is presented here as the procedure is repetitive.

Design moment: $M_{Ed} := 75.872 \cdot MN \cdot m$

Design shear force: $V_{Ed} := 7.4900 \cdot MN$

Design axial force: $N_{Ed} := 0.9956 \cdot MN$

Design displacement: $U_{Ed} := -0.0993 \cdot m$

Design moment range: $\Delta M_{Ed} := 36752712 \cdot N \cdot m$

Note. This stress range includes the dynamic factor ϕ.

For the box girder bridge, the torsion moment is also retrieved from Brigade Plus.

Design torsion moment: $M_{T.Ed} := 0.4259 \cdot MN \cdot m$

F.4.1 Control of normal stress

Normal stresses: $$\sigma_{y.Ed} := \frac{N_{Ed}}{A_s} + \frac{M_{Ed}}{\left|W_{el.bottom}\right|} = 228.994 \cdot MPa$$

Utilization ratio for normal stress: $$UR_\sigma := \frac{\sigma_{y.Ed}}{f_{yk}} = 64.505 \cdot \%$$

F.4.2 Control of shear stress

Control of shear stress differs for the two cross-section types, due to the two different ways that torsion is introduced to the bridge.

I-girder bridge

Calculation of shear strength according to SS-EN 1993-1-1 Chapter 6. Shear.

Shear area: $$A_{v.s} := 1.2 \cdot \left(H - t_{tf.s} - t_{bf.s}\right) \cdot t_{w.s} = 0.046\ m^2$$

Shear strength: $$V_{pl.Rd} := \frac{A_{v.s} \cdot \left(\frac{f_{yk}}{\sqrt{3}}\right)}{\gamma_{M0}} = 9.484 \times 10^3 \cdot kN$$

Note. This eq. is ok to used for curved open sections, since resistance by warping results in added component to shear.

Utilisation ratio for shear force: $$UR_V := \frac{V_{Ed}}{V_{pl.Rd}} = 78.976 \cdot \%$$

Box girder bridge

Calculation of shear strength in combination with torsion is performed according to *Design of steel-concrete composite bridges to Eurocode* Chapter 9. Note. The utilisation ratios listed in this section will not correspond to any real calculations, as the sectional properties and the shear force is given for the I-girder bridge. This only serves as an illustrative example of how the calculations are performed for a box girder.

Shear area: $A_{v.s.web} := 1.2\left(H - t_{tf.s} - t_{bf.s}\right)\cdot t_{w.s} = 0.046\,m^2$

$A_{v.s.bottom} := 1.2 b_{bf.s}\cdot t_{bf.s} = 0.065\,m^2$

Enclosed area: $A_0 := t_{slab}\cdot CC + t_{bf.s}\cdot CC + t_{w.s}\cdot CC = 1.579\,m^2$

Reduction for shear buckling have to be made if the slenderness of the webs are under a threshold.

Buckling: $\eta := 1.2$ For steel grades up to S460.

$\kappa_\tau := 5.34$

Slenderness: $\lambda_w := \dfrac{H - t_{tf.s} - t_{bf.s}}{37.4\cdot t_{w.s}\cdot\varepsilon\cdot\sqrt{\kappa_\tau}} = 2.142 \qquad > 1.08$

$$\chi_w := \begin{cases} \dfrac{1.37}{0.7 + \lambda_w} & \text{if } \dfrac{H - t_{tf.s} - t_{bf.s}}{t_{w.s}} > 60\cdot\varepsilon \\ 1 & \text{if } \dfrac{H - t_{tf.s} - t_{bf.s}}{t_{w.s}} \le 60\cdot\varepsilon \end{cases} = 0.482$$

Shear strength: $\gamma_{M1} := 1.0$

$V_{bw.Rd.web} := \chi_w\cdot A_{v.s.web}\cdot\dfrac{f_{yk}}{\sqrt{3}\cdot\gamma_{M1}} = 4.572\times10^3\cdot kN$

$V_{bw.Rd.bottom} := \chi_w\cdot A_{v.s.bottom}\cdot\dfrac{f_{yk}}{\sqrt{3}\cdot\gamma_{M1}} = 6.402\times10^3\cdot kN$

Shear flow: $v_{MT.Ed} := \dfrac{M_{T.Ed}}{2\cdot A_0} = 1.348\times10^5\,\dfrac{kg}{s^2}$

Shear in webs: $V_{Ed.web.inner} := V_{Ed} - v_{MT.Ed}\cdot\left(H - t_{tf.s} - t_{bf.s}\right) = 7.165\times10^3\cdot kN$

$V_{Ed.web.outer} := V_{Ed} + v_{MT.Ed}\cdot\left(H - t_{tf.s} - t_{bf.s}\right) = 7.815\times10^3\cdot kN$

Shear in bottom flange: $V_{Ed.bottom} := v_{MT.Ed}\cdot CC = 566.356\cdot kN$

Utilisation ratio for shear force:

$$UR_V := \frac{V_{Ed.web.inner}}{V_{bw.Rd.web}} = 156.728 \cdot \%$$

$$UR_V := \frac{V_{Ed.web.outer}}{V_{bw.Rd.web}} = 170.945 \cdot \%$$

$$UR_V := \frac{V_{Ed.bottom}}{V_{bw.Rd.bottom}} = 8.846 \cdot \%$$

F.4.3 Control of fatigue

Fatigue control according to SS-EN 1993-2 Chapter 9. Fatigue assessment.

Detail category:

$$\Delta\sigma_R := 80 \cdot MPa$$

Damage equivalence factor:

$$\lambda := \min(0.63 \cdot 1.0 \cdot 1.0 \cdot 1.0 , 1.4) = 0.63$$

Stress range at the top fibre:

$$\Delta\sigma_{E.top} := \lambda \cdot \frac{\Delta M_{Ed}}{W_{el.top}} = 20.545 \cdot MPa$$

Stress range at the bottom fibre:

$$\Delta\sigma_{E.bottom} := \lambda \cdot \frac{\Delta M_{Ed}}{W_{el.bottom}} = -68.451 \cdot MPa$$

Utalisation ratios for fatigue:

$$UR_{F.top} := \frac{\gamma_{Ff} \cdot \Delta\sigma_{E.top}}{\frac{\Delta\sigma_R}{\gamma_{Mf}}} = 29.534 \cdot \%$$

$$UR_{F.bottom} := \left| \frac{\gamma_{Ff} \cdot \Delta\sigma_{E.bottom}}{\frac{\Delta\sigma_R}{\gamma_{Mf}}} \right| = 98.398 \cdot \%$$

F.4.4 Control of displacement

Requirements for rail way bridges:

$$U_{lim} := \frac{\max(L_1 , L_2 , L_3)}{600} = 102 \cdot mm$$

Utilisation ratio for displacement:

$$UR_U := \frac{|U_{Ed}|}{U_{lim}} = 97.353 \cdot \%$$

G

Supplementary result: Case study

Result from optimisation for box girder bridge.					
Radius	150 m	300 m	500 m	700 m	900 m
Result from first optimisation					
H	2300	2300	2300	2300	2300
$t_{w.field}$	18	18	16	16	16
$t_{w.support}$	24	24	24	24	22
$t_{w.end}$	16	16	16	16	16
$b_{tf.field}$	250	250	250	250	250
$b_{tf.support}$	300	300	300	300	300
$b_{tf.end}$	250	250	250	250	250
$t_{tf.field}$	20	20	20	20	20
$t_{tf.support}$	28	28	28	28	28
$t_{tf.end}$	20	20	20	20	20
$t_{bf.field}$	10	10	10	10	10
$t_{bf.support}$	25	25	25	25	25
$t_{bf.end}$	10	10	10	10	10
$UR_{moment.field}$ [1)]	15,0%	13,7%	13,4%	13,3%	13,2%
$UR_{moment.support}$	71,8%	67,7%	66,6%	66,1%	67,1%
$UR_{moment.end}$	11,8%	10,7%	10,3%	10,2%	10,1%
$UR_{shear.field}$	95,6%	85,7%	100,2%	98,2%	96,9%
$UR_{shear.support}$	94,6%	89,5%	87,2%	86,2%	99,1%
$UR_{shear.end}$	96,5%	90,2%	87,6%	86,7%	86,2%
$UR_{fatigue}$	102,7%	99,6%	99,7%	99,9%	101,7%
$UR_{displacement}$	136,1%	114,7%	111,1%	109,6%	110,0%
Result from second optimisation					
H	2700	2500	2500	2500	2400
$t_{bf.field}$	10	10	10	10	10
$t_{bf.support}$	30	25	25	25	30
$t_{bf.end}$	10	10	15	15	10
$UR_{moment.field}$	13,3%	12,9%	12,6%	12,5%	12,7%
$UR_{moment.support}$	53,9%	61,7%	60,5%	60,0%	56,8%
$UR_{moment.end}$	10,5%	10,0%	7,9%	7,8%	9,7%
$UR_{shear.field}$	94,3%	84,5%	98,7%	96,6%	96,9%
$UR_{shear.support}$	91,3%	87,5%	85,1%	84,1%	97,9%
$UR_{shear.end}$	94,2%	88,7%	86,2%	85,2%	84,9%
$UR_{fatigue}$	77,0%	90,4%	90,2%	90,4%	86,0%
$UR_{displacement}$	99,5%	97,8%	94,7%	93,3%	94,2%
Volume	33,1859	30,7484	30,1138	30,1138	29,6935

1) Utilisation ratio (UR)

Result from optimisation for I-girder bridge with lower plan bracing.					
Radius	150 m	300 m	500 m	700 m	900 m
Result from first optimisation					
H	2600	2400	2300	2300	2300
$t_{w.field}$	12	12	12	12	12
$t_{w.support}$	16	16	18	16	16
$t_{w.end}$	14	14	14	14	14
$b_{tf.field}$	350	350	350	350	350
$b_{tf.support}$	450	450	450	450	450
$b_{tf.end}$	350	350	350	350	350
$t_{tf.field}$	25	25	25	25	25
$t_{tf.support}$	30	30	30	30	30
$t_{tf.end}$	25	25	25	25	25
$b_{bf.field}$	600	600	600	600	600
$b_{bf.support}$	900	900	900	900	900
$b_{bf.end}$	600	600	600	600	600
$t_{bf.field}$	40	40	40	40	40
$t_{bf.support}$	60	60	60	60	60
$t_{bf.end}$	40	40	40	40	40
$UR_{moment.field}$	13,0%	12,9%	12,7%	13,0%	13,0%
$UR_{moment.support}$	67,2%	69,3%	68,1%	71,0%	70,8%
$UR_{moment.end}$	10,2%	9,9%	9,7%	9,9%	9,8%
$UR_{shear.field}$	61,6%	63,6%	62,5%	64,8%	64,5%
$UR_{shear.support}$	74,4%	81,7%	82,3%	86,1%	86,2%
$UR_{shear.end}$	47,5%	49,2%	48,4%	50,3%	50,1%
$UR_{fatigue}$	101,8%	105,1%	103,5%	108,3%	108,2%
$UR_{displacement}$	124,1%	115,1%	108,6%	115,3%	114,8%
Result from second optimisation					
H	3000	2700	2500	2500	2500
$b_{bf.field}$	600	600	600	600	600
$b_{bf.support}$	900	800	900	900	900
$b_{bf.end}$	600	600	600	600	600
$UR_{moment.field}$	11,8%	11,8%	12,3%	12,2%	12,2%
$UR_{moment.support}$	58,1%	65,8%	63,9%	64,6%	64,5%
$UR_{moment.end}$	9,2%	9,1%	9,4%	9,3%	9,2%
$UR_{shear.field}$	53,7%	56,1%	60,0%	59,5%	59,2%
$UR_{shear.support}$	64,6%	72,5%	70,0%	78,9%	79,0%
$UR_{shear.end}$	41,6%	43,9%	46,5%	46,2%	46,0%
$UR_{fatigue}$	87,4%	99,8%	97,0%	98,5%	98,4%
$UR_{displacement}$	99,5%	96,9%	99,4%	98,3%	97,4%
Volume	33,4233	31,1877	31,1506	30,6784	30,6784

Result from optimisation for I-girder bridge without lower plan bracing.					
Radius	150 m	300 m	500 m	700 m	900 m
Result from first optimisation					
H	2700	2500	2400	2400	2400
$t_{w.field}$	12	12	12	12	12
$t_{w.support}$	18	16	16	16	16
$t_{w.end}$	14	14	14	14	14
$b_{tf.field}$	350	350	350	350	350
$b_{tf.support}$	450	450	450	450	450
$b_{tf.end}$	350	350	350	350	350
$t_{tf.field}$	25	25	25	25	25
$t_{tf.support}$	30	30	30	30	30
$t_{tf.end}$	25	25	25	25	25
$b_{bf.field}$	600	600	600	600	600
$b_{bf.support}$	900	900	900	900	900
$b_{bf.end}$	600	600	600	600	600
$t_{bf.field}$	40	40	40	40	40
$t_{bf.support}$	60	60	60	60	60
$t_{bf.end}$	40	40	40	40	40
$UR_{moment.field}$	14,7%	13,5%	13,4%	13,1%	13,0%
$UR_{moment.support}$	68,9%	70,3%	70,8%	69,7%	69,2%
$UR_{moment.end}$	11,2%	10,3%	10,1%	9,8%	9,7%
$UR_{shear.field}$	67,9%	66,1%	65,8%	64,4%	63,7%
$UR_{shear.support}$	63,1%	78,7%	82,5%	82,6%	82,6%
$UR_{shear.end}$	54,1%	51,6%	51,2%	50,1%	49,6%
$UR_{fatigue}$	103,7%	106,8%	107,8%	106,3%	105,5%
$UR_{displacement}$	128,8%	113,9%	113,1%	109,6%	107,9%
Result from second optimisation					
H	3000	2700	2600	2600	2500
$b_{bf.field}$	600	600	600	600	600
$b_{bf.support}$	1200	900	900	900	900
$b_{bf.end}$	600	600	600	600	600
$UR_{moment.field}$	13,7%	12,8%	12,6%	12,3%	12,6%
$UR_{moment.support}$	50,7%	64,9%	65,1%	64,1%	66,3%
$UR_{moment.end}$	10,4%	9,7%	9,5%	9,3%	9,4%
$UR_{shear.field}$	61,8%	61,3%	60,7%	59,4%	61,1%
$UR_{shear.support}$	56,1%	72,6%	75,9%	76,0%	79,2%
$UR_{shear.end}$	49,5%	47,9%	47,3%	46,3%	47,6%
$UR_{fatigue}$	76,1%	99,0%	99,6%	98,1%	101,3%
$UR_{displacement}$	97,4%	98,9%	96,9%	93,8%	99,6%
Volume	34,4680	30,4868	29,9381	29,9381	29,3897

1) The value exceeds 100% due to the tolerance of the genetic algortihm.